INVESTIGATION OF PEPTIDE FOLDING

BY NUCLEAR MAGNETIC RESONANCE SPECTROSCOPY

A Dissertation

by

SOYOUN HWANG

Submitted to the Office of Graduate Studies of
Texas A&M University
in partial fulfillment of the requirements for the degree of

DOCTOR OF PHILOSOPHY

May 2012

Major Subject: Chemistry

Investigation of Peptide Folding by Nuclear Magnetic Resonance

Spectroscopy

INVESTIGATION OF PEPTIDE FOLDING

BY NUCLEAR MAGNETIC RESONANCE SPECTROSCOPY

A Dissertation

by

SOYOUN HWANG

Submitted to the Office of Graduate Studies of
Texas A&M University
in partial fulfillment of the requirements for the degree of

DOCTOR OF PHILOSOPHY

Approved by:

Chair of Committee,	Christian Hilty
Committee Members,	Janet Bluemel
	Paul Cremer
	J. Martin Scholtz
Head of Department,	David H. Russell

May 2012

Major Subject: Chemistry

ABSTRACT

Investigation of Peptide Folding by Nuclear Magnetic

Resonance Spectroscopy. (May 2012)

Soyoun Hwang, B.S., Chungnam National University;

M.S., Pohang University of Science and Technology

Chair of Advisory Committee: Dr. Christian Hilty

Understanding structure and folding of a protein is the key to understanding its biological function and potential role in diseases. Despite the importance of protein folding, a molecular level understanding of this process is still lacking. Solution-state nuclear magnetic resonance (NMR) is a powerful technique to investigate protein structure, dynamics, and folding mechanisms, since it provides residue-specific information. One of the major contributions that govern protein structure appears to be the interaction with the solvent. The importance of these interactions is particularly apparent in membrane proteins, which exist in an amphiphilic environment. Here, individual peptide fragments taken from the disulfide bond forming protein B (DsbB) were investigated in various solvents. The α-helical structures that were obtained, suggest that DsbB follows the two-stage model for folding. However, side chains of polar residues showed different conformations compared to the X-ray structure of full-length protein, implying that polar side-chains may re-orient upon helix packing in order to form the necessary tertiary interactions that stabilize the global fold of DsbB. Model

peptides in general represent attractive systems for the investigation of non-covalent interactions important for protein folding, including those with the solvent. NMR structures of the water soluble peptide, BBA5, were obtained in the presence an organic co-solvent, methanol. These structures indicate that the addition of methanol stabilizes an α-helix segment, but disrupts a hydrophobic cluster forming a ß-hairpin. Since dynamic effects reduce the ability for experimental observation of individual, bound solvent molecules, results were compared with molecular dynamics simulations. This comparison indicates that the observed effects of NMR structures are due to preferred binding of methanol and reduction of peptide-water hydrogen bonding. NMR structures, such as those determined here, represent a distribution of conformations under equilibrium. The dynamic process of protein unfolding can nevertheless be accessed through denaturation. A method was developed to probe thermal denaturation by measuring the temperature dependence of NOE intensity. Applied to a model peptide, trpzip4, it was confirmed that the ß-hairpin structure of this peptide is stabilized by the hydrophobic cluster formed by tryptophan residues. Together, the peptides investigated here illustrate the important roles that solvent-peptide interactions and side chain-side chain hydrophobic interactions play in forming stable secondary and tertiary structures.

DEDICATION

My Love Jesus

ACKNOWLEDGEMENTS

I am deeply indebted to Christian Hilty who has been a great advisor ever since I joined his group. I still remember the first meeting with him when I did not have so much expectation of joining his group. I had decided to study other biophysical tools rather than NMR after I spent some time using NMR during master degree. However, the moment made me end up thinking "why not NMR? I want to learn more from him!" I am really grateful to have him as my advisor, and he has helped me to think more scientifically and to be more curious about science.

I also would like to thank my committee members, Dr. Bluemel, Dr. Cremer, and Dr. Scholtz, for their guidance and support throughout the course of this research. I also would like to thank to Dr. Gao for his help and encouragement on the co-project.

Thanks also go to Hilty group members, Sean Bowen, Hsueh-Ying Chen, Youngbok Lee, Mukundan Ravagan, Giri Sekar, for useful discussion on the projects and department staffs for making good experience at Texas A&M University. Special thanks go to Mingchien Li, Ms. Myong Ledesma, Younhee Cho, Jaibir Kherb, Hyejin Chun, Eunhwa Ko, Youngbok Lee, Jenny Chen, Jesus Lopez, Xiangming Kong, for being such nice friends to me and sharing your life with me. I also want to extend my gratitude to the VMC friends including my pastor and his wife for praying for us and being good family to us.

Last, but not least, I thank to my family, mom, my husband Sangwoo, and my son Siwon for their love and support during long journey.

NOMENCLATURE

NMR	Nuclear Magnetic Resonance
2D	Two Dimensional
COSY	Correlation SpectroscopY
TOCSY	TOtal Correlation SpectroscopY
HSQC	Heteronuclear Single Quantum Correlation
NOESY	Nuclear Overhauser Effect SpectroscopY
ROESY	Rotational frame Overhauser Effect SpectroscopY
DsbB	Disulfide Bond Forming Protein B
BBA5	Beta Beta Alpha 5
Trpzip4	Tryptophan Zipper Peptide 4
16-DSA	16-DoxylStearic Acid
5-DSA	5-DoxylStearic Acid
SDS	Sodium Dodecyl Sulfate
DPC	DodecylPhosphoCholine
CD	Circular Dichroism Spectroscopy
Gd-DTPA	N,N-Bis(2-[bis(carboxymethyl)amino]ethyl)glycine gadolinium complex)
DSS	Sodium 2,2-dimethyl-2-silapentane-5-sulfonate
MD	Molecular Dynamics
TFE	Trifluoroethanol

GdmCl	Guanidinium Chloride
LDAO	Lauryldimethylamine-oxide

TABLE OF CONTENTS

Page

LIST OF FIGURES

LIST OF TABLES

CHAPTER I

INTRODUCTION

An interesting property of proteins is their capability to fold into a characteristic conformation on a short timescale (μs – h) under physiological conditions.[1] For even a relatively small protein with 100 amino acids, the number of possible conformations is 10^{100} if one residue has an average of 10 conformations.[1] Nevertheless, the protein selectively folds into a unique three dimensional structure, which is essential for fulfilling its biological function. Failing to fold into this structure generally leads to the malfunctioning of the protein and consequently to various disorders such as Alzheimer's, Parkinson's, and Huntington's diseases.[2-3] With this reason, it is important to understand the mechanism of protein folding which continues to be one of the central problems in biochemistry, biophysical chemistry, and molecular biology.

Often, short peptides have been used as model systems even though they do not systematically adopt well-defined tertiary structures in contrast to proteins. They still provide insight into specific noncovalent interactions which play an important role in secondary structure formation in order to explain early events in protein folding.[4-6] Hydrophobic interactions, intramolecular hydrogen bonds, and electrostatic interactions are important factors that affect protein folding. In this study, we investigated the folding determinants of several peptides, including alpha-helical membrane protein fragments, as well as model peptides that include α-helical and β-hairpin elements.

This dissertation follows the style of Journal of Physical Chemistry.

1.1 Secondary Structure in Proteins

Secondary structure is the local structure of the polypeptide. Typical structures include α-helices, 3_{10}-helix, parallel and anti-parallel ß-sheets, and ß-turn structures. Backbone torsion angles and hydrogen bond paring patterns can be used as criteria to recognize the secondary structure. Torsion angles are rotations about bonds, usually described with values between -180° and +180°. Rotation about the N-C^{α} bond of the peptide backbone is defined as φ and rotation about the C^{α}-C' bond is defined as ψ. With torsion angle information, φ and ψ in α-helices are -60° and -45° in folded proteins and φ and ψ in ß-sheet are -135° and 135°. A Ramachandran plot is a plot of the torsional angles ψ and φ of the amino acid residues contained in a peptide (Figure 1.1), and through the Ramachandran plot, permitted torsion angles in the peptide can be determined, which gives insight into the peptide structure.

1.2 Hydrophobic Interaction

When a protein folds, most of the nonpolar side chains are buried in the core of the protein where the protein is protected from water, and those side chains are tightly packed with other side chain groups. This phenomenon is known as the hydrophobic effect, which is a major driving force in determining protein stability and folding. There has been a long standing question about how the hydrophobic interaction can favorably contribute to protein stability. Usually, the magnitude of the hydrophobic interactions is measured by the free energy ΔG of nonpolar molecules. In 1962, Tanford et al. developed the concept that the free energy of transfer of amino acids from organic

solvents to water could be used to establish a hydrophobicity scale which is useful for estimating the contributions to the protein stability from buried residues.[7] At the end, they concluded that the stability of the native conformation in water entirely depends on the hydrophobic interactions of the nonpolar residue. Furthermore, by mutating a single amino acid in the protein sequence which is involved in hydrophobic interactions and measuring the stability difference between the wild type and the mutant, one can also answer whether the hydrophobic interaction can favorably contribute to protein stability. For example, Pace et al. investigated contributions of hydrophobic interactions to protein stability by measuring the protein conformations Δ(ΔG) of hydrophobic mutants of several proteins including the villin headpiece subdomain (VHP), a surface protein from Borrelia burgdorferi (VlsE), and ribonuclease Sa and T1. For example, VHP has a Δ(ΔG) of about 0.6±0.3 kcal/mol per –CH2– group, and VlsE 1.6±0.3 kcal/mol per –CH2– group. Based on this study, hydrophobic interaction is the predominant driving force in stabilizing the globular protein conformation.[8] Several recent studies, including MD simulations, emphasized the inter-strand hydrophobic side chain – side chain interactions play an important role in stabilizing the ß-hairpin structure of a trpzip peptide, which is one of the model peptides studied in this thesis.[9-10]

1.3 Hydrogen Bond

A hydrogen bond occurs between a hydrogen atom attached to an electronegative atom, and an electronegative atom nearby. Hydrogen bonds in proteins frequently involve the C=O and N-H groups of the polypeptide backbone, where they stabilize the secondary structure. Figure 1.2 shows the hydrogen bond pattern in the secondary

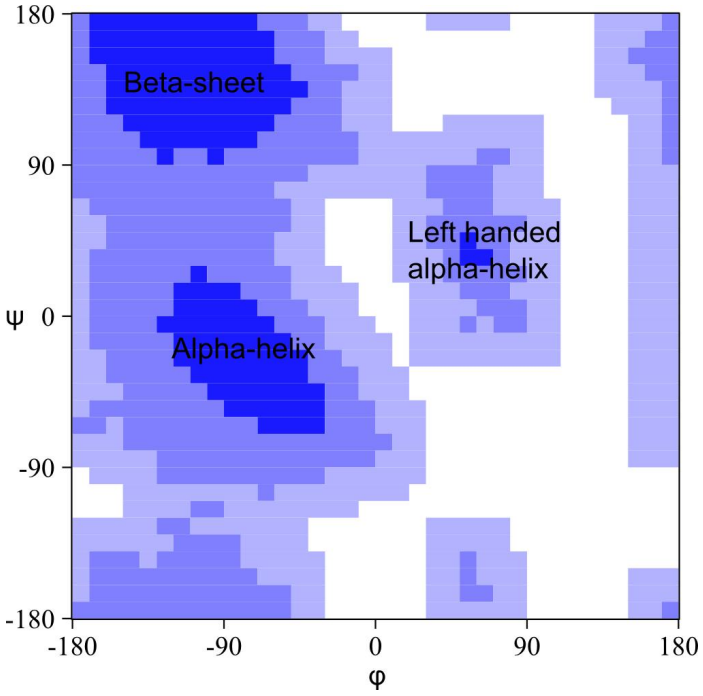

Figure 1.1: Ramachandran plot showing allowed torsion angles for different secondary structure elements. The white and brightest blue color regions are sterically disallowed for all amino acids except glycine, and the slightly darker blue regions correspond to generously allowed regions where there are no steric clashes. The darkest blue color areas show the favored regions Ramanchandran plot was made by the cyana[12] program, and revised.

structure α-helix and ß-sheet. The estimated ΔG value resulting from stabilization is around 2.2 kcal/mol per hydrogen bond,[11] for a distance of 3.04 Å.

During the protein folding process, a significant population of the polar side chains is buried in the interior of the protein and these groups form hydrogen bonds with other polar groups. Whether or not these hydrogen bonded polar groups contribute to overall globular protein stability has been controversial. Several theoretical studies claim that hydrogen bonds do not make any contribution to protein stability.[13-14] However, Myer et al. performed experiments measuring the stability difference between mutant and wild-type proteins where one residue of a hydrogen bonding pair has been replaced with a residue incapable of hydrogen bonding, concluding that hydrogen bonds make a favorable contribution to stability.[11] Other experimental evidence, shown by Huyghues-Despointes et al., measured the contribution of an interaction between (i)th Gln and (i+4)th Gln to the stability of the α-helical form of a peptide. They used NMR to show that the Asp carboxyl group forms a specific hydrogen bond with the amide group of Gln. Furthermore, by measuring the free energy, they calculated that this interaction stabilizes the α-helix by 0.4 kcal/mol when the Asp is uncharged and by 1.0 kcal/mol when the Asp is charged indicating that hydrogen bonds are important in stabilizing α-helices in water.[15]

1.4 Electrostatic Interaction

Electrostatic interaction occurs between charged amino acid residues. There are ionized groups of the side chains, including Lys, Arg, His, Asp, and Glu residues, plus

the α-amino and α-carboxyl oxygen atoms. Interactions between close oppositely charged groups in a protein are known as salt bridges, and those interactions usually consist not only of electrostatic interactions but also of some degree of hydrogen bond.

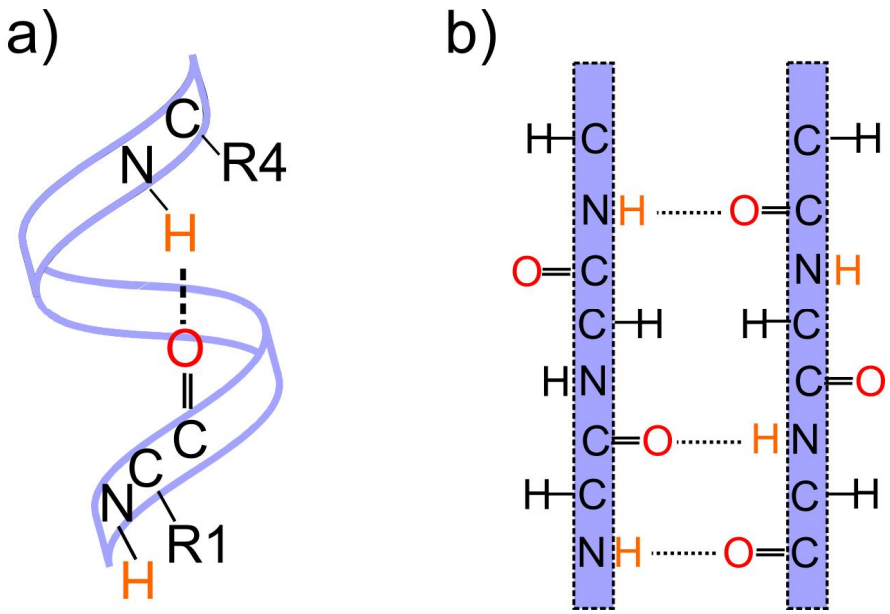

Figure 1.2. Hydrogen bond topology of α-helix and anti-parallel ß-sheet structure. a) alpha helix has 3.6 amino acids per turn of the helix which places the carbonyl group of the first amino acid in line with the amide group of the fourth amino acid. b) anti-parallel β sheet makes the planar hydrogen bond between carbonyl groups and amides from each ß-strand which results in the strong inter-strand stability.

Many polar and charged residues are often observed in the protein-protein interface and those are creating salt bridges which often arises from the ionizable side

chains such as histidine, lysine, and glutamate. For example, one of the transmembrane proteins, Disulfide bond forming protein B, also includes a salt bridge between His 91 of helix 3 and Glu 47 of helix 2.[16]

1.5 Influence of Solvent

Protein structure and dynamics are strongly dependent on specific interactions with solvent molecules in addition to intramolecular interactions in the polypeptide. Various solvent-solute interactions can cause protein folding or protein denaturation,[17-20] and despite their importance, it is not immediately clear how these interactions cause protein folding and denaturation. A number of studies of the solvent effect on protein structure have been done by NMR. Sonnichsen et al. studied the effect of the solvent TFE on the protein secondary structure of a synthetic actin peptide using NMR and CD.[17] The peptide was largely unstructured in an aqueous solution, but in 80% TFE solution, the peptide contained well-defined α-helices. Searle et al. also showed the organic solvent effect on N-terminal 20 residues of a native-like β-hairpin structure in an isolated fragment from ferredoxin using NMR and CD.[18] The peptide was unstructured in a purely aqueous solution, but native like β-hairpin formed after the addition of a small amount of organic co-solvent, suggesting that the stabilizing influence from an organic co-solvent can be one of the tertiary interactions which occur in the complete ferredoxin folding sequence. The importance of the solvent effect is illustrated by the results of interactions with various solutes, leading to protein folding or denaturation. Often, it is challenging to identify the specific solvent-solute interaction using experimental techniques, therefore several studies have been performed employing a

molecular dynamics simulation and possibly combined with experimental approaches.[19-21] For example, there was a study showing that polar/electrostatic interactions between denaturants and polypeptide chains can be the driving force to cause a polypeptide to unfold.[20] O'Brien et al. observed direct interactions between guanidinium cation and charged/polar residues of the protein.They did not observe similar interactions for urea and concluded that direct electrostatic interaction is a stronger driving force for denaturation mediated by GdmCl than it is for urea.[20] In this thesis, combined research including experimental study with MD simulation is used to examine specific peptide-solvent interactions.

1.6 Membrane Proteins

Integral membrane proteins play a central role including transport, signaling, and energy transport.[22] Unlike soluble proteins, integral membrane proteins contain a hydrophobic surface area in the transmembrane region. The amphipathic property of integral membrane proteins gives rise to several technical challenges associated with crystallizing or solubilizing membrane proteins. Therefore, determining the structure and folding mechanisms of membrane proteins is more challenging than for soluble proteins. However, important progress has been made in this field in recent years.

First, structures were determined for ß-barrel membrane proteins. Arora et al. determined the 3D-structure of the transmembrane domain of the outer membrane protein A (OmpA) of *Escherichia coli* in DPC with a solution NMR spectroscopy.[23] Furthermore, Hiller et al., using NMR, announced the structure of human voltage-dependent anion channels (VDAC) which mediate trafficking of small molecules and

ions across the outer mitochondrial membrane. Recombinant human VDAC-1 was reconstituted in LDAO micelles, and the 3D-structure included a 19-strand ß-barrel.[24] β-barrels represent a small class of membrane proteins found in the outer membrane of gram-negative bacteria, chloroplasts, and mitochondria. The vast majority of membrane proteins are alpha-helical structures, and they typically have helix bundles. There has also been progress on the study of structure and function of α-helical membrane proteins. For example, Doyle et al. determined the X-ray structure of the potassium channel from *Streptomyces lividans* which is an integral membrane protein. Detailed structural information explained the principle of selectivity of the K^+ channel.[25] Inaba et al. also used X-ray crystallography to determine the disulfide bond generation protein complex DsbA-DsbB structure.[16] A short time later, Zhou et al. announced the NMR structure of DsbB and proposed the mechanism of catalysis for this enzyme.[26]

Several sequence motifs in transmembrane proteins are known to stabilize the helix bundlesby helix-helix interaction. First of all, the GXXXG motif allows the formation of hydrogen bonds. Replacing Gly with other amino acids affects the interaction energy between helices.[27] A Leu zipper is also one of the lateral association domains for stabilizing transmembrane helices.[28] Also, hydrogen bonding between transmembrane helices involving strongly electronegative atoms has been found to stabilize the helix bundle. For example, one Val residue mutated to Asp in the fourth membrane span of cystic fibrosis transmembrane conductance regulator (CTFR) results in the formation of a hydrogen bond between Asp232 and Gln207 of the third membrane

span that stabilizes formation of a helical hairpin and affects the CFTR function in vivo.[29]

1.6.1 The two stage model for membrane protein folding

Alpha-helical membrane proteins are thought to typically fold according to a two-stage model initially proposed by Popot and Engelman. The two-stage model implies that individual stable helices form first in the membrane, and subsequently reassemble into a helix bundle (Figure 1.3).[30] Experimental evidence that bacteriorhodopsin fragments completely refold into a native structure clearly shows that bacteriorhodopsin supports a two-stage model. It has also proven to refold in lipid bilayers and the structure of refolded protein was compared to a crystal structure and is shown to be indistinguishable from that of native bacteriorhodopsin.[31] Furthermore, Mackenzie et al. calculated the free energy of transmembrane domain dimerization of the Glycophorin A, the major sialoglycoprotein from human red cell membranes that also supports the two-stage model.[32]

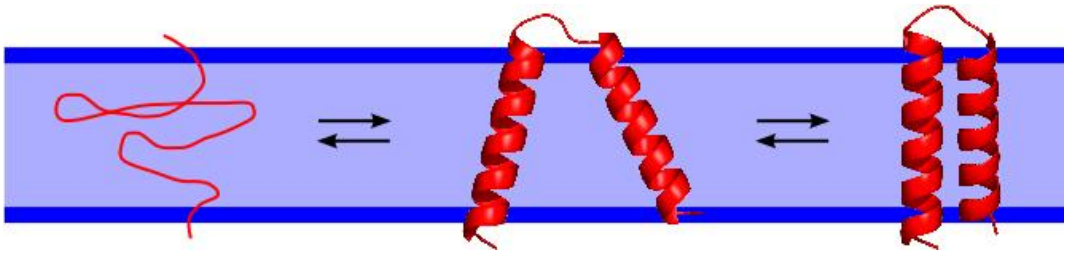

Figure 1.3. The two-stage model for alpha helical membrane protein folding suggested by Popot and Engelman.

Some alpha helical membrane proteins have been found to follow a folding scheme that is more complicated than the two-stage model. The glycerol facilitator from *E. coli* and the KcsA potassium channel are defined as a three-stage model due to the hydrophobic partitioning of short helices and extended polypeptides into the transbilayer region.[33] A three-stage model also applies when proteins are involved in ligand binding, insertion of peripheral domains, or the formation of quaternary structures.

In order to transform from a soluble state to a transmembrane configuration, a protein has to pass through the membrane interface and adopt a different conformation. The interaction between membrane and polypeptide plays an important role in membrane protein folding and insertion. Therefore, it is necessary to know the transfer free energy when the amino acid is partitioning into the membrane interface. Wimley et al. determined hydrophobicity scales for showing this free energy change when unfolded peptides partition from water to octanol.[34] They also measured the free energy change for model peptides partitioning from water to the membrane interfacial region of 1-palmitoyl-2-oleoyl-sn-glycero-3-phosphocholine (POPC) bilayers.[35]

1.7 Methods Used to Study Protein Folding

Since there has been intense interest in protein folding in the past, various new experimental and theoretical approaches have been applied to the protein folding problem. In particular, methods from structural biology, including NMR and X-ray crystallography, as well as computational methods enhance the understanding of fundamental questions on a molecular level. Time resolved information can be obtained from stopped-flow CD and fluorescence measurements. Stopped-flow CD has been

extensively used to examine the properties of the early intermediates in protein folding. Radfold et al. showed the study of the refolding of hen egg white lysozyme using a combined method of stopped-flow CD and NMR, concluding that there is more than one folding pathway.[36] Elove et al. investigated the kinetics of protein folding for horse ferricytochrome c using stopped-flow methods including far-UV CD, near-UV CD, and tryptophan fluorescence.[37]

1.7.1 Nuclear Magnetic Resonance

NMR has been used for studies related to protein folding because it can deliver unique structural and dynamic information. In the vast majority of cases, NMR is used under equilibrium conditions. Nevertheless, it is possible to access parameters that may be relevant for folding. These experiments may use chemically or thermally denatured proteins, partially denatured proteins, or protein fragments. For example, Neri et al. found the structures of residual hydrophobic clusters of a urea-denatured protein using solution NMR.[38] Numerous NMR investigations also include the measurement of dynamics in folded proteins.[39] Additional work has aimed at applying real-time NMR to the study of protein folding. Band-selective optimized flip-angle short transient (SOFAST) 2D-NMR spectroscopy was developed by Schanda et al., which showed the conformational transition of α-lactalbumin from a molten globular to the native state.[40]

1.7.2 NMR parameters relevant to protein folding

1.7.2.1 Chemical shift

Chemical shift is a sensitive probe of molecular structure. The chemical shift of each nucleus depends on the electronic environment. In structural biology, chemical shifts are commonly used to predict regions of secondary structure in native and denatured states of proteins. A well known method for this purpose is the chemical shift index (CSI), which wasdeveloped by Wishart et al. based on chemical shift differences with respect to random coil values.[41]

The temperature dependence of amide proton chemical shifts correlates to the presence of hydrogen bonds. Using amide proton temperature coefficients, $\Delta\sigma_{HN}/\Delta T$, offers a simple way to confirm the existence of hydrogen bonds within a peptide or with surrounding solvents. In the well-defined secondary structures, amino acid residuesthat participate in intramolecular hydrogen bonds and are protected from solvent, show $\Delta\sigma_{HN}/\Delta T > -4.6$ ppb/K, whereas exposed amino acids typically show -6 to -10 ppb/K.[42]

1.7.2.2 Spin relaxation

Relaxation is the process by which the spin system returns to thermal equilibrium in the magnetic field. Typically, the process is classified into spin-lattice relaxation (T_1), which acts on population difference, and spin-spin relaxation (T2), which acts on coherence. Both relaxation processes are caused by local fluctuations of magnetic field, which are due to various interactions that are modulated by molecular motions.

Among those, most prominent interactions in liquid state NMR of proteins are dipole-dipole coupling and chemical shift anisotropy. Dipole-dipole coupling arises due to the interaction between the magnetic moment of a spin I and the magnetic dipole field created by the magnetic moment of a spin S. It is modulated by molecular motions because of its dependence on the angle of the distance vector between the two spins with the magnetic field. Chemical shift anisotropy relaxation of a nucleus is caused by a locally fluctuating magnetic field due to different molecular orientation of a molecule with anisotropic electron density relative to the external magnetic field.

Molecular motions are described by the spectral density

$$J(\omega) = \frac{2}{5}\left(\frac{\tau_c}{1+\omega^2 {\tau_c}^2} \right)$$

where ω is the angular frequency of spin precession and τ_c the correlation time for global motion.Relaxation rate constants depend on the spectral density. They can therefore be used as probes for molecular motions, both global and local.

In addition to causing auto-relaxation, dipolar interactions give rise to cross-relaxation effects. Cross-relaxation causes a change of magnetization of a spin I, when a second, coupled spin S is perturbed. This effect is known as the nuclear Overhauser effect (NOE).[43] The cross-relaxation rate is strongly dependent on the distance between the two spins. Therefore, in protein NMR, the NOE effect forms the basis for structure determination. Two types of NOE experiments are used, which are the steady-state NOE and transient NOE experiment. The steady-state NOE experiment measures the change

in peak intensity of the I spin under RF irradiation on the S spin. The transient NOE experiment inverts the S spin with a 180° pulse, and the magnetization is transferred to the I spin by cross-relaxation. The transient NOE experiment can be implemented as a 2D spectrum, where cross-peaks appear for correlated spins. This experiment is particularly well suited for protein structure determination, since it yields simultaneously all NOE correlations.

Specific NOEs are characteristic for the presence of secondary structures I proteins, even though ^{1}H-^{1}H NOE is not observed directly at the location of the hydrogen bond. Specifically, NOEs between $H^{\alpha}(i)$ and $H^{\beta}(i+3)$ [$d_{\alpha\beta}(i,i+3)$], as well as between $H^{\alpha}(i)$ and $H^{N}(i+4)$ [$d_{\alpha N}(i,i+4)$] are indicative of α-helix structure. NOEs observed between $H^{\alpha}(i)$ and $H^{\alpha}(j)$ [$dH^{\alpha}H^{\alpha}(i,j)$], $H^{N}(i)$ and $H^{N}(j)$ [$dH^{N}H^{N}(i,j)$], and $H^{\alpha}(i)$ and $H^{N}(j)$ [$dH^{\alpha}H^{N}(i,j)$] are characteristic of the presence of anti-parallel β-sheet structures, and NOEs between $H^{N}(i)$ and $H^{N}(j)$ [$dH^{N}H^{N}(i,j)$] and between $H^{\alpha}(i)$ and $H^{N}(j)$ $dH^{\alpha}H^{N}(i,j)$ for parallel β-sheet structures.

Cross-relaxation also depends strongly on molecular dynamics. In the fast motion limit ($\omega_0\tau_c << 1$), we expect to see positive NOE enhancement due to $W_2 > W_0$. ($(W_2 - W_0)$ defines the cross-relaxation rate constant, W_2 and W_0 indicate the relaxation pathways between the αα and ββ states and between the αβ and βα states shown in Figure 1.4.) In contrast, in the slow motion limit ($\omega_0\tau_c >> 1$), the NOE will become negative due to $W_0 > W_2$.

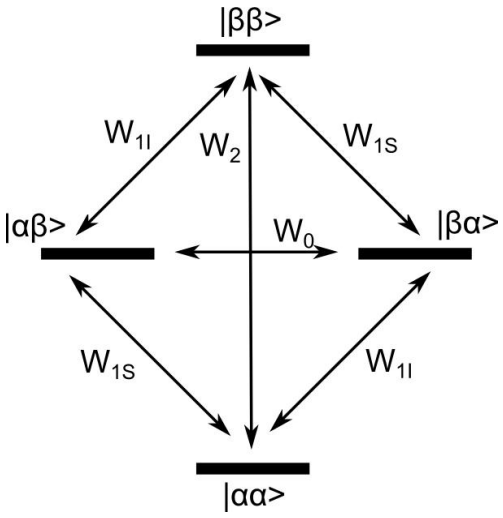

Figure 1.4. Energy levels in a two-spin-1/2 system with transition rates. α and β represent the states with magnetic quantum number of +1/2 and -1/2 of the I and S spins. W_{1I} and W_{1S} are the transitions, where the I and S spin are flipped, respectively. W_2 ("flip-flip") and W_0 ("flip-flop") involve both spins simultaneously.

Due to their dependence on molecular motions, auto-and cross-relaxation rate constants contain information on the dynamics of individual moieties in proteins. For example, Kay et al. developed the pulse sequence that allows measurements of heteronuclear NOE, spin-lattice (T1), and spin-spin (T2) ^{15}N or ^{13}C relaxation times.[44] They applied the pulse sequence to study the backbone dynamics of staphylococcal nuclease (S. Nase) complexed with thymidine 3',5'-bisphosphate and Ca^{2+}. In order to employ this sequence, it is necessary to uniformly label the protein with a stable isotope. Through the NMR measurement, T_1, T_2, and NOE values were obtained for each residue from the protein, and the order parameter (S) was calculated from determined T1 values.

In another example, Volkman et al. characterized the motions of NtrC in three functional states which are unphosphorylated (inactive), phosphorylated (active), and a partially active mutant indicative of exchange between inactive and active conformations.[45] They measured three relaxation parameters including rate constants for T_1 and T_2 for backbone amide nitrogen and ^{1}H-^{15}N NOE of the regulatory domain of NtrC in different functional states, which enabled them to extract order parameters. Spin relaxation methods can also be used to study the side-chain dynamics.[46-47] Muhandiram et al. investigated a new method to measure relaxation properties of deuterated methyl groups, and applied the method to the C-terminal SH2 domain from phospholipase $C_{\gamma 1}$ protein, which was uniformly ^{13}C labeled and fractionally deuterated.[46] By measuring ^{2}H longitudinal and transverse relaxation rates, order parameters that characterize the degree of spatial restriction of the motions and correlation times that describe their rates can be obtained.

1.7.2.3 Amide proton exchange

Amide proton exchange, is observed using NMR to confirm the secondary structure present in the peptide.[48-50] Generally, atoms that exchange slowly are from folded proteins and are involved in hydrogen bonding in the core, and atoms that exchange quickly are exposed to solvent. Slow exchange can be measured by proton/deuterium exchange, and fast exchange rates are accessed using 2D exchange spectroscopy (EXSY).[51]

1.8 Using Model Peptides to Study Protein Folding

Alongside the instrumental techniques, chemical and biochemical approaches can be used to aid in understanding protein folding. Synthesized peptides can be used as simplified models that exhibit many of the features and complexities of proteins. In general, protein structure and folding is determined by the competition between hydrogen bond formation, solvent effect, hydrophobic interaction, and salt bridge formation determines protein stability and folding.[52] Although peptides do not typically form tertiary structure, many of these interactions are still present, permitting the use of peptides as simplified models for the behavior of proteins. Cochran et al. synthesized ß-hairpin stabilized peptides and investigated the origin of their stability pointing out the importance of cross-strand tryptophan interactions.[53] Furthermore, by genetically engineering the peptide or protein sequence, one can study the role of an individual side chain in the folding and the stability of a protein.[54-58] Bellapadrona et al. compared the stability of the dodecameric Listeria monocytogenes Dps with the Listeria innocua protein mutating two amino acids from Lys 114 to Gln and from Asp 126 to Asn. This mutation caused protonation of Asp 126, and therefore removed the salt-bridge between Lys 114 and Asp 126 characteristic of L. innocua Dps.[58] In another example, an in-vitro peptide model for the folding of a nascent polypeptide chain in vivo has been studied in the chymotrypsin inhibitor 2 system.[59] A series of peptides which have increasing length from the N-terminus were structurally characterized by CD and NMR spectroscopy to determine folding propensities. As a result, higher populations of folded conformations were detected in the longer peptides. Wu et al. showed that small fragments of

cytochrome c can undergo spontaneous noncovalent association to form subdomains with native-like secondary and tertiary structural features.[60] This indicates that dissection to peptide fragment and reassembly can be a general method to study protein folding.

Unlike full-length proteins, it is common that secondary structure elements are less well-defined in peptides, since short peptides typically exhibit a large amount of conformational flexibility.[61] Non-aqueous solvents can be used to induce secondary structure formation, even though these solvents are further removed from physiological conditions. Various peptide fragments have been studied in different organic solvents. Dmitriev et al. solved the structure of the membrane domain of subunit b of *E. coli* F0F1 ATP synthase using a membrane mimetic solvent mixture which is a 4:4:1 ratio of chloroform, methanol, and water. Reddy et al. used a TFE solvent to find the structure of fragments of the alpha-factor receptor protein.[62] Those peptide fragments retained native-like secondary structures in the applied solvent systems. Klivanov et al. even showed that enzyme activities can be improved by replacing water-only environments with anhydrous organic solvents.[63]

1.9 Peptides Used in This Work

Three model peptides were chosen to examine driving forces that influence the secondary and tertiary structure formations. Since different systems may require different driving forces to form the structures, various types of peptides, including membrane protein fragments, as well as water soluble model peptides were employed.

1.9.1 Disulfide bond forming protein (DsbB)

DsbB is an alpha-helical membrane protein, which was chosen here to examine the two stage model of membrane protein folding. In *E.coli*, disulfide bond formation in proteins exported from the cytoplasm is catalyzed by two proteins DsbA and DsbB.[64] DsbA is the disulfide bond introducing enzyme, which catalyzes the disulfide bond formation. The function of DsbB is to re-oxidize the reduced form of DsbA. DsbB is an integral membrane protein, which spans the cytoplasmic membrane four times and contains a membrane embedded quinone molecules representing the active site of the enzyme. Inaba et al. determined the crystal structure of the DsbB-DsbA complex at 3.7 Å resolution,[16] and later refined it and compared it with the structure of a DsbB-Fab complex at 3.4 Å resolution.[65] Shortly afterward, Zhou et al. determined the solution NMR structure of DsbB.[26]

1.9.2 BBA5

BBA5 is an artificial peptide designed to exhibit a β-haripin, β-turn, and α-helix structure in water.[66] Because of its well-defined secondary structures, BBA5 represents an ideal model to test the stability of secondary structures. In the ß-hairpin sequence (Tyr1—Phe8), a D-proline provides a structural nucleation element, and several hydrophobic residues were employed to stabilize the structure through hydrophobic interactions. The BBA5 structure was previously determined by NMR, and the motif is particularly interesting because it forms a tertiary contact between the β-hairpin segment and α-helix segment (Arg10—Gly23).[66] Its globular structure is stabilized by the hydrophobic core cluster constructed by Tyr1, Val3, Tyr6, and Phe8 from the hairpin

segment and Leu14, Leu17, and Leu18 from the helix segment. Using this peptide, we examined the solvent effect on peptide structure using NMR and MD simulations.

1.9.3 Tryptophan zipper peptide

Tryptophan zipper peptides (trpzip 1-4) exhibit well folded ß-hairpin structures with strong cross-strand interactions. Trpzip peptides were designed by Cochran et al. and have been shown by NMR spectroscopy to adopt ß-hairpin conformations in an aqueous solution.[53] The same authors also examined the thermal unfolding of trpzip peptides with CD spectroscopy, and found the main stabilization factor for these peptides was resulted from cross-strand tryptophan interactions. Trpzip4 is triple mutated for the stable ß-hairpin structure, and it is most studied ß-hairpin peptide with 16 amino acid residues. Trpzip4 is more stable than other trpzip peptides, and the thermal denaturation curve of trpzip4 is much more cooperative than the wild type gb1 peptide. Among trpzip 1-4, we chose trpzip4 as a model system for thermal denaturation.

CHAPTER II

FOLDING DETERMINANTS OF DISULFIDE BOND FORMING PROTEIN B EXPLORED BY SOLUTION NMR SPECTROSCOPY*

2.1 Introduction

The majority of transmembrane proteins are comprised of a bundle of helices, which are stabilized due to the absence of solvent hydrogen bonding in the membrane. Even with knowledge of the native structure of a protein, the mechanism for its folding is however not predictable from basic principles.[67] A two-stage model for the folding of α-helical membrane proteins postulates that individual helices form first, and are subsequently packed against each other.[30] This model has been based on theoretical calculations of the gain of free energy upon helix formation.[68] The recent advent of membrane protein structures at atomic resolution may suggest that the tools of structural biology can also be applied to obtain more detailed information about these processes in protein folding. For example, the assembly of bacteriorhodopsin from fragments has been verified by X-ray crystallography and supports the two-stage model for membrane protein folding.[31] Since the methods with high structural fidelity – such as X-ray crystallography and nuclear magnetic resonance (NMR) – typically call for extended data acquisition time, they do however not permit direct measurements of the protein folding process.

---

* Reprinted from *Proteins,* 79, Hwang S. and Hilty C. 'Folding Determinants of Disulfide Bond Forming Protein B Explored by Solution NMR Spectroscopy' pp 1365-375, 2011 with the permission of Wiley-Liss, Inc. a subsidiary of John Wiley & Sons, Inc.

Nevertheless, these methods can be used to study conformations along the folding pathway, if such conformations are stable for the duration of the measurement time. Typical methods for stabilizing unfolded or partially folded conformations include thermal denaturation, as well as chemical denaturation using various solvents. Using solution state NMR, the structures of residual hydrophobic clusters in proteins denatured using urea or guanidine hydrochloride have been determined for soluble proteins,[38] as well as for β-barrel membrane proteins.[69] Further along on the folding pathway, it is of interest to also examine the formation of individual secondary structure elements. Peptide fragments from membrane proteins have been studied in organic solvents, foremost trifluoroethanol (TFE),[62,70-72] chloroform/methanol[73-75], and dimethyl sulfoxide (DMSO),[76-79] as well as in detergent micelles.[80-81] For the α-helical membrane protein bacteriorhodopsin, NMR spectroscopy indicated that the protein retained considerable secondary structure in chloroform/methanol solution and also retained some elements of native tertiary structure.[82-84] Further, NMR structures of isolated transmembrane peptides derived from bacteriorhodopsin[74,81,85] in a chloroform/methanol mixture, as well as in aqueous solutions of SDS micelles, allowed comparison of side chain rotamers of a two helix peptide fragment with single helix fragments.[75] Those peptide fragments retained native-like secondary structure in the applied solvent systems. The structures of the individual transmembrane helices of bacteriorhodopsin determined in dimethyl sulfoxide (DMSO) have been shown to superimpose well with the structure of full-length protein.[77] Other α-helical membrane proteins that have been studied in a partially denatured state include the potassium channel KcsA, which separated from tetrameric

structure into the monomeric two helix subunit when solubilized in 50% trifluoroethanol (TFE) containing 1% trifluoroacetic acid.[86] To investigate secondary structure formation, the structure and stability of polypeptide fragments taken from full-length protein sequences have further been studied using a variety of techniques, including, for example, circular dichroism (CD) spectroscopy and NMR,[70,80,87] sometimes also accompanied by site-directed mutagenesis of key amino acid residues.[88] A systematic structural study that aims at the determinants for secondary structure formation in transmembrane helices is however at present lacking. As a step towards this goal, we have determined NMR structures of two individual transmembrane helices taken from an α-helical membrane protein, the disulfide bond forming protein B (DsbB). DsbB is a protein from the inner membrane of *E. coli*, with a topology of four membrane spanning helices (Fig. 2.1). The function of DsbB lies in the regeneration of the periplasmic protein DsbA, which is involved in disulfide bond formation. For this purpose, DsbB contains an embedded oxidant, the ubiquinone molecule. DsbB presents an ideal target for the study of transmembrane helix assembly, since several structures of the full-length protein are available. X-ray crystal structures have been determined initially in complex with DsbA at 3.7 Å resolution,[16] and later refined and compared with a structure of a DsbB-Fab complex at 3.4 Å resolution.[65] Further, an NMR structure of DsbB has been determined in dodecyl phosphocholine micelles.[26] Here, we compare the structural features of isolated peptides corresponding to transmembrane helices 2 and 3, which contain a large contact surface, to full-length DsbB in order to determine the individual propensity of these transmembrane peptides to form native structure prior to assembly.

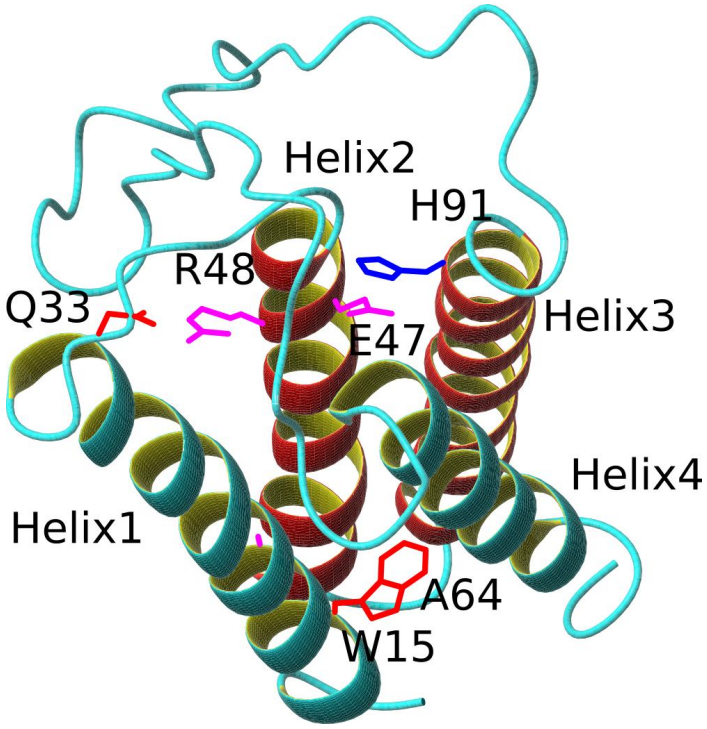

Figure 2.1. Rendering of the X-ray crystal structure of DsbB in the DsbB-Fab complex (from PDB ID 2ZUQ).[89] Helices 2 and 3 are colored red. Side-chains for the amino acids involved in salt bridges and hydrogen bonds in these helices are drawn (W15 – A64; Q33 – R48; E47 – H91).

2.2 Experimental Methods

2.2.1 Sample preparation

Peptides corresponding to transmembrane helices 2 and 3 of full-length DsbB, in the following referred to as DsbB2 and DsbB3, were synthesized commercially using solid phase synthesis (Anaspec, Fremont, CA). Peptide sequences were H-Lys-Lys-Leu-Ser-Ile-Tyr-Glu-Arg-Val-Ala-Leu-Phe-Gly-Val-Leu-Gly-Ala-Ala-Leu-Ile-Gly-Ala-Leu-

Ala-Pro-Lys-Lys-OH (DsbB2) and H-Lys-Lys-Arg-Tyr-Val-Ala-Met-Val-Ile-Trp-Leu-Tyr-Ser-Ala-Phe-Arg-Gly-Val-Gln-Leu-Thr-Tyr-Glu-His-Thr-Met-Leu-Gln-Lys-Lys-OH (DsbB3). The lysine residues at the N- and C-termini were added to increase solubility during purification. Samples in 100% trifluoroethanol (TFE) or 70% TFE were prepared by dissolving the DsbB peptides in 300 µl 2,2,2-trifluoroethanol-1-D_2 (Cambridge Isotope Laboratories, Andover, MA), or in 210 µl 2,2,2-trifluoroethanol-1-D_2 mixed with 90 µl sodium phosphate buffer (30 mM PO_4, pH 6.5, 90% H_2O, 10% D_2O). For the sample in dodecyl phosphocholine (DPC), lyophilized peptide was added to phosphate buffer containing 80 mM DPC-D_{38} (Cambridge Isotopes Laboratories, Andover, MA) and mixed by vortexing. The sample in sodium dodecyl sulfate (SDS) was prepared in an identical way, using 80 mM SDS-d_{25} (Cambridge Isotope Laboratories, Andover, MA). Peptide concentrations for NMR spectroscopy were 1 mM. For the titrations with spin labels, 16-doxyl stearic acid or Gd-DTPA (N,N-Bis(2-[bis(carboxymethyl)amino]ethyl)glycine gadolinium complex) (Sigma-Aldrich, St. Louis, MO) was added to the samples to a final concentration of 1 mM and 4 mM, respectively. For CD spectroscopy, peptide samples were diluted to final concentrations between 40 and 70 µM. Exact concentrations were determined by UV-Vis spectrophotometry using the calculated molar absorptivities at 280 nm of 1615 M^{-1} cm^{-1} and 9970 M^{-1} cm^{-1} for DsbB2 and DsbB3, respectively. In the DPC and SDS micelle samples used for CD spectroscopy, detergent concentration was 12 mM and 15 mM, respectively.

2.2.2 NMR spectroscopy and structure calculation

Two-dimensional DQF-COSY,[90] TOCSY,[91] and NOESY[92] spectra were recorded of all samples. For the NOESY spectra, mixing times of 200 ms and 300 ms were used for TFE samples, and 50 ms and 100 ms for micelle samples. TOCSY experiments used the MLEV-17[93] scheme with mixing times of 60 ms and 100 ms for TFE samples, and of 20 ms and 60 ms for micelle samples. All NMR experiments were performed on a Varian 600 MHz spectrometer using a 5 mm HCN probe with z-gradient. The NOESY experiments (100 ms mixing time) with the DPC sample were performed on a Bruker 800 MHz spectrometer using a 5 mm TXI cryo probe with z-gradient. Samples in TFE were measured at 298 K, and micelle samples were measured at 313 K. The measurement temperature in micelles was chosen to alleviate spin-relaxation due to slow molecular tumbling, and was identical to the measurement temperature that was used for the NMR structure of full-length protein.[26] TFE, on the other hand, exhibits low viscosity, and molecular tumbling is rapid in this solvent. Many NOEs would not be observable at the high temperature due to reduced cross-relaxation.[43] Therefore, a temperature of 298 K was chosen for the measurements in TFE. An external standard of sodium 2,2-dimethyl-2-silapentane-5-sulfonate (DSS) was used for ^{1}H chemical shift referencing. All of the NMR data were processed with NMR pipe[94] and analyzed with the CARA program.[95] Chemical shift assignments were obtained from TOCSY and NOESY spectra. Distance restraints for structure calculations were obtained from NOESY spectra.[96] Structures were calculated with the program CYANA,[12] using 100 randomized starting structures. The 20 conformers with the lowest target function values

were selected to represent the NMR structure. Figures were prepared with the program MOLMOL.[97]

2.2.3 Circular dichroism

CD spectra were acquired on a AVIV 26DS spectrometer. Data points were taken in steps of 1 nm between 190 and 260 nm, with 15 s integration time. The blanked CD signal Δm was converted to mean residue ellipticity,

$$\theta = \frac{\Delta m}{cN_{res}l} \tag{1}$$

where N_{res} is the number of amino acid residues in the peptide, c the peptide concentration and l the optical path length.

2.3 Results and Discussion

2.3.1 DsbB peptides in trifluoroethanol

CD spectra of the DsbB peptides were measured to determine the prevalent secondary structure elements in the solvents used. In all cases, the CD spectra of DsbB2 and DsbB3 show negative ellipticity at 208 nm and at 222 nm, characteristic of α-helical structures (Fig. 2.2).

A numeric value for the fractional helix content, p_h, of a peptide may be estimated using

$$p_h = \frac{\theta_{222\,nm(obs)} - \theta_{222\,nm(coil)}}{\theta_{222\,nm(helix)} - \theta_{222\,nm(coil)}} \tag{2}$$

where the θ is the mean residue ellipticity at the wavelength indicated, of the sample ($\theta_{222nm(obs)}$), a random coil reference ($\theta_{222nm(coil)}$= 640 deg cm^2 dmol^{-1}), and a helical reference ($\theta_{222nm(helix)}$ = [– 42,500 deg cm^2 dmol^{-1}] ·[1 – 3/N_{res}]).[43] At a temperature of 298 K, the helix content was estimated to lie between 49% (DsbB2 in 70% TFE) and 73% (DsbB2 in 100% TFE). A similar result was obtained at 313 K, where helix content was estimated to lie between 44% and 68%.

TOCSY spectra of DsbB2 and DsbB3 both in 100% TFE and in 70% TFE are well dispersed in the fingerprint region (Fig. 2.3), hinting at a well defined secondary structure. Complete chemical shift assignments could be obtained in both cases, as indicated in the figure. Medium range NOEs indicative of α-helical secondary structure were identified from NOESY spectra of the peptides (Fig. 2.4). Specifically, NOEs between H^{α}(i) and H^{β}(i+3) [$d_{\alpha\beta}$(i,i+3)], as well as between H^{α}(i) and H^{N}(i+4) [$d_{\alpha N}$(i,i+4)] were observed throughout the regions of the peptides that would be membrane embedded in the full-length protein. In the same region, a negative secondary shift of H^{α} [$\Delta\delta(H^{\alpha})$] was observed, which is also expected for α-helical structure.[40] The pattern of NOEs and secondary shifts are surprisingly similar when comparing the same peptide in 70% TFE and in 100% TFE. They indicate that both solvents are equally capable of stabilizing the transmembrane helices of DsbB.

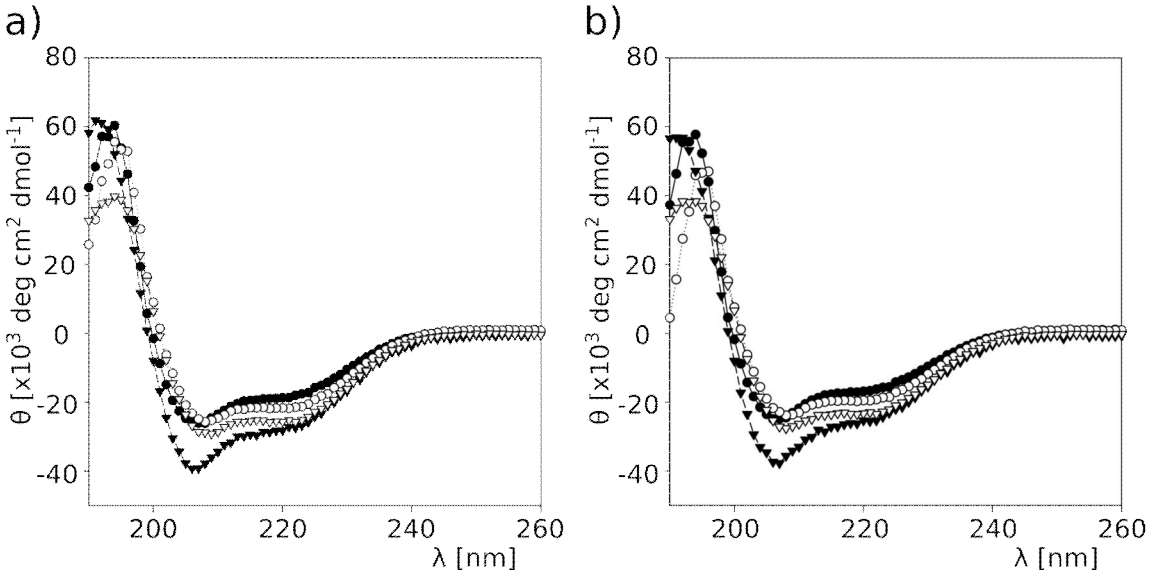

Figure 2.2. CD spectra of DsbB2 in 70% TFE / 30% water (—●—), DsbB3 in 70% TFE / 30% water (·····○·····), DsbB2 in 100% TFE (– – ▼ – – –) and DsbB3 in 100% TFE (— · ▽ · —) measured at a temperature of a) 298 K, b) 313 K.

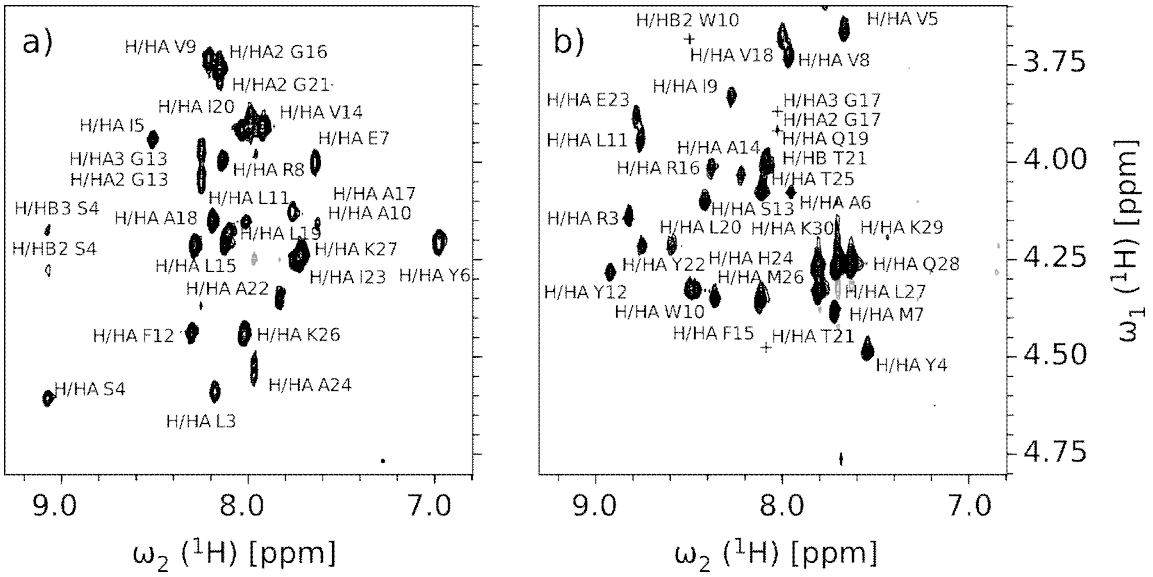

Figure 2.3. Fingerprint region of 2D TOCSY spectra of a) DsbB2 and b) DsbB3 peptides in 70% TFE / 30 % water mixture at T = 298 K.

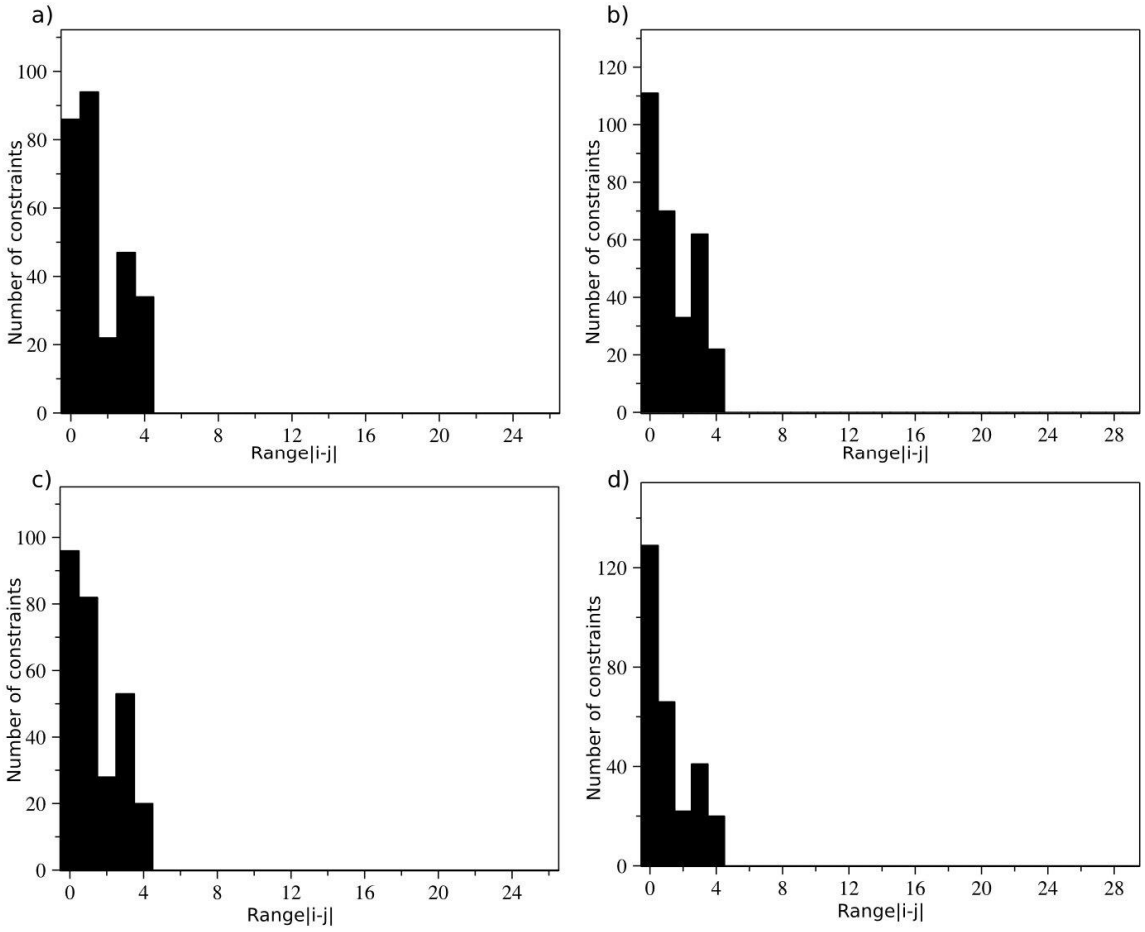

Figure 2.4. Histograms of the number of distance constraints *vs.* separation in residue number. a) DsbB2 in 70% TFE. b) DsbB3 in 70% TFE. c) DsbB2 in 100% TFE. d) DsbB3 in 100% TFE.

The observed medium-range NOE patterns reliably convey information about the secondary structure of the peptides.[96] Additionally, the NMR structures of both peptides were calculated using the observed NOEs as distance constraints (for statistics, see Fig. 2.5). The structures for the peptides in 100% TFE and in 70% TFE appear similar (Fig.

2.6). All of the structures contain well-defined α-helical secondary structure in the central part of the peptides. The terminal residues, including the lysine residues that were added to facilitate the solid phase synthesis are less well defined, as might be expected due to increased mobility of this part of the polypeptide.

In general, it would be expected that the peptides in organic solvent exhibit considerable flexibility. Conformational flexibility is indeed evident in the NMR data by coupling constants between H^{α} and H^{N} in the range of 6 – 8 Hz. This value is larger than the maximum of 5 Hz expected for a fully stable α-helical conformation. Similar observations have been made in other NMR structures of α-helical peptides.[80] Furthermore, the CD spectra indicate an α-helix content of 40 – 70%. When compared to the NMR structures, this observation may indicate the presence of a conformational exchange process, where the peptide occupies a non-helical conformation for a fraction of time.

2.3.2 Comparison of peptide structures to crystal and NMR structures of DsbB

Since the crystal- and NMR structures of full length DsbB are known, it is possible to compare the corresponding parts of these structures to the NMR structures of the peptides. From Fig. 2.6, it is apparent that in TFE, the α-helical structure comprises residues Ile 5 – Ile 20 for DsbB2 and Val 5 – Met 26 for DsbB3. This is in good agreement with the crystal structure, where helix 2 ranges from Ile 45 – Ile 60, and helix 3 from Val 72 – Met 93. Likewise, the backbone fold of the NMR structures of the peptides superimpose well with the crystal structure (bold line in Fig. 2.6). The

backbone RMSD between the mean structure of DsbB2 in 70% TFE and helix 2 (residues Ile 45 – Ile 60) in the crystal structure is 1.70 Å, and the backbone RMSD between the mean structure of DsbB3 in 70% TFE and helix 3 (residues Val 72 – Met 93) in the crystal structure is 1.56 Å. Superposition of all of the heavy atoms, including the side chains, yields a RMSD value; 3.23 Å for DsbB2 in 70% TFE and 2.78 Å for DsbB3 in 70% TFE. These deviations are smaller than the resolution of the crystal structure, which is reported at 3.4 Å [65] and 3.7 Å.[16] In order to assess local differences between crystal structure and NMR structure, local RMSD values for the crystal structure can further be calculated from the B-factors:[98]

$$RMSD = \sqrt{\frac{3B}{8\pi^2}} \tag{3}$$

For helix 2 and 3, these values are 1.96 ± 0.14 Å. By comparison, for the NMR structure, local RMSD values are 0.63 ± 0.21 Å for backbone heavy atoms (DsbB2, residues Ile 45 – Ile 60) and 1.08 ± 0.31 Å for backbone heavy atoms (DsbB3, residues Val 72 – Met 93). Fig. 2.7 shows the thus calculated RMSD values for the x-ray structure, as well as for the NMR structures of the individual helices. These values are compared to the RMSD between the NMR and x-ray structures calculated for backbone heavy atoms. The average backbone RMSD values between the NMR structures of the peptides and the X-ray crystal structure are below 2 Å, and indicate good agreement between the structures.

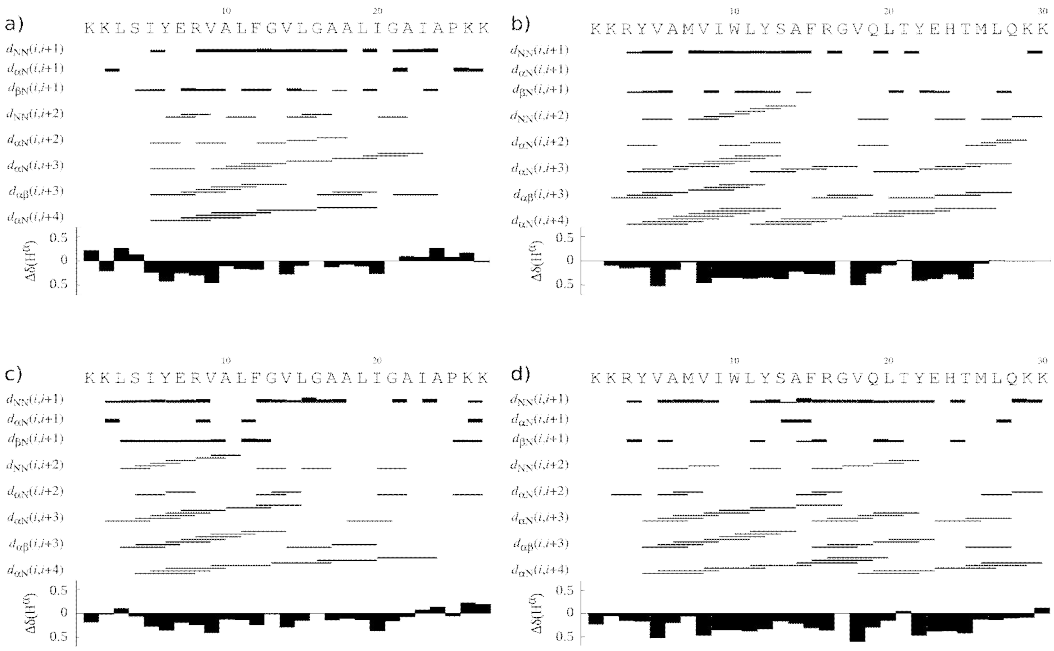

Figure 2.5. Short-and medium range NOEs taken from NOESY spectra with 200 ms mixing time, and $^{1}H^{\alpha}$ chemical shift deviations from random coil values, $\Delta\delta(H^{\alpha})$, for DsbB peptides in TFE solvents. a) DsbB2 in 70% TFE. b) DsbB3 in 70% TFE. c) DsbB2 in 100% TFE. d) DsbB3 in 100% TFE.

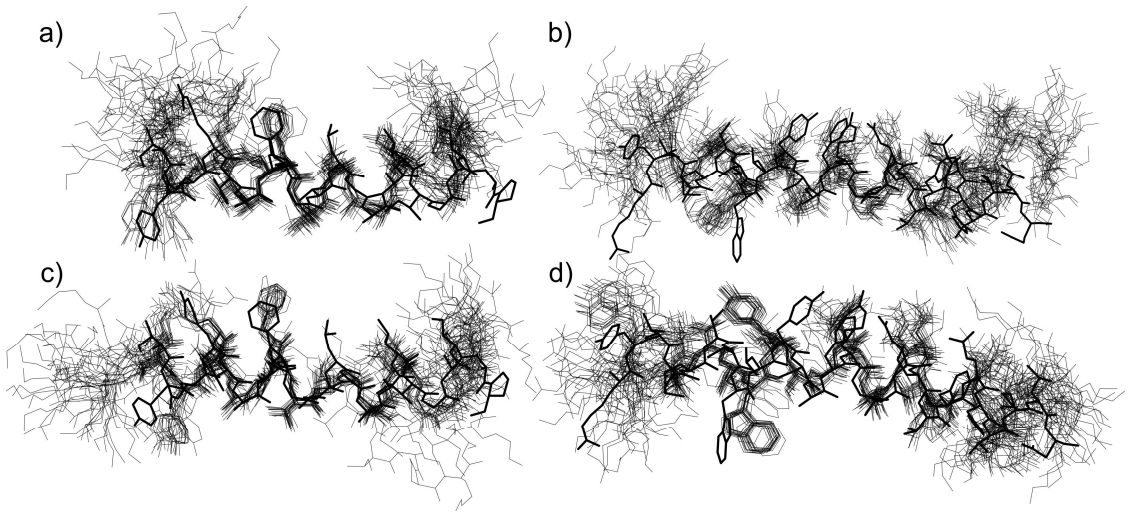

Figure 2.6. NMR structures of the DsbB peptides, represented by bundles of 20 conformers shown using thin lines. The corresponding segments of the X-ray crystal structure from DsbB-Fab complex are overlaid using thick lines. a) DsbB2 in 70% TFE (fit range I5-I20; backbone RMSD: 0.45 Å, heavy atom RMSD: 1.08 Å). b) DsbB3 in 70% TFE (fit range V5-M26; backbone RMSD: 0.93 Å, heavy RMSD: 1.44 Å). c) DsbB2 in 100% TFE (fit range I5-I20; backbone RMSD: 0.60 Å, heavy RMSD: 1.21 Å). d) DsbB3 in 100% TFE (fit range V5-M26; backbone RMSD: 0.70 Å, heavy atom RMSD: 1.26 Å).

The structures of the DsbB peptides were also compared to the NMR structure of the full-length protein.[26] The extent of α-helical secondary structure coincides, spanning Ile 5 - Ile 20 for the DsbB2 peptide compared to Ile 45 – Ile 60 for full-length DsbB, and Val 5 – Met 26 for the DsbB3 peptide compared to Val 72 – Met 93 for full-length DsbB. Backbone RMSDs between the peptide structures and the NMR structure of full-length protein are between 1.67 Å and 2.0 Å. Since the overall structures of the peptides

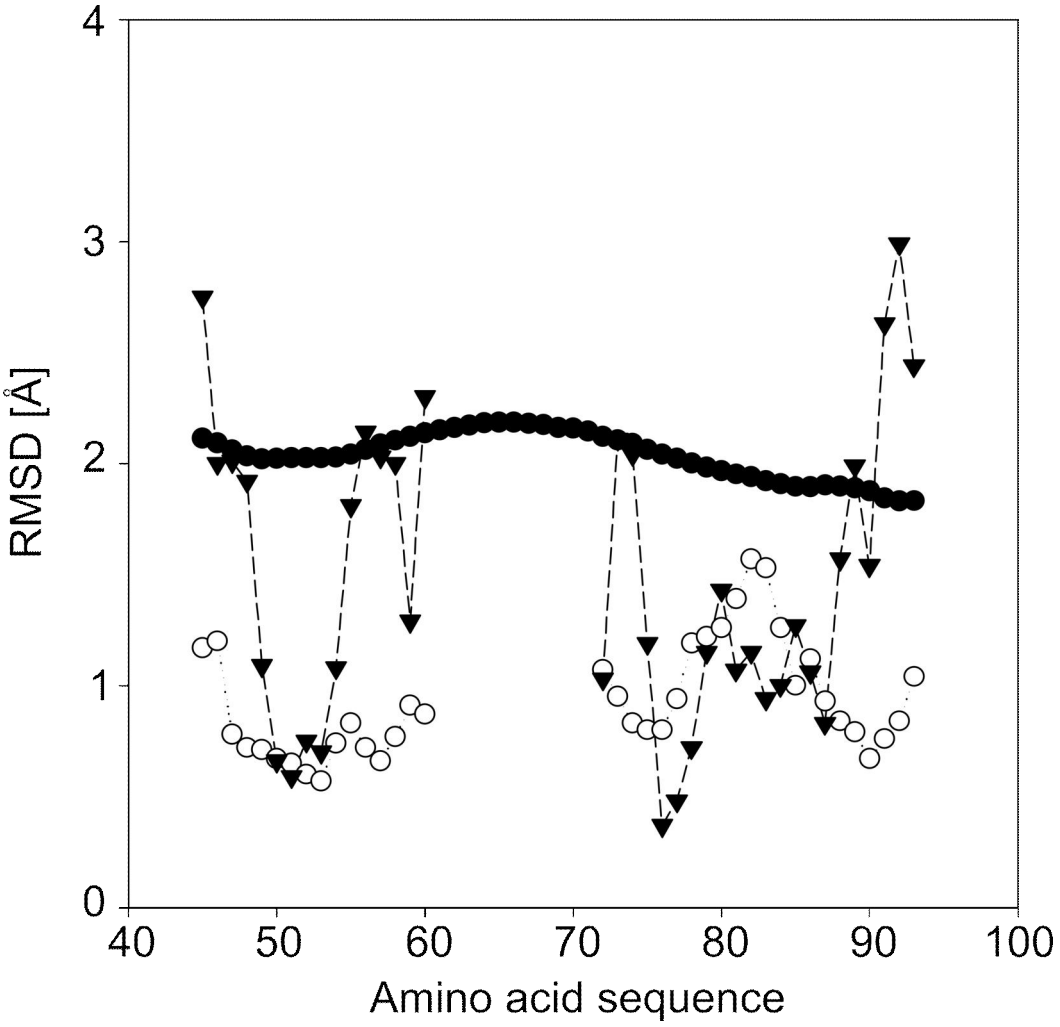

Figure 2.7. Average backbone heavy atom RMSD values obtained by fitting the 20 conformers of the NMR structures in 70% TFE to the mean NMR structure from 20 conformers with lowest target function values (·····○·····). RMSD values of X-ray structure calculated using equation 3 from B-factors in PDB ID 2ZUQ of the crystal structure from DsbB-Fab complex (——●——).[99] B-factors for each residue were calculated as average from backbone heavy atoms. Average backbone heavy atom RMSD calculated between the mean NMR structure of the peptides and the X-ray structure (– – –▼– – –).

superimpose well with the structures of full-length DsbB, it may be interesting to undertake a more detailed comparison of side chain conformation, even if structural differences are near the limit of resolution. In particular for the crystal structure of DsbB-Fab complex, which has the higher resolution, side chain structure at least for bulky amino acids in the transmembrane region was observable.[65]

In Fig. 2.8, a comparison of individual side-chain orientations between the NMR structures of the DsbB peptides in 70% TFE and two of the X-ray crystal structures is shown. The structures in 70% TFE were chosen because these contain a larger number of NOE distance constraints to side-chains than the structures in 100% TFE. For each image of a side chain, the backbone structures were superimposed over a range starting two amino acid residues prior to and ending two amino acid residues after the residue of interest. None of the side chain atoms were included in the fit. This local comparison removes any influence of global structural differences that may arise because the structures have been obtained by different methods. The NMR structure, which is based on NOE distance constraints, would be expected to most faithfully reproduce local structure, whereby the structure obtained is an average over conformers present in solution. Differences in side-chain conformation that are observed in Fig. 2.8 should be interpreted based on these considerations. Further, the number of NOE distance constraints that are available for each side chain (shown with dashed lines) indicates the level of support for the respective structure. It can be seen that most side chains, including most of the hydrophobic amino acids (Val 49, Ala 50, Leu 51, Phe 52, Val 54, Leu 55, Ala 57, Ala 58, Leu 59, Ile 60 in the helix 2, Val 72, Ala 73, Val 75, Ile 76, Leu

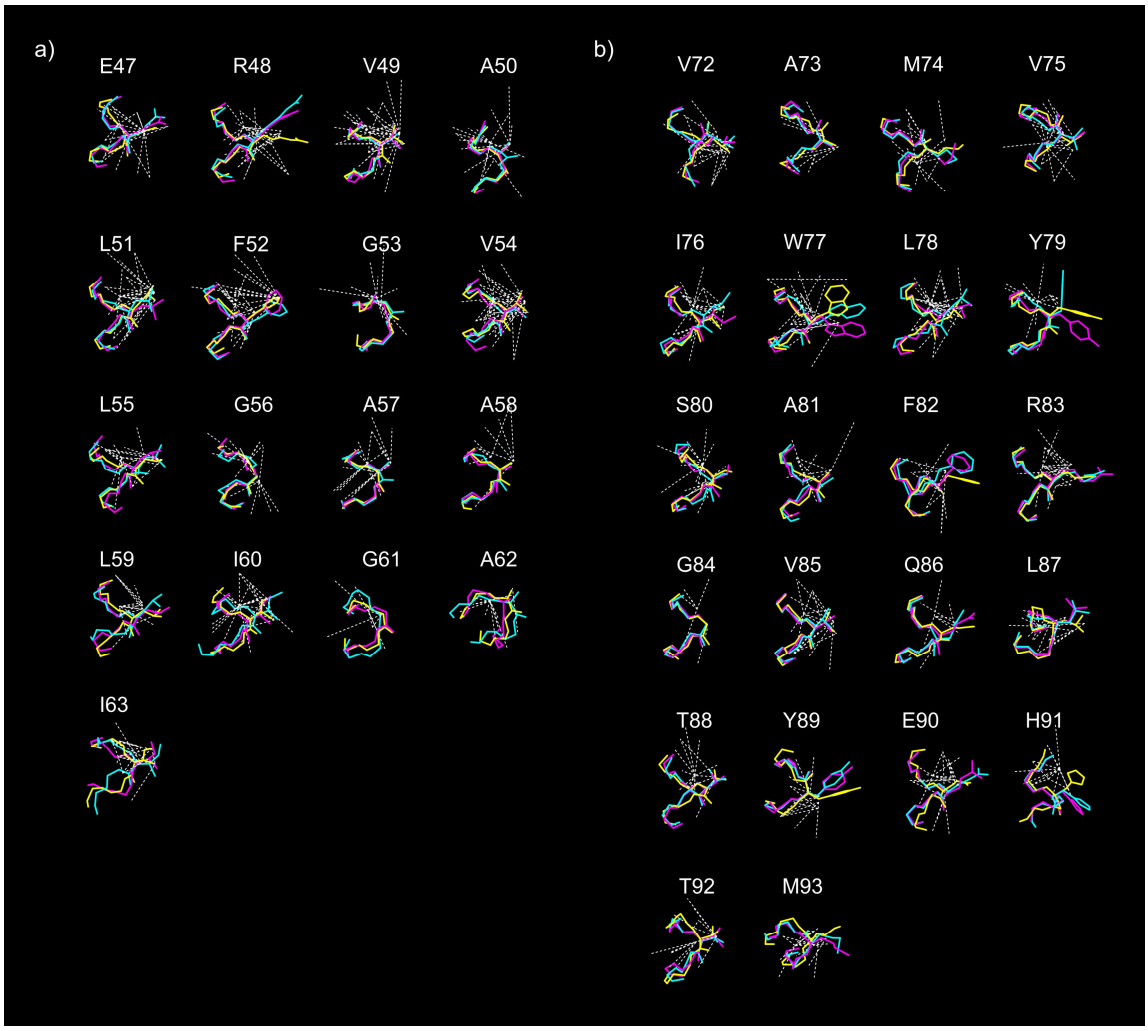

Figure 2.8. Overlay of side-chain orientation in a) DsbB2 or b) DsbB3 peptide in 70% TFE (yellow); DsbB from DsbB-Fab complex (magenta); and DsbB from DsbB-DsbA complex (cyan). Overlaid structures were fitted for backbone heavy atoms in the range starting two amino acids prior to and ending two amino acids after the side-chain shown. NOE distance constraints to the backbone and side-chain shown are indicated with dashed lines.

78, Ala 81, Val 85, and Leu 87 in the helix 3) superimpose well with the crystal structures. Some aromatic amino acids (Tyr 79, Phe 82, and Tyr 89 of helix 3) are lacking NOE constraints in the aromatic ring, and do not lend themselves to comparison of ring orientation.

The observation that side-chain structure coincides with the X-ray crystal structure may be less surprising for amino acids with short side-chain such as alanine, but appears non-trivial for longer side-chains. Similar side-chain conformations may indicate that TFE does not significantly interfere with the intramolecular hydrophobic interaction, in agreement with findings based on FT-IR spectroscopy, which show that TFE appears to interact only weakly with nonpolar residues.[100] Some of the polar side chains (Glu 47 of helix 2 and Ser 80, Gln 86, Thr 88, Thr 92 of helix 3) also coincide well with the crystal structure. On the other hand, the orientations of the side chains of Arg 48 and His 91 are different, even though those also contain significant NOE support in the NMR structures of the peptides. Interestingly, in the crystal structure of full length DsbB-Fab and DsbB-DsbA complex, these side-chains are involved in tertiary interactions. Specifically, His 91 of helix 3 is salt bridged to Glu 47 of helix 2, and Arg 48 of helix 2 is hydrogen bonded to Gln 33 of helix 1 (Fig. 2.1). It appears reasonable to conclude that these polar side-chains would re-orient upon helix packing, in order to form the needed tertiary interactions that stabilize the global fold of DsbB.

2.3.3 DsbB peptides in micelles

Even though the TFE solvents are capable of solubilizing the DsbB transmembrane peptides, their physical properties are different from those of the natural lipid bilayer. More realistic solvents for membrane proteins that are also compatible with solution state NMR spectroscopy are aqueous detergent micelle solutions. CD spectra of the DsbB peptides in SDS and DPC micelle solutions are shown in Fig. 2.10. Based on this data, the calculated helix content at 298 K lays in-between 23% (DsbB2 in DPC) and 47% (DsbB3 in DPC). Upon increasing the temperature to 313 K, the helix content remains between 21% and 33%. Clearly, all of the peptides showed helical structure under the conditions used for CD spectroscopy, albeit at a reduced level when compared to the peptides in the TFE solvents.

NMR spectra of the peptides in micelles are shown in Fig. 2.9. Comparing to Fig. 2.4, it is apparent that the amide proton chemical shift dispersion is lower than for the measurements in TFE. Nevertheless, it was possible to obtain chemical shift assignments for DsbB2 in DPC, the second half of DsbB3 in DPC, and DsbB3 in SDS micelles. Of the peptide samples in detergent micelles, only DsbB2 in DPC and DsbB3 in SDS yielded medium range NOEs characteristic for α-helical secondary structure (see Fig. 2.11). On the other hand, the number of intraresidual NOEs in micelle samples is comparable to those of the samples in TFE. For example, DsbB2 in 70% TFE, 100% TFE, and DPC micelles gave rise to 86, 96, and 75 intraresidual NOEs, respectively. DsbB3 in 70% TFE, 100% TFE, and SDS micelles gave rise to 112, 128, and 102 intraresidual NOEs, respectively (see Fig. 2.4 and 2.9).

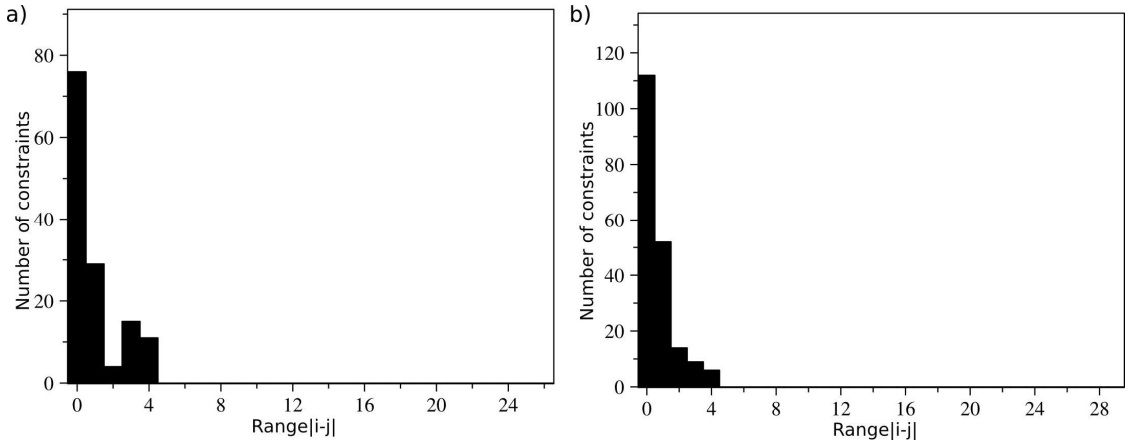

Figure 2.9. Histograms of the number of distance constraints *vs.* separation in residue number. a) DsbB2 in DPC. b) DsbB3 in sodium docecyl sulfate (SDS).

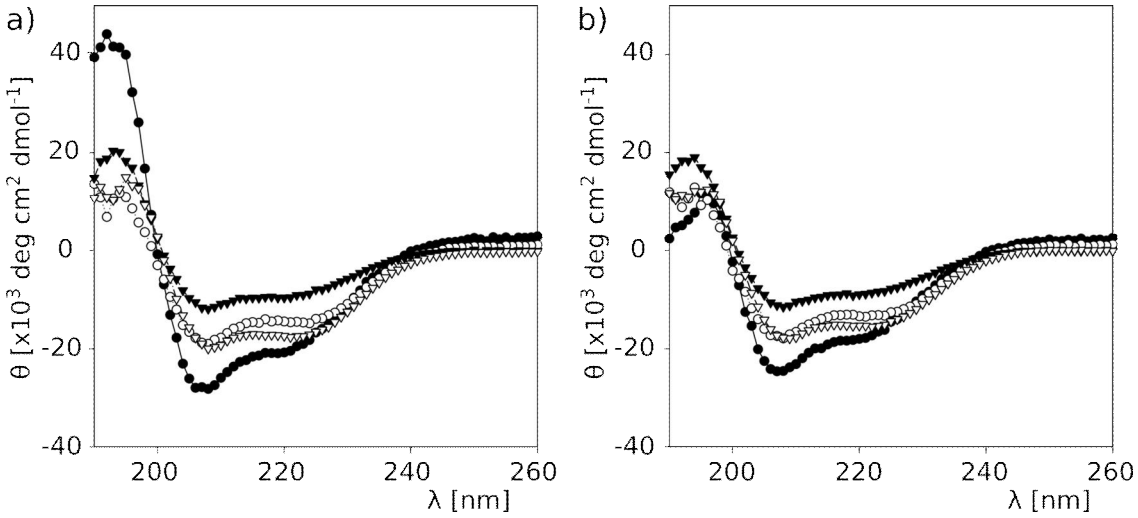

Figure 2.10. CD spectra of DsbB2 in SDS micelles (—●—), DsbB2 in DPC micelles (– –▼– –), DsbB3 in DPC micelles (·····○·····) and DsbB3 in SDS micelles (—·▽·—) measured at a temperature of a) 298 K, b) 313 K.

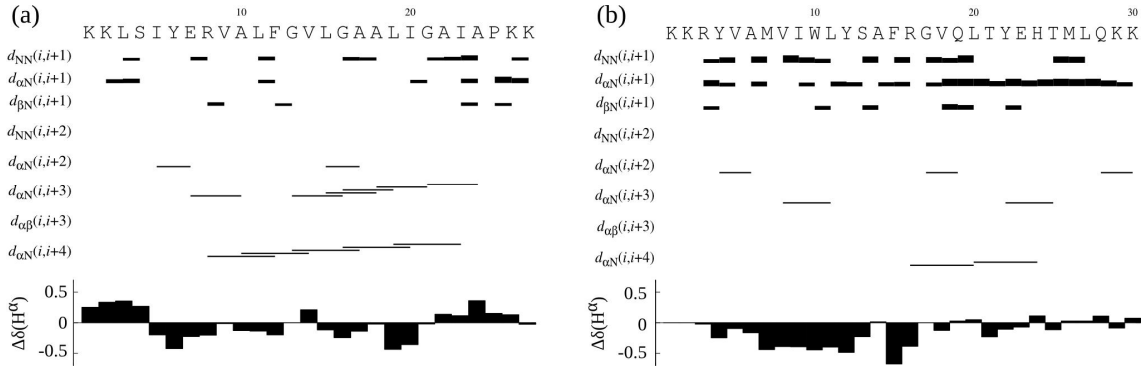

Figure 2.11. Short-and medium range NOEs taken from NOESY spectra with 100 ms mixing time, and $^{1}H^{\alpha}$ chemical shift deviations from random coil values, $\Delta\delta(H^{\alpha})$, for DsbB peptides in micelles. a) DsbB2 in DPC. b) DsbB3 in SDS.

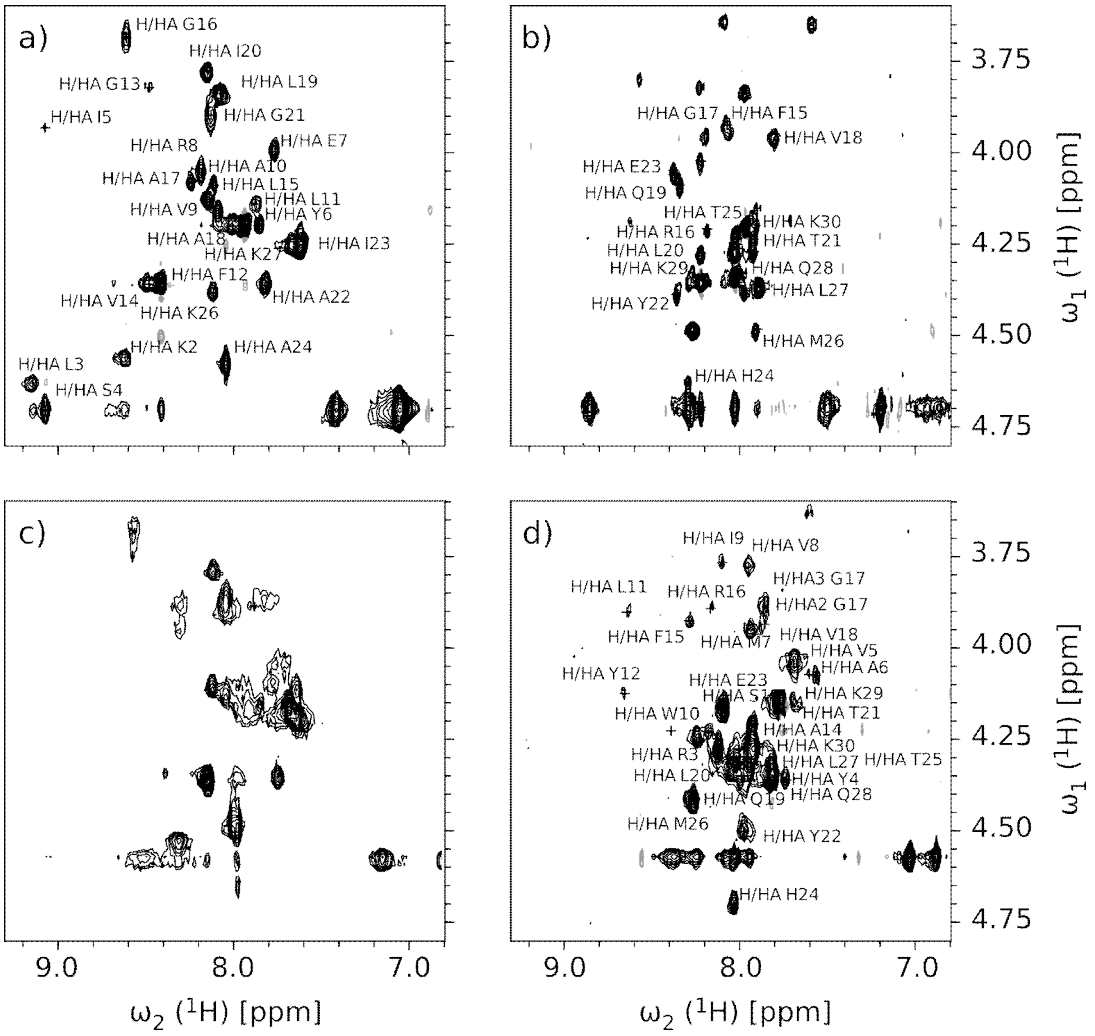

Figure 2.12. Fingerprint region of 2D TOCSY spectra of a) DsbB2 in DPC micelles, b) DsbB3 in DPC micelles, c) DsbB2 in SDS micelles, d) DsbB3 in SDS micelles, at T = 313 K.

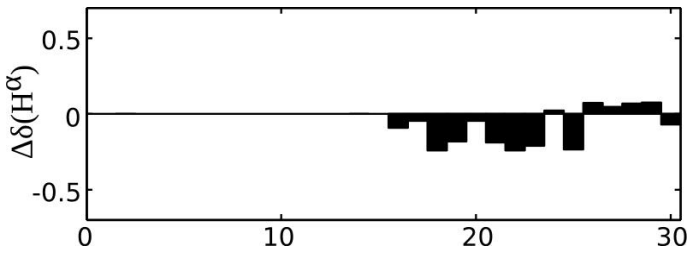

Figure 2.13. $^{1}H^{\alpha}$ chemical shift deviations from random coil values, $\Delta\delta(H^{\alpha})$, for DsbB3 in DPC. (DsbB3 in DPC is half-sequence assigned)

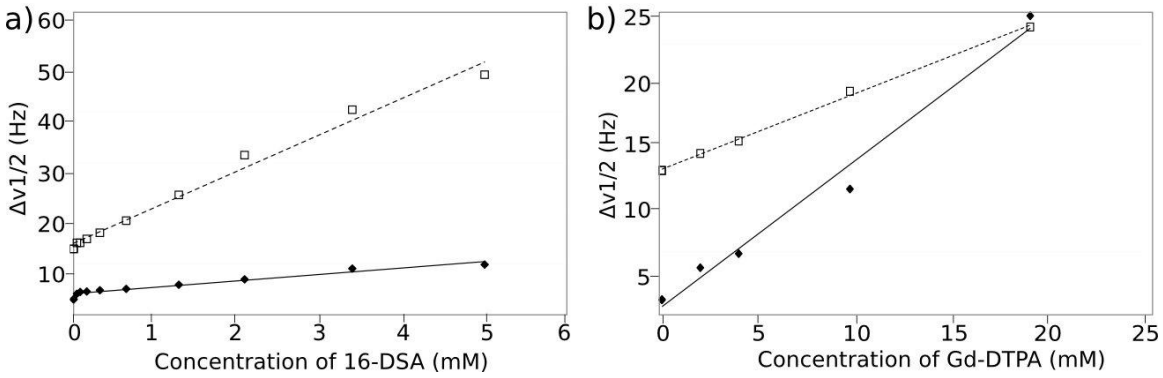

Figure 2.14. Full with at half maximum of ^{1}H resonance lines from $(CH_3)_3$-N hydrophilic headgroups (◆) and $(CH_2)_{10}$ hydrophobic tail groups (□) of dodecyl phosphocholine (DPC) micelles at 80 mM concentration, titrated with paramagnetic relaxation agents. Paramagnetic relaxation enhancements ε were calculated from linear regressions according to a) Titration with 16-doxyl stearic acid (16-DSA), yielding ε = 4.0 $s^{-1}mM^{-1}$ for $(CH_3)_3$-N and ε = 22.6 $s^{-1}mM^{-1}$ for $(CH_2)_{10}$. b) Titration with N,N-Bis(2-[bis(carboxymethyl)amino]ethyl)glycine gadolinium complex (Gd-DTPA), yielding ε = 3.3 $s^{-1}mM^{-1}$ for $(CH_3)_3$-N and ε = 1.7 $s^{-1}mM^{-1}$ for $(CH_2)_{10}$.

It appears, therefore, that the reduced number of medium range NOEs is not simply due to increased spin relaxation in the micelles, but rather due to an actual difference in the structure of the peptides. This difference cannot be explained simply by the temperature difference between the NMR measurements in TFE and in micelles. As determined from the CD spectra, the difference in α-helix content between the two temperatures is only marginal when compared to the difference in α-helix content

between TFE and micelle solvents. Additionally, it should be noted that in the NMR structure of full-length DsbB, which was determined at the same temperature as the structures of the DPC micelle samples, all of the helices were stable.[26]

Both by the H^N chemical shift dispersion and by the NOE patterns (Fig. 2.9 and Fig. 2.11), DsbB2 seems to exhibit slightly increased helix propensity in micelles compared to DsbB3. This may be due to a larger number of hydrophobic amino acid residues in the center of DsbB2, which stabilize the structure of the peptide in the center of the micelle. DsbB3, on the other hand, contains a number of polar amino acids, which could reduce its hydrophobicity below the threshold for insertion into detergent micelles.[101-103]

For DsbB2 in DPC micelles, paramagnetic relaxation enhancement mediated by spin labels was used to determine whether the peptide was inserted into the micelle (Fig. 2.15). The unpaired electron spins in spin labels cause rapid relaxation of nearby nuclear spins, allowing the determination of the relative position of nuclear spins with respect to a spin label.[104] 16-DSA is a spin label that inserts into the micelle, while Gd-DTPA remains in the bulk water (see Fig. 2.14).[105] Fig. 10a shows the reduction of the intensity of H^N-H^α cross peaks in a 2D TOCSY experiment in the presence of 1 mM 16-DSA. A dramatic decrease in peak volume can be observed in the center of the peptide (residues 5 – 20). In contrast, Gd-DTPA most effectively broadened the resonances from the beginning of the amino acid sequence (residues 2 – 5), while residues 10 – 15 appear most protected (Fig. 2.15b). The complementary effect of 16-DSA and Gd-DTPA leads to the conclusion that the peptide is indeed inserted in the micelle.

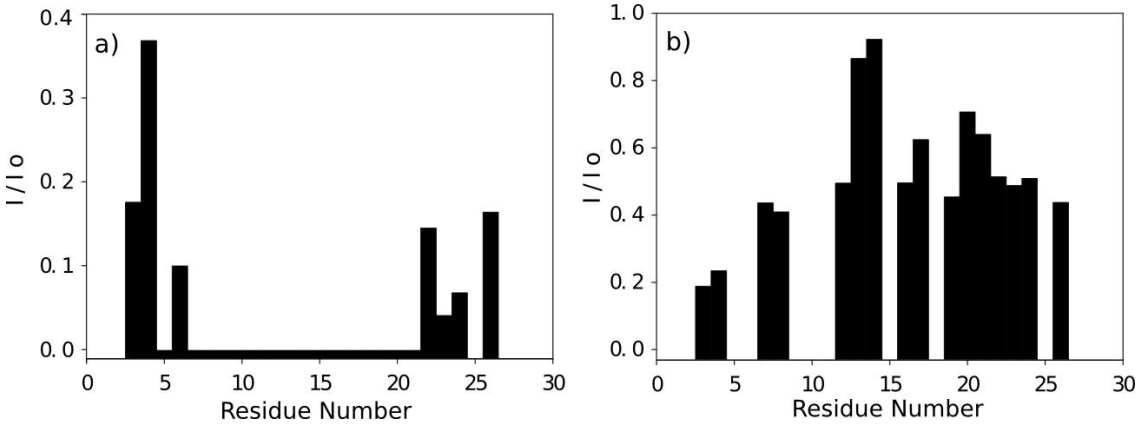

Figure 2.15. Relative H^N-H^α cross peak volumes in 2D TOCSY spectra (20 ms mixing time) of DsbB2 peptide in DPC, in the presence of a) 1 mM 16-DSA and b) 4 mM Gd-DTPA. Short bars represent a relative peak volume of zero, whereas missing bars indicate that the peak volume could not reliably be determined for the respective residue.

Table 1.1. Table of conformational constraints and statistics of the structure calculation for DsbB2 and DsbB3 in 70% TFE and 100% TFE with the program Cyana.

Quantity	Value for DsbB2 in 70% TFE	Value for DsbB3 in 70% TFE	Value for DsbB2 in 100% TFE	Value for DsbB3 in 100% TFE
NOE upper-distance limits	276	289	266	244
Residual target function value [$Å^2$]	0.12 +/- 0.04	0.09 +/- 0.06	0.28 +/- 0.08	0.27 +/- 0.08
Average backbone RMSD	(Residue 4-25) 0.63 +/- 0.21	(Residue 4-28) 1.08 +/- 0.31	(Residue 4-25) 1.18 +/- 0.75	(Residue 4-28) 0.91 +/- 0.53
Average heavy atom RMSD	(Residue 4-25) 1.18 +/- 0.25	(Residue 4-28) 1.71 +/- 0.32	(Residue 4-25) 1.69 +/- 0.96	(Residue 4-28) 1.46 +/- 0.54

2.4 Conclusions

A detailed study of the structure of peptides corresponding to individual transmembrane helices of the DsbB protein yields an account of the individual propensity of these peptides for the formation of native structure. In agreement with the common knowledge that TFE is a helix stabilizing solvent,[106-107] peptide structures in TFE and TFE/water mixtures showed high α-helical content. The extent of helical structure was found to be similar to that in the structures of full length DsbB from DsbB-Fab and DsbB-DsbA complex except for the terminal proline, as well as added lysine residues. The individual propensity of these peptides to form helices similar to those in full-length DsbB seems to confirm that the two-stage model for membrane protein folding indeed applies to the DsbB protein. However, differences in side-chain

conformation between the crystal structures of full-length protein and the NMR structures of the individual transmembrane helices were found, including in some of the residues participating in tertiary interaction in the full length protein. The observed differences appear to be indicative of a rearrangement of side chain conformation upon helix packing. The data that was obtained in detergent micelles indicate that the DsbB peptides form less structured α-helices in detergent micelles than in TFE. Since full-length DsbB is well structured in DPC micelles,[32] these results may indicate that in the full-length protein, tertiary interactions such as salt bridges, hydrogen bonds and hydrophobic contacts play a role in further stabilizing the structure of the transmembrane helices. Additional insights into these and other more subtle interactions may well be the key to a deeper understanding of many aspects of membrane protein folding and function.

2.5 Further Studies

2.5.1 Investigation of helix-helix interactions between DsbB2 and DsbB3 peptides

Tertiary interactions in proteins influence many aspects of their behavior, including their stability and folding. Such interactions between amino acid side chains can play an important role in stabilizing specific secondary structures and also in mediating protein-protein recognition.[108] In full-length DsbB, there are tertiary interactions between His 91 of helix 3 and Glu 47 of helix 2 and Arg 48 of helix 2 and Gln 33 of helix 1.

Here, we examine whether specific side chain interaction between the two helices DsbB2 and DsbB3 are also present when they were mixed together under the same conditions, under which the individual peptides were studied.

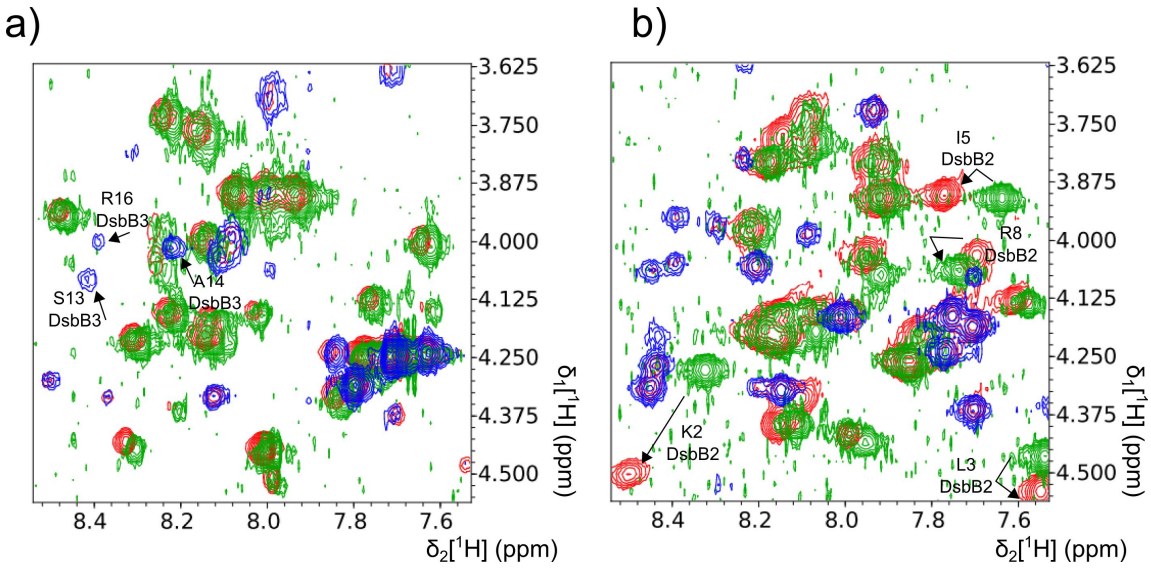

Figure 2.16. Comparison of finger print region of TOCSY spectra of individual peptide and mixture sample in a) 70% TFE and b) 100% TFE. Red peaks indicate TOCSY spectrum of peptide mixture and green peaks belongs to TOCSY of DsbB2 and blue peaks belong to DsbB3.

TOCSY spectra of DsbB2 and DsbB3 in 70% TFE and in 100% TFE were measured separately, and then two samples were combined to measure the TOCSY spectrum of the mixtures. As can be seen in Figure 2-16 (a), the spectra from the individual DsbB2 and DsbB3 peptides agree with the spectrum of the peptide mixture, except for a few peaks including those from Ser 13, Ala 14, and Arg 16. Also, spectra measured in 100% TFE

show only relatively small difference in chemical shift of several amino acid residues. Small changes of chemical shift may be expected due to changes in sample condition when two peptides are mixed. Since no significant changes were observed in particular for residues in the central region of the helices, it appears that under these conditions no conclusive evidence for helix-helix interaction could be found. In the full-length protein, these two helices are connected with a linker, which may increase the likelihood for specific helix-helix interactions due to an entropic effect, or due to structural positioning of the two helices. As a future study, it would be interesting to perform the same experiment using a peptide that contains both helices and the linker.

2.5.2 Determination of correlation times with off-resonance ROESY experiment

In addition to the investigation of peptide structure, spin relaxation parameters can be used for determining intrinsic molecular motions. For isotopically enriched proteins, heteronuclear ^{1}H-^{15}N NOE, as well as ^{15}N T1 and T2 measurements are often used for this purpose.[44] In the case of homonuclear NMR, similar information can be obtained from off-resonance ROESY experiments. In this experiment, the dependence of ROE intensity on the frequency offset of off-resonance irradiation allows to determine internuclear dynamics and chemical exchange.[109-110]

Figure 2.17 shows the ratio of the dipolar cross and direct-relaxation rates as a function of $\omega\tau_c$, where ω is the Larmor frequency and τ_c is the correlation time for isotropic Brownian rotation. As can be seen in the graph, the ratio is constant regardless of the values of $\omega\tau_c$ when θ, the angle between z-axis and effective magnetic field in the

rotating frame, is 54.7°. When θ is 35.3°, cross-relaxation contributions disappear for $\omega\tau_c >> 1$.

Off-resonance ROESY experiments were measured for DsbB peptides. Figure 2.18 shows on-resonance and off-resonance ROESY spectra of DsbB in 100% TFE. The reduction in crosspeak intensity in the off-resonance spectrum can clearly be seen. Using integrated peak volumes from these spectra, correlation times were calculated according to Figure 2.19. Obtained correlation times ranged between 0.4 ns and 1 ns. Values for several representative peaks are shown in Table 1.2. For comparison, an α-helix forming peptide (GFSKAELAKARAAKRGGY) in water has a correlation time of about 1 ns[111] for backbone C_α-H bonds and a ß-hairpin forming monocyclic-AMPB (4-aminomethyl)-phenylazobenzoic peptide in DMSO also has a correlation time of about 1.5 ns for backbone ^{15}N-H bonds which are close to the one we observed.[112]

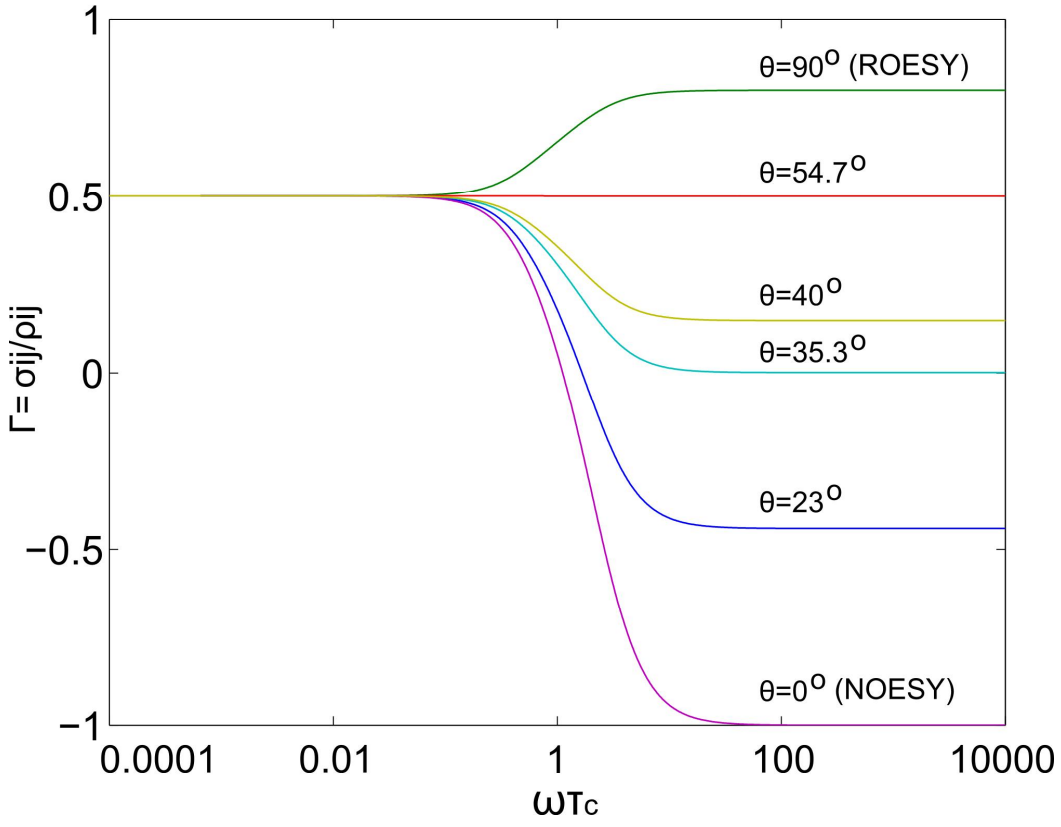

FIGURE 2.17: Ratio of the dipolar cross and direct-relaxation rates as a function of $\omega\tau_c$,where ω is Larmor frequency and τ_c is the correlation for isotropic Brownian rotation.[109] θ indicates the angle between z-axis (static magnetic field) and the effective field magnetic field in the rotating frame.

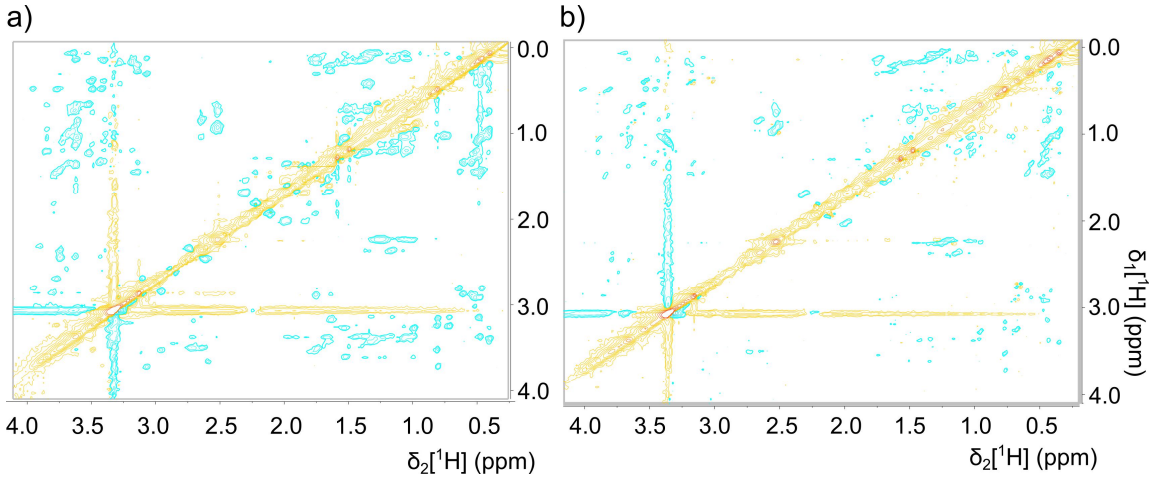

Figure 2.18. a) on-resonance ROESY b) off-resonance ROESY spectrum ($\theta = 40^{\circ}$) of DsbB3 in 100% TFE at 298K measured with the spin-lock pulse carrier frequency 9kHz above the center of the spectrum.

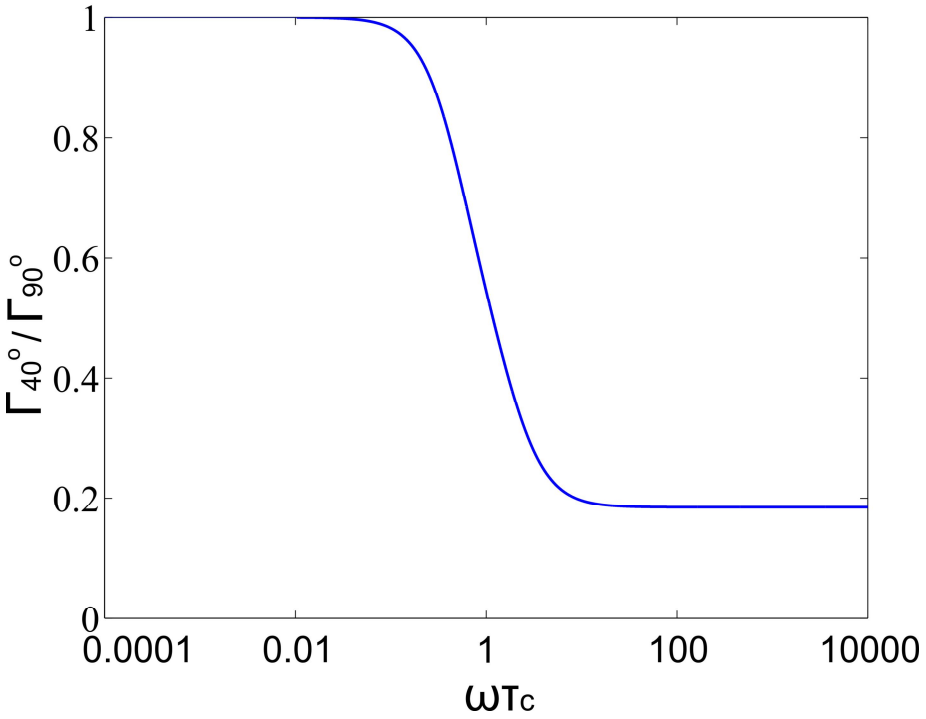

Figure 2.18. Plot showing the ratio between off-resonance ROE (θ = 40°) and on-resonance ROE as a function of $\omega\tau_c$. Calculated ratio provides correlation time of selected cross peaks from several amino acids which is shown below in the table.

Table 1.2. Correlation time obtained from a selection of cross-peaks in ROESY spectra of DsbB3 in 100% TFE measured at 298 K.

Residue	Correlation time (τ_c)
HA/HD2 of K2	0.9 ns
HA/HG3 of R3	1.15 ns
HA/HB of A6	1.15 ns
HA/HB of M7	0.88 ns
HA/HB2 of F15	0.62 ns
HA/HB2 of Q19	1.15 ns
HA/HD2 of L20	1.28 ns
HA/HG2 of T25	1.15 ns
HA/HB2 of K29	0.42 ns

CHAPTER III

METHANOL STRENGTHENS HYDROGEN BONDS AND WEAKENS HYDROPHOBIC INTERACTIONS IN PROTEINS—A COMBINED MOLECULAR DYNAMICS AND NMR STUDY*

3.1 Introduction

Protein structure can be investigated with increasing ease and precision using the modern techniques of structural biology. Not surprisingly, research focus has shifted to the study of the structure and function of large proteins, protein complexes or even membrane embedded proteins; yet, even the basic determinants of protein structure and folding are still poorly understood. In addition to intramolecular interactions, protein structure appears to be governed by contributions from solvation effects. The importance of the latter is illustrated by the effects of the interaction with various solutes, leading to the protein folding or denaturation. Observing interactions between solvent species and a protein remains challenging using the currently available experimental techniques for various reasons. For example, X-ray crystallography requires the artificial environment of a crystal, and furthermore cannot observe disordered conformations, while in nuclear magnetic resonance (NMR) spectroscopy, dynamic effects reduce the ability to observe intermolecular solvent/protein interactions.

On the other hand, the techniques of computational chemistry give access to a complete set of molecular parameters, in addition to the high time resolution, and they present a unique opportunity to further the understanding of the processes governing protein structure and function. The interpretation of computational results without physical data is often problematic. However, if results are compared to experimentally determined structures, they become capable of filling in mechanistic information that experimental structures alone cannot provide.

The solvation effects during protein folding remain one of the most intriguing problems in physical chemistry. Examination of protein structural changes occurring as a result of the changes in solvation environment can serve as a useful model system for understanding the various molecular interactions in determining protein structures. A typical case is the alcohol-induced conformational change of protein: it was observed in various experiments that the addition of alcohol into the aqueous solution generates the structure of protein similar to the molten globule (H) state, a common folding intermediate state for small globular proteins.[113-114] As a result alcohols (particularly methanol and trifluoroethanol (TFE)) have been widely used in the protein folding and structure investigations, the experimental approaches used in which include NMR, circular dichroism (CD), Fourier transform infrared spectroscopy (FTIR), light scattering, fluorescence and so on.[107,114-126] The previous experimental and theoretical studies have shown that the addition of methanol to aqueous solutions of proteins stabilizes (or even induces) the α-helical structure and can also at the same time, “denature” other protein structures, accompanied by the accumulation of methanol near the protein

surfaces.[114,126-127] Recent molecular dynamics (MD) simulations combined with NMR studies are largely consistent with these studies.[128]

In this work, we report a combined MD simulation and NMR experimental study to show the details how methanol affects the structure and various molecular interactions in BBA5. The BBA5 peptide is from a family of peptides designed to exhibit a ββα fold in water: BBA5 forms a stable tertiary structure consisting of a β-hairpin segment (Tyr1—Phe8) and an α-helix segment (Arg10—Gly23); its globular structure is stabilized by the hydrophobic core cluster constructed by Tyr1, Val3, Tyr6, and Phe8 from the hairpin segment and Leu14, Leu17, and Leu18 from the helix segment.[66] Because of its well-defined secondary structures, BBA5 represents an ideal model to test the stability of secondary structures.[129] In this study the computation was first used to make predictions, NMR and CD experiments were then used to test the calculated results. These studies show that the change of the solvation environment has a strong effect on the structure of BBA5: the backbone hydrogen bond interaction is strengthened, and the side-chain hydrophobic interaction is weakened in the presence of methanol. As a result, the solution structure has significantly more helical components, while the overall structure becomes more open.

3.2 Experimental Methods

3.2.1 Sample preparation

BBA5 (NH_2-YRV^{D}PSYDFSRSDELAKLLRQHAG-COO^-) peptide samples were obtained from solid phase synthesis (Anaspec, Fremont, CA), and used without further purification.[66] The lyophilized powder was dissolved in 90% H_2O/10% D_2O, or

in 50% (v/v) deuterated methanol/water (90% H_2O / 10% D_2O), to a peptide concentration of 1 mM. Buffer was not used and the pH was adjusted to pH 4.5. For CD spectroscopy, samples were further diluted to a concentration of 20 μM. Concentrations were determined by spectrophotometry, using a calculated molar extinction coefficient $\varepsilon = 2980\ M^{-1}cm^{-1}$.

3.2.2 Structure determination

CD spectra were acquired using an AVIV 26DS spectrometer, from 190 to 260 nm in steps of 1 nm, at a temperature of 280 K. α-Helix content was estimated from mean residue ellipticity at 222 nm,[130] neglecting any contributions from β-sheet-like secondary structure to the CD signal. Solution NMR structures of the peptides were determined using two-dimensional ^1H NMR.[96] NMR spectra were measured on a Varian INOVA 600 MHz spectrometer with triple resonance probe and z-gradient, and on a Bruker ARX 500 MHz spectrometer with triple resonance probe and z-gradient. All spectra were measured at 280 K. Amino acid spin systems were identified in TOCSY spectra (70 ms mixing time),[91] and sequence specific resonance assignments were obtained from NOESY spectra (150 ms mixing time).[92] All of the NOE assignments and structure calculations were performed by the same automated procedure using the program CYANA,[12] to ensure objective results. In each of seven cycles, distance constraints were automatically identified in the NOESY spectra, and were used for a structure calculation by simulated annealing starting from 100 randomized structures. From the last cycle, a bundle of the 10 conformers with lowest target function were retained to represent the NMR structure.

3.3 Results and Discussion

CD spectroscopy of BBA5 samples indicated that the peptide adopts a predominantly α-helical structure both in water and in 50% (v/v) MeOH/water solutions, under the experimental conditions used (Figure 3.1). As judged from the ellipticity at 222 nm, the α-helix content in MeOH/water solution is significantly increased (Table 2.1). More detailed structure information is available from the NMR experiments.

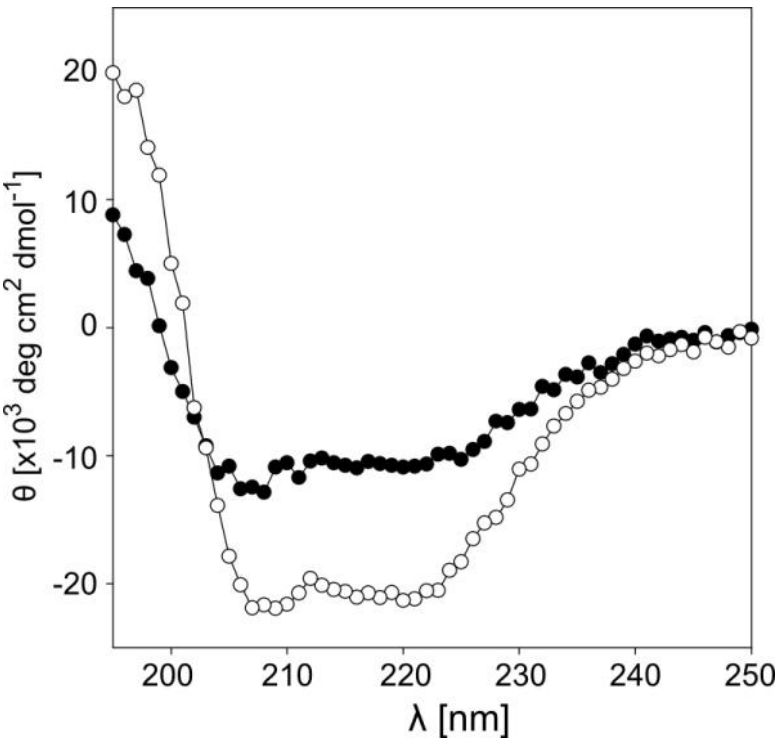

Figure 3.1. CD spectra of BBA5 in water (—●—), and MeOH/water solution (—○—) at a measurement temperature 280 K.

Table 2.1. Mean residue ellipticity at 222 nm (θ_{222}) and estimated α-helix content from CD spectra of BBA5. Estimates of α-helix content are based on θ_{222} and neglect any contribution of β-sheet like secondary structure to the CD signal.

	In MeOH/Water		In Water	
T [K]	θ_{222} [$\times 10^3$ deg·cm^2·dmol^{-1}]	Estimated α-helix content	θ_{222} [$\times 10^3$ deg·cm^2·dmol^{-1}]	Estimated α-helix content
280	-20582.92	56%	-10662.21	30%
288	-19928.82	55%	-9612.04	27%
298	-17878.03	49%	-9297.66	26%
308	-17039.25	47%	-8229.65	24%
318	-15184.69	42%	-7560.76	22%
328	-13487.88	38%	-7157.19	21%

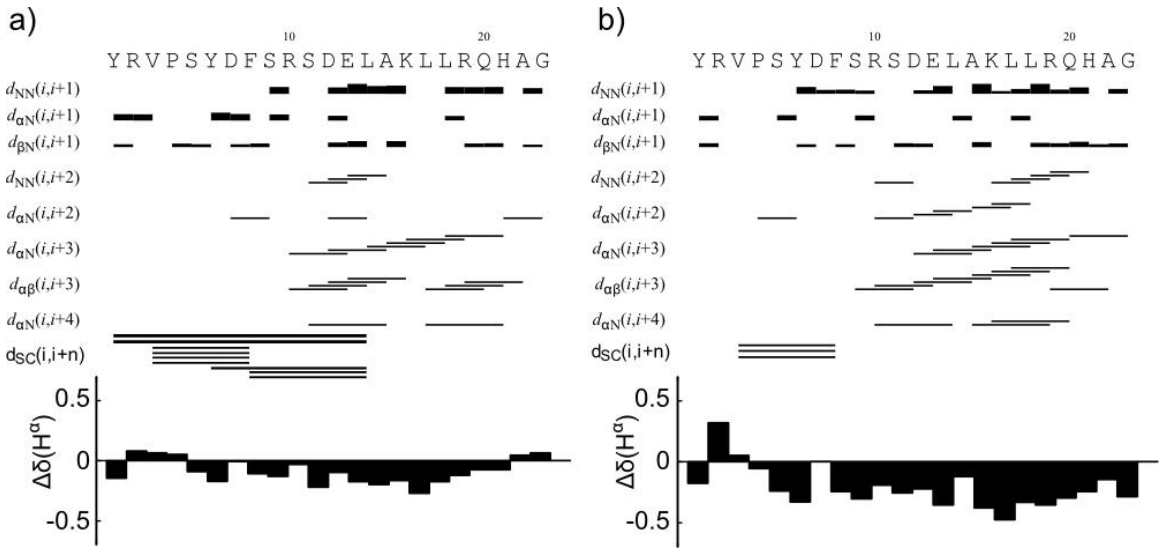

Figure 3.2. BBA5 in a) water, and b) MeOH/water solution. The top panels indicate observed NOEs in the respective spectra. The bottom panels show the deviation of H^{α} chemical shift from random coil values. SC denotes “side-chain”.

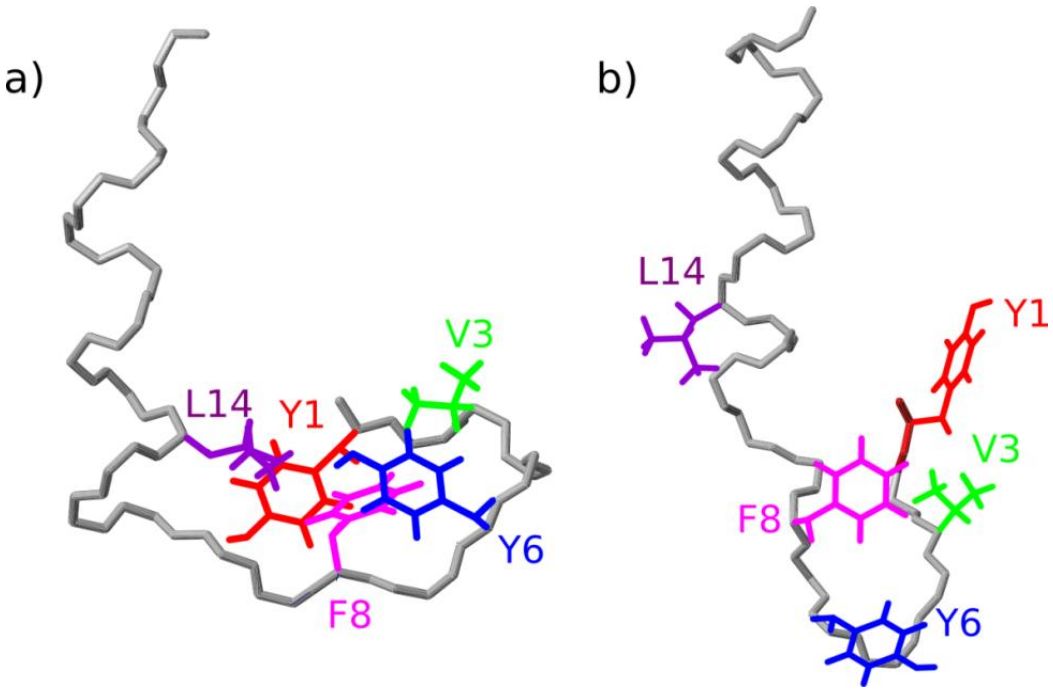

Figure 3.3. NMR structure of BBA5 in a) water, and b) MeOH/water solution. The side-chains of hydrophobic residues participating in the hydrophobic cluster in water are indicated.

NOE distance constraints were collected from NOESY spectra (Figure 3.2). Based on these constraints, structures of BBA5 in water and in MeOH/water solutions were calculated (Figure 3.3). The NMR structure in water is similar to a previously determined structure, with a few small differences mainly in the side-chain packing.[66] In the following comparisons, we use the newly calculated structure in order to avoid the bias that may otherwise arise due to the differences in methodology.

In water, $d_{\alpha\beta}(i,i+3)$ and $d_{\alpha N}(i,i+3)$ NOEs, indicative of helical secondary structure, were observed between residues R10 and A22 (Figure 3.3). The helix extent in MeOH/water solution was slightly larger (S9 to G23), and overall more medium-range

NOEs were observed, indicating an increased propensity for the α-helix. This observation is in agreement with the results from CD spectroscopy. With other peptides, alcohols have also been observed to increase α-helix content, an effect presumed to arise because of a reduced number of hydrogen bonds between the solvent and the peptide backbone when compared to water.[18,107,125-126]

The β-hairpin-like element in water is defined by cross-strand NOEs between V3 and F8. Additionally, a number of long-range interactions with the α-helix indicate a tertiary contact (Y1–L14, Y6–L14 and F8–L14). These NOEs are part of a hydrophobic cluster, which appears to stabilize the β-hairpin structure. In contrast to its effect on the α-helix, MeOH/water solution appears to de-stabilize the β-hairpin-like structure. Fewer cross strand NOEs are observed, and the tertiary interaction is lost (Figure 3.2). A direct, visual indication of the loss of these contacts is also obtained by comparing the NOESY spectra acquired under the two conditions, shown in Figure 4. A significant reduction in the number of crosspeaks involving the side-chains of aromatic residues in the hydrophobic core cluster can be seen in MeOH/water solution.

To compare MD simulations with experiments, we show in Table 2.2 the population of the individual backbone hydrogen bond (HB)s calculated from the simulations. It is apparent that the addition of methanol increases the population of the protein backbone hydrogen bonds, in particular those belonging to the α-helix.

Table 2.2. Average number of individual backbone hydrogen bonds of BBA5 formed in water, and MeOH/water solutions respectively from MD simulation data. The average is over the entire simulation trajectory. (*This table is made by Dr. Gao's laboratory in Peking university in China)

Backbone HB	In MeOH/Water	In Water	Backbone HB	In MeOH/Water	In Water
F8O-Y1H	0.000	0.000	E13O-L17H	0.326	0.000
Y1O-F8H	0.590	0.603	L14O-L18H	0.335	0.492
Y6O-V3H	0.950	0.978	A15O-R19H	0.252	0.222
V3O-Y6H	0.204	0.282	K16O-Q20H	0.325	0.029
R10O-L14H	0.311	0.000	L17O-H21H	0.044	0.265
S11O-A15H	0.416	0.188	L18O-A22H	0.270	0.541
D12O-K16H	0.363	0.000	R19O-G23H	0.273	0.003

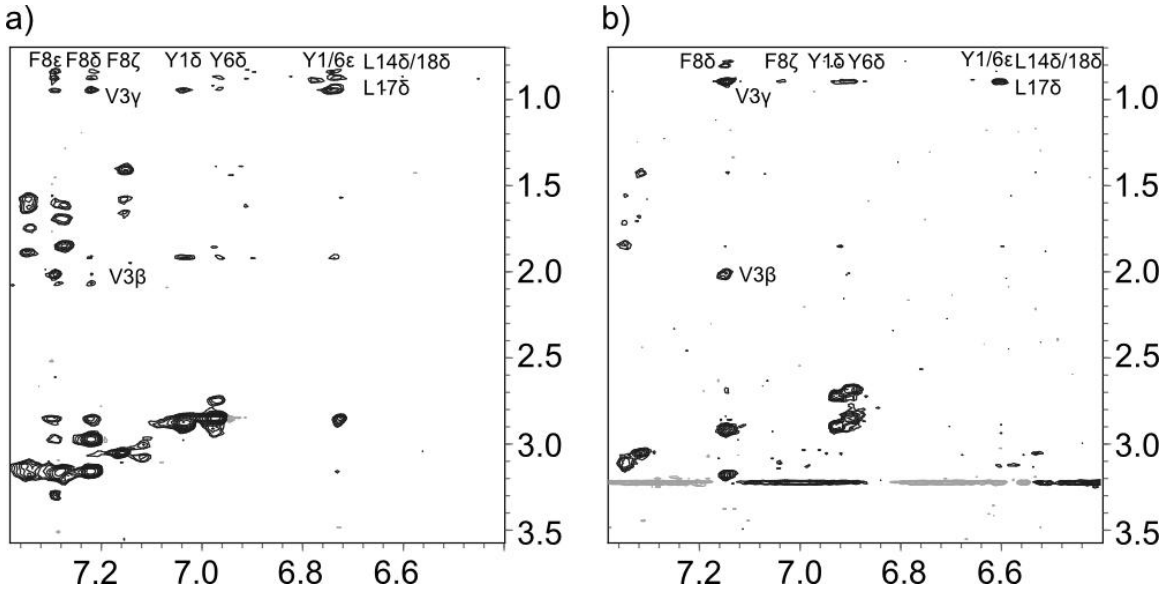

Figure 3.4. Regions taken from NOESY spectra of BBA5 in a) water, and b) MeOH/water solution. NOE crosspeaks corresponding to long-range interactions are shown.

The average number of α-helix hydrogen bonds in MeOH/water solution is about 1.7 times of that in pure water. This number is similar to the ratio of α-helical secondary structure content estimated from the CD spectra in MeOH/water and water samples, which is about 1.9 at the room temperature (Table 2.1). Although the hydrogen bond numbers calculated from the simulations does not compare directly to the helicity in CD experiment in a quantitative manner, these results show that the helix formation is enhanced in MeOH/water solution as compared to in pure water.

To further assess the propensity of the individual segments of the peptide to form regular secondary structures, the temperature coefficients for amide proton chemical shifts ($-\Delta\sigma_{HN}/\Delta T$) were determined for each sample (Figure 3.5 a & b). Values of $-\Delta\sigma_{HN}/\Delta T < 4.6$ ppb/K are generally taken as an indication of the presence of an intramolecular hydrogen bond, where the amide proton is protected from the solvent.[42] For BBA5 in water, the C-terminal part exhibits a significant number of values smaller than 4.6 ppb/K, indicating the presence of the α-helix. The N-terminal segment, where the β-hairpin structure is located, shows the temperature coefficient values predominantly larger than 4.6 ppb/K. This difference may be rationalized considering that for β-hairpin structure in BBA5, the stabilization by the hydrophobic core cluster may play a more important role than the hydrogen bonding. In MeOH/water solution, the α-helix region (A15– Q20) exhibits unusually large temperature coefficients. Such an effect has previously been observed for peptides solvated in TFE, where it was hypothesized that it could be due to the hydrophobic interactions between the helix and the organic solvent.[131]

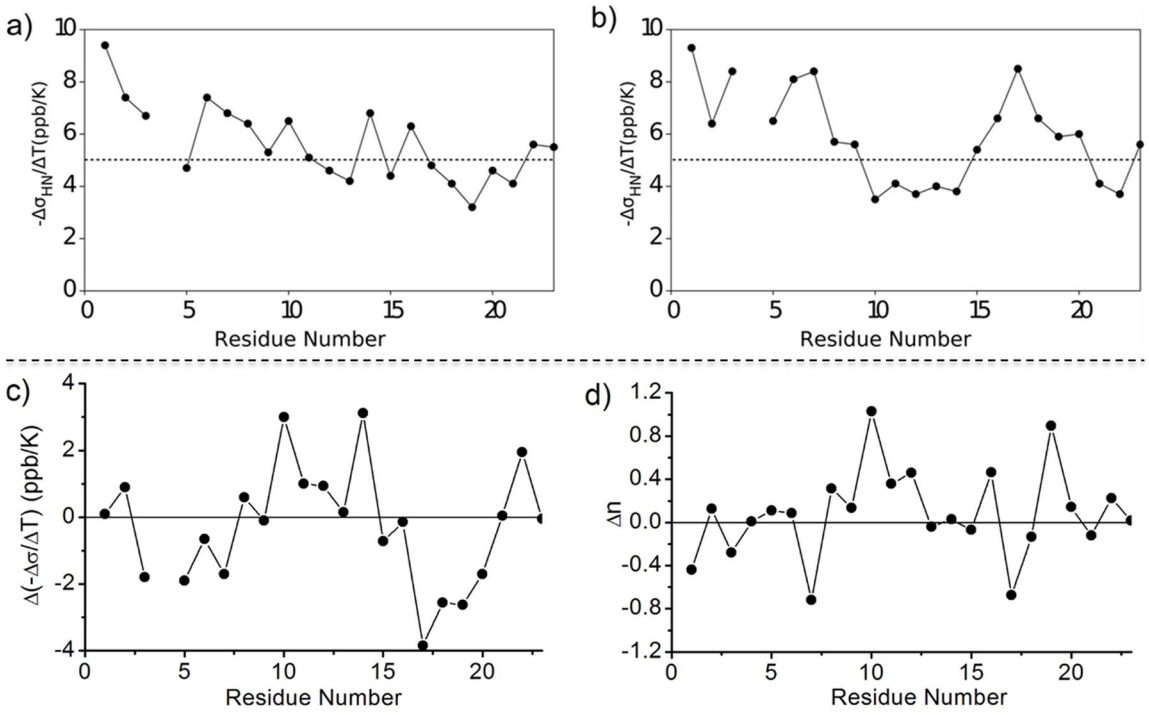

Figure 3.5. a) Amide proton temperature coefficients ($-\Delta\sigma_{HN}/\Delta T$) for BBA5 in water. b) Temperature coefficients for BBA5 in MeOH/water solution. The dashed line at $-\Delta\sigma_{HN}/\Delta T$ = 4.6 ppb/K indicates a typical cutoff value for the identification of secondary structure elements (see text). c) Difference in temperature coefficients for BBA5 between water and MeOH/water solutions, $\Delta(-\Delta\sigma_{HN}/\Delta T) = (-\Delta\sigma_{HN,\ water}/\Delta T) - (-\Delta\sigma_{HN,\ methanol}/\Delta T)$. d) Difference in the average number of hydrogen bonds from solvent molecules, between MD simulations of BBA5 in water and in MeOH/water solutions, Δn = (*HBs from water*) $_{in\ water}$ - (*HBs from water +HBs from methanol*)$_{in\ MeOH/water}$.

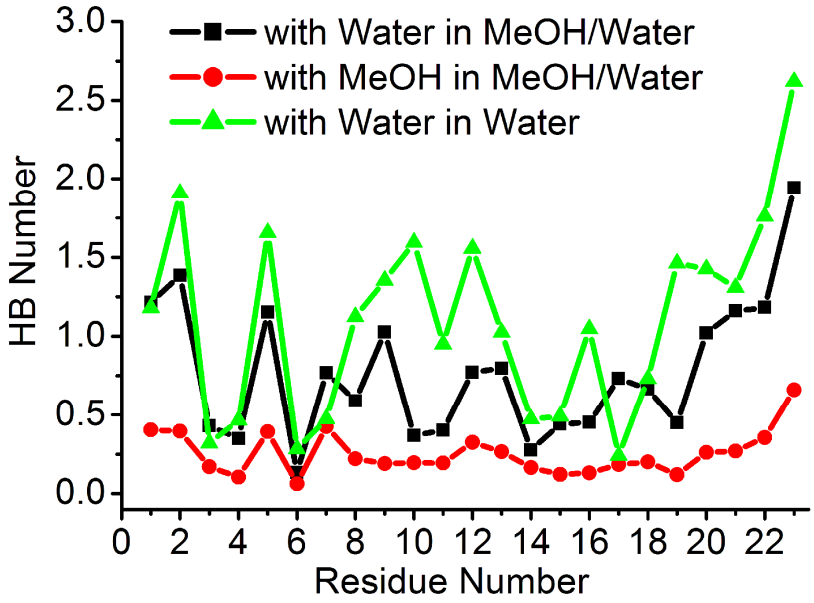

Figure 3.6. Average number of hydrogen bonds formed between the backbone amide (-NH) or carbonyl (C=O) group of individual residues with solvent molecules, from MD simulation data. The numbers of hydrogen bond formed are shown in black for those between individual residues and water, in red for those between individual residues and methanol in MeOH/water solution, and in green for those between individual residues and water in pure water. The average is over the entire simulation trajectory. (*This figure was made by Dr. Gao's laboratory at Peking University in China)

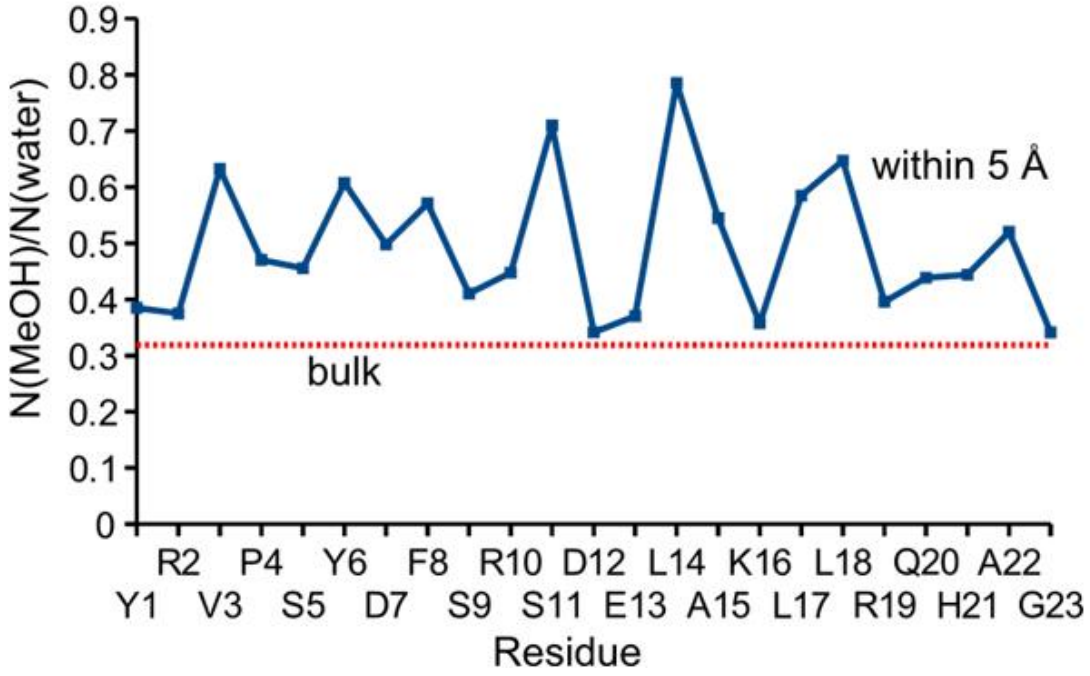

Figure 3.7. Average number of solvent molecules within 5 Å of each individual residue of BBA5 was calculated and provided the ratio between the numbers of methanol and water molecules accumulated around each residue of BBA peptide, from MD simulation data. (*based on data by Dr. Gao's laboratory at Peking University in China)

It may be of interest to further examine this point based on the simulation results. In Figure 3.6, we show the effects of methanol on the hydrogen bonds between protein backbone and solvent molecules, for each residue in the simulations (In MeOH/water solution, the hydrogen bonds between the backbone and solvent include not only those from water molecules but also those from methanol molecules, both are calculated and shown in Figure 3.6). For most of the residues, the hydrogen bonding from water is largely reduced by the addition of methanol, which is to some extent compensated by the

hydrogen bonding from methanol. Meanwhile, the overall hydrogen bonding between protein backbone and solvent including water and methanol is only slightly changed compared to that in pure water (the total number of hydrogen bonds between the backbone of the 23 residues of BBA5 and solvent averaged over the simulation trajectory is 23.53 in MeOH/water and 25.45 in water). Most noticeably, the number of hydrogen bonds decreases significantly around residue R10 and R19, and increases for residue L17 in MeOH/water solution. This result correlates with the observed change in temperature coefficients from the NMR measurement (Figure 3.5c).

In MeOH/water solution, the small change of the total number of the protein-solvent hydrogen bonds but the significant decrease of the total number of protein-water hydrogen bonds, accompanying with the structural exposure of BBA5, might be attributed to the methanol accumulation near the protein surface and the consequent replacement of the water molecules. The preferred binding of methanol to the protein is calculated as the ratio R_{MW} between the numbers of methanol and water molecules within 5 Å of the protein surface. The resulting values of the MeOH/water ratios are greater than 0.32 for all residues as shown in Figure 3.7, and the average of R_{MW} over all residues is 0.49, indicating the preferred binding of methanol over water to the protein surface. The more favored interaction between methanol and the protein reduces the hydrophobic effect and therefore results in a higher degree of solvent exposure of the peptide.

On the other hand, the accumulation of methanol in general reduces the protein-water hydrogen bonding as well as the local dielectric constant near protein surface. This

change is not uniform along the protein: the reduction of protein-water interaction and the increase of the protein-protein hydrogen bonding mainly occur in the α-helix region, as shown in Figure 3.6 and Table 2.2 respectively. The overall decrease of protein-water hydrogen bonding for residues from R10 to R19 correlates well with the increase of the corresponding protein-protein hydrogen bonding, revealing the fact that the source of the protein-protein hydrogen bond disruption is from the water hydrogen bonding. Furthermore, even along the helix portion, the change in protein-water hydrogen bonding also varies with the sequence. In fact, the protein-water hydrogen bonding is mostly weakened for the polar residues (e.g., R10, S11, D12, K16, and R19) but little changed or even strengthened for the apolar ones (e.g., L14, A15, L17 and L18). Consequently, the protein-protein hydrogen bonds formed by the carbonyl groups from polar residues (R10O-L14H, S11O-A15H, D12O-K16H, E13O-L17H, K16O-Q20H, and R19O-G23H) are strengthened, whereas the stability of the hydrogen bonds formed by the carbonyl groups from apolar residues (L14O-L18H, A15O-R19H, L17O-H21H, and L18O-A22H) are either weakly affected or decreased. These results are consistent with the difference between the temperature coefficients obtained in pure water and in MeOH/water solution: Figure 3.5 indicates that the helix becomes more structured in the position where the polar residues are gathered, e.g., the N-terminal segment (residues R10 – E13), rather than the more apolar part (A15 –R19) in MeOH/water solution. It is also interesting to point out that the residues that form the better secondary structure are more likely to hydrogen bond with methanol than with water when compared to those associated with broken secondary structures, as shown by the ratio between the numbers

of their hydrogen bonds to methanol and water (Figure 3.6). This observation indicates that protein-water hydrogen bonds are likely more capable of breaking the protein secondary structure than those formed between protein and methanol.

3.4 Conclusions

In this work, we performed MD simulation and NMR/CD studies to investigate the effects of methanol on a short peptide that serves as a model system for proteins. The combined theoretical and experimental data show that the addition of methanol enhances the formation of secondary structure, especially the α-helical segment of the BBA5 peptide. This enhancement of backbone-backbone interactions is accompanied by the weakening of hydrophobic interactions between the side-chains, which disrupts a hydrophobic core cluster in BBA5. The peptide structure in MeOH/water solution is therefore expanded, but contains highly ordered secondary structures, consistent with earlier studies.

The present study suggests that the accumulation of methanol near the protein surface induces the expansion of protein structure, presumably by the reduction of hydrophobic effects. At the same time, the replacement of water molecules from the local environment of the protein surface decreases the hydrogen bonding of water to protein, and on average increases the protein-protein hydrogen bonds. The hydrogen bonding of methanol to the protein backbone, on a per molecule basis, is less favorable than the hydrogen bonding of water. These effects together *locally* decrease the polar interaction between the solvent and protein and therefore result in a higher propensity for secondary structure formation, in particular for the α-helix, although the introduction of

methanol increases the exposure of the protein to the solvent. The effects of methanol on the secondary structure are not uniform along the α-helix but dependent on the sequence and/or the residue position: the backbone hydrogen bonds formed by the carbonyl groups from polar residues are strengthened whereas those from apolar residues are weakened. The effect of methanol on the protein structure is thus a combination of direct (preferred binding of methanol) and indirect (e.g., reduced protein-water hydrogen bonding) effects, although these two are closely related, and manifested differently in local and global structures. The balance between these effects determines whether methanol tightens or loosens the local protein structure, which heavily depends on the local sequence and environment.

CHAPTER IV

FOLDING OF A TRYPTOPHAN ZIPPER PEPTIDE INVESTIGATED BASED ON NUCLEAR OVERHAUSER EFFECT AND THERMAL DENATURATION*

4.1 Introduction

Peptides present attractive, simplified models for the study of protein folding. Short peptides however typically exhibit a large amount of conformational flexibility. Unlike in full-length proteins, it is by consequence common that secondary structure elements are not well-defined in peptides. The use of non aqueous solvents is a popular way to induce secondary structure formation, albeit at the expense of being further removed from physiological conditions. Peptide sequences can also be designed to give rise to intrinsically higher structural stability by exploiting specific interactions. A set of peptides that adopt a remarkably stable β-hairpin secondary structure in water has been introduced by Cochran et al.[53] These tryptophan zipper peptides are mutants of the B1 domain of Protein G. They contain several tryptophan residues that seem to confer stability through side chain – side chain interaction. Since their introduction, the stability and folding of trpzip peptides has been studied in various ways, including by circular dichroism (CD) and infrared spectroscopy.[53,132-134]

Du et al. found that the key factors stabilizing ß-hairpins are a turn-promoting sequence which increases the folding rate, as well as interstand hydrophobic side chain – side chain interactions which decrease the unfolding rate.[133] Wu et al. observed a strong impact of Trp-Trp interactions on the stability of the ß-hairpin by substituting Trp with Val residues.[135] Takekiyo et al. also investigated the stability of the trpzip1 peptide by substituting Trp with Tyr, concluding that the mutation reduced the extent of ß-hairpin structure and decreased the ß-hairpin stability.[136] Based on studies by Waters et al., aromatic-aromatic interactions give rise to more stable ß-hairpin structure than aliphatic-aromatic interactions.[137-139] In addition, trpzip peptides are often used as a model system to study the folding mechanism of ß-hairpins by molecular dynamics simulation.[134,140] Gao et al. analyzed the thermodynamics involved in the folding of trpzip2, suggesting the existence of various short-lived folding intermediates that result in a zip-out folding mechanism. They also found that hydrophobic interaction between tryptophan residues of trpzip4 plays an important role in stabilizing the peptide structure.[10,141]

While several structures of trpzip peptides have been solved by nuclear magnetic resonance (NMR), folding and stability was predominantly investigated by other methods. NMR would present a significant opportunity to elucidate folding mechanisms, since sequence positions can be individually addressed. Although a wealth of information on protein dynamics is in principle available from heteronuclear relaxation experiments, due to the low cost for the solid-phase synthesis of unlabeled peptides, homonuclear NMR remains a mainstay for structural study of small peptides. Peptide folding may be studied by NMR through observation of chemical shift changes, such as

H^{α} and H^{N} NOEs traditionally are not often used in combination with thermal denaturation, perhaps due to the dependence of the NOE not only on the structure, but also on other parameters such as motional correlation time that changes in function of temperature. Here, we make the case that despite these effects, NOEs may still contain more information than other experimentally accessible parameters, and provide a different perspective on peptide folding.

4.2 Experimental Methods

4.2.1 Sample preparation

Peptide with the trpzip4 sequence GEWTWDDATKTWTWTE (with sequence position numbers 41-56)[53] was obtained commercially from solid phase synthesis (Anaspec, Fremont, CA), and used without further purification. Peptide was dissolved to 1 mM final concentration in 92% water / 8% deuterium oxide, containing potassium phosphate (30 mM PO_4, pH 6.0) and a small amount of 4,4-dimethyl-4-silapentane-1-sulfonic acid (DSS) for chemical shift referencing. The pH was adjusted to 6 using HCl, and the NMR sample was sealed under argon.

4.2.2 NMR spectroscopy

NMR spectroscopy was performed on a spectrometer with 500 MHz ^{1}H frequency equipped with a cryoprobe (Bruker, Billerica, MA). A set of NOESY (300 ms mixing time), ROESY (200 ms mixing time, with a spinlock field of 3.54 kHz), and TOCSY (100 ms mixing time) spectra was acquired for each of the following temperatures: 9 °C, 19 °C, 29 °C, 40 °C, 49 °C, 59 °C, 69 °C. 1D H/D exchange

experiments were measured at 9 °C immediately after lyophilized peptide was dissolved in 100% D_2O (30 mM PO_4, pD 6.0).

4.2.3 Data processing

NMR spectra were processed with the program TOPSPIN (Bruker). Peak volumes were determined using the program CARA.[95] Experimental data was fitted in MATLAB (Mathworks, Natick, MA). Calculated curves for signal intensity were plotted using Mathematica (Wolfram Research, Champaign, IL). Figures with protein structures were prepared using PyMOL (open source version, Schrödinger LLC, Portland, OR).

4.3 Results and Discussion

In order to assess thermal denaturation of trpzip4, NMR measurements were carried out over an accessible temperature range between 9 °C and 69 °C (see Materials and Methods). Loss of the folded structure of the peptide in this temperature range can also be assessed by circular dichroism (CD) spectroscopy. According to CD measurements (from [53], and in agreement with data collected of the samples used here; figure 4.1), the peptide has approximately reached the mid-point of thermal denaturation at 69 °C, the highest temperature used. Since the CD spectrum of trpzip4 is dominated by exciton coupling between the aromatic chromophores of tryptophan, the parameter that is accessible in these measurements is not directly the amount of secondary structure, but rather the mutual proximity of tryptophan side chain moieties.

4.3.1 NMR chemical shifts

Generally, the chemical shift of amide protons in the polypeptide is expected to decrease as temperature increases, *i.e.* the amide proton becomes more shielded.[142-147] In trpzip4, the majority of amino acids follow this pattern (Figure 4.2). However, Thr 49 and Thr 51 show opposite behavior. It can also be seen that the chemical shifts of the amide protons of Trp 45 and Trp 54 are most temperature dependent, such that it may be hypothesized that a change in local structure, such as side chain orientation of tryptophan residues may have a dominating effect on the chemical shift.[145-146] On this premise, chemical shift – while indicating structural changes in the peptide – may not be a faithful measure specifically for the loss of the hydrogen bonds that define β-sheet secondary structure. Furthermore, previous studies have found that amide proton temperature coefficients do not correlate well to hydrogen bonding in peptides.[145,148]

Apart from amide protons, alpha proton chemical shift values can be used to estimate the secondary structure of a protein.[41] In Figure 4.2, changes in the chemical shift of H^{α} protons are relatively small, possibly because the highest temperature accessible in the NMR experiments reaches only the mid-point of denaturation as indicated by CD spectroscopy.

4.3.2 Nuclear overhauser effect

Since the nuclear Overhauser effect is highly sensitive to changes in inter proton distance, it would appear to be a natural choice for assaying denaturation. Moreover, while the ^{1}H-^{1}H NOE is not observed directly at the location of the interstrand hydrogen bond, distances $dH^{\alpha}H^{\alpha}(i,j)$, $dH^{N}H^{N}(i,j)$ and $dH^{\alpha}H^{N}(i,j)$ observed by NOE are deemed

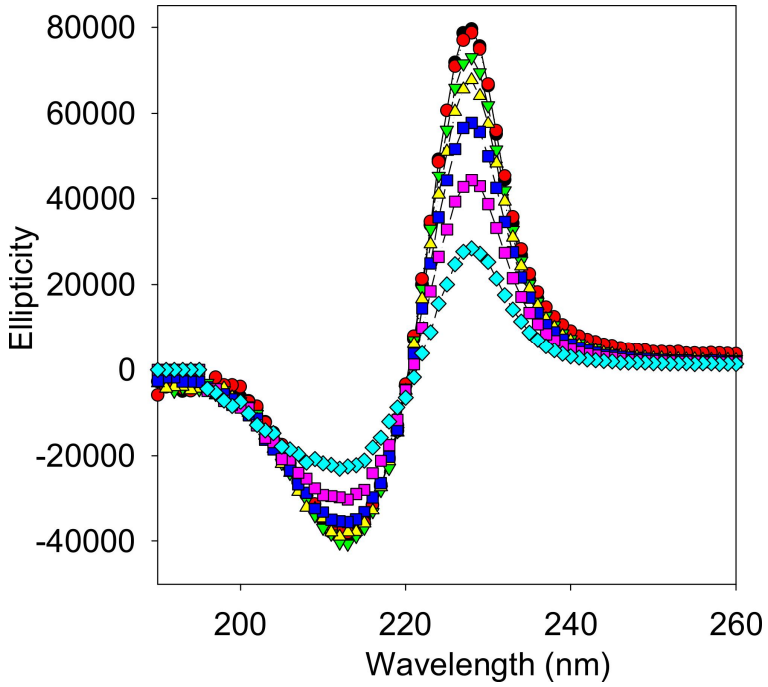

Figure 4.1. CD spectra of trpzip4 measured from 15 °C to 75 °C. As temperature increases, the fraction of folded structures is lost.

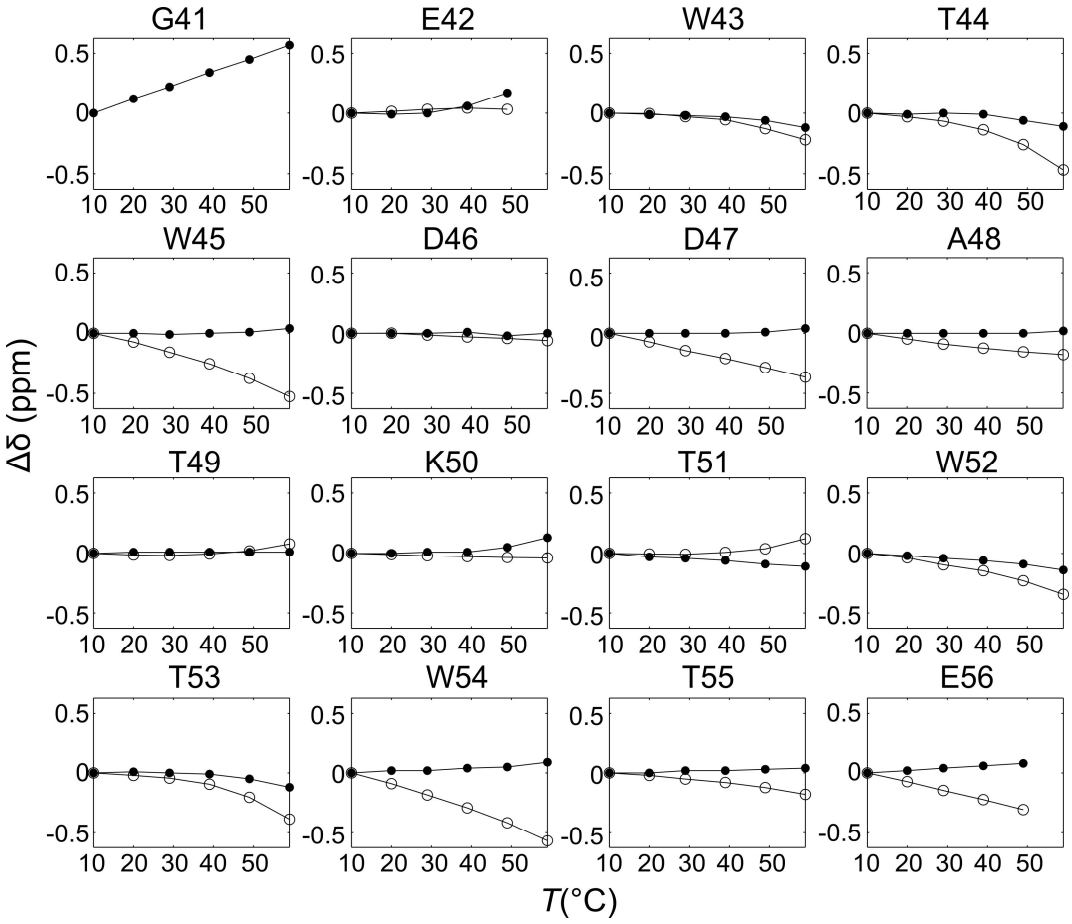

Figure 4.2. Chemical shift change of amide protons (-o-) and alpha protons (..●..) in function of temperature.

characteristic for the presence of antiparallel β-sheet structure, and distances $dH^NH^N(i,j)$ and $dH^\alpha H^N(i,j)$ for parallel β-sheet structure.[96] When attempting to use the NOE for assaying thermal denaturation, it is necessary to consider various factors that can give rise to a change in NOE intensity upon changing the temperature. For an isolated pair of protons, the cross peak intensity in a transient NOE experiment is given as

$$I_{NOE} = \sinh(-\sigma t_{mix}) \exp(-\rho t_{mix}) \tag{4}$$

where t_{mix} is the NOE mixing time, and the autorelaxation rate ρ and cross-relaxation rate σ are given as

$$\rho = \frac{\gamma^4 \hbar^2 {\mu_0}^2}{64\pi^2 r^6}\left(J(0) + 3J(\omega) + 6J(2\omega)\right) \tag{5}$$

$$\sigma = \frac{\gamma^4 \hbar^2 {\mu_0}^2}{64\pi^2 r^6}\left(-J(0) + 6J(2\omega)\right). \tag{6}$$

Here, r is the distance between the two protons, ω the angular frequency of spin precession, γ the gyromagnetic ratio, $\hbar$ Planck's constant, and μ_0 the vacuum permeability [149]. In spin relaxation experiments, the spectral density is often approximated by the model free expression of Lipari and Szabo.[150-151]

$$J(\omega) = \frac{2}{5}\left(S^2 \frac{\tau_c}{1+\omega^2 {\tau_c}^2} + (1-S^2)\frac{\tau'_f}{1+\omega^2 {\tau'_f}^2} \right). \tag{7}$$

τ_c is the correlation time for global motion, S^2 an order parameter for the accessible local conformations, and $\tau'_f = \tau_f / (\tau_f / \tau_c + 1)$ with τ_f as a correlation time for fast internal motions. In the case of a rigid molecule (S^2 = 1), this spectral density reduces to the

usual expression, and depends only on the global correlation time. The temperature dependence of τ_c can be approximated as

$$\tau_c = \frac{4\pi\eta a^3}{3kT} \tag{8}$$

with a the radius of gyration of the polypeptide, k Boltzmann's constant and T the temperature.[96] Over the temperature range used, the most significant effect of the temperature on τ_c lies in the change in the dynamic viscosity of the solvent, which for water is approximated by $\eta = (0.4508\,\mathrm{Nsm^{-2}})e^{-(0.02076\,\mathrm{K^{-1}})T}$, based on data encompassing the temperature range between 9 °C and 69 °C.[152] The effect of the temperature dependence of τ_c on the observed NOE crosspeak intensity is examined in Figure 4.3 under the assumption of a pair of protons in a rigid molecule, using parameters similar to those expected for a peptide the size of trpzip4. The absolute NOE intensity is strongly distance dependent (see Figure 4.3a). However, its relative reduction as a function of increasing temperature is nearly equal for the typically observed distances between 0.2 and 0.5 nm (Figure 4.3b). This observation forms the basis for considering the NOE crosspeak intensity as an indicator for protein denaturation. Any differences in the intensity as a function of temperature among the various observed crosspeaks would be expected to arise from changes in the peptide itself, as opposed to merely from differences in initial proton – proton distance.

NOE crosspeak intensities are influenced both by structural and dynamic factors, which need to be considered. The strong dependence on internuclear distance (Figure 4.3a) is well known. It may further be noted that this plot assumes an isolated pair of

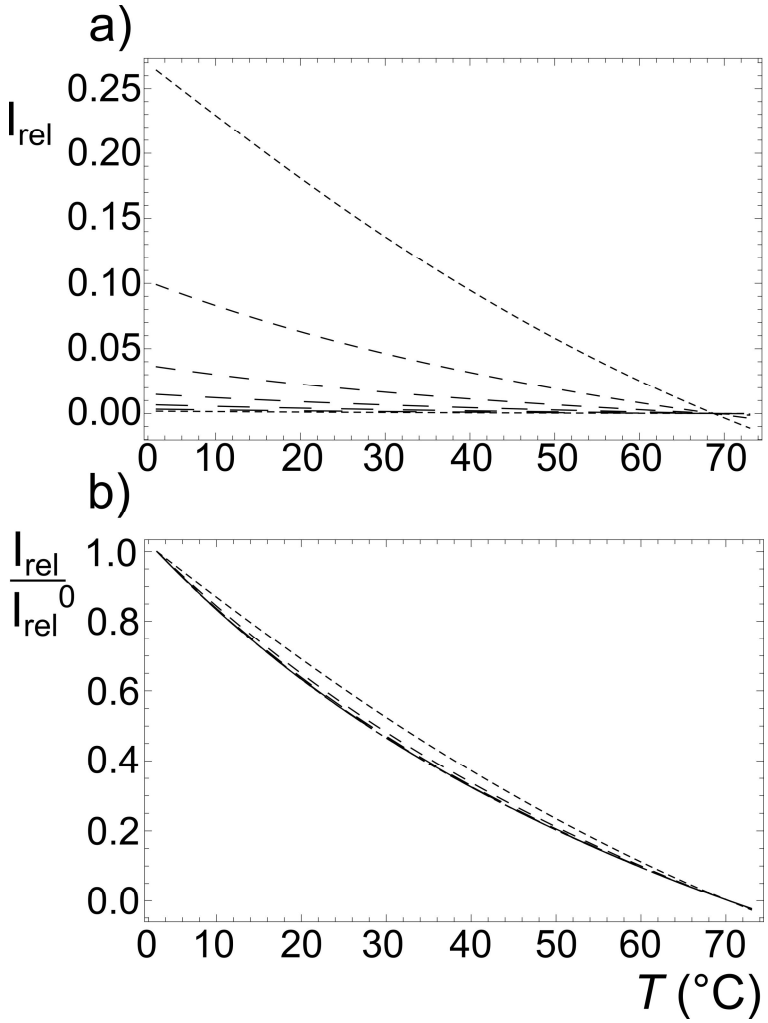

Figure 4.3. a) NOE cross peak intensity calculated for an isolated pair of protons in a rigid molecule, in function of temperature. In b), each curve was scaled to unit intensity at 0 °C (273 K). Dashed lines indicate inter proton distances from 0.2 nm to 0.5 nm, in steps of 0.05 nm, from shortest to longest dash. Curves were calculated for a particle with radius of gyration of 1.0 nm, field strength of 11.74 T, and a NOE mixing time tmix = 0.3 s. The temperature axis has been converted to °C for readability.

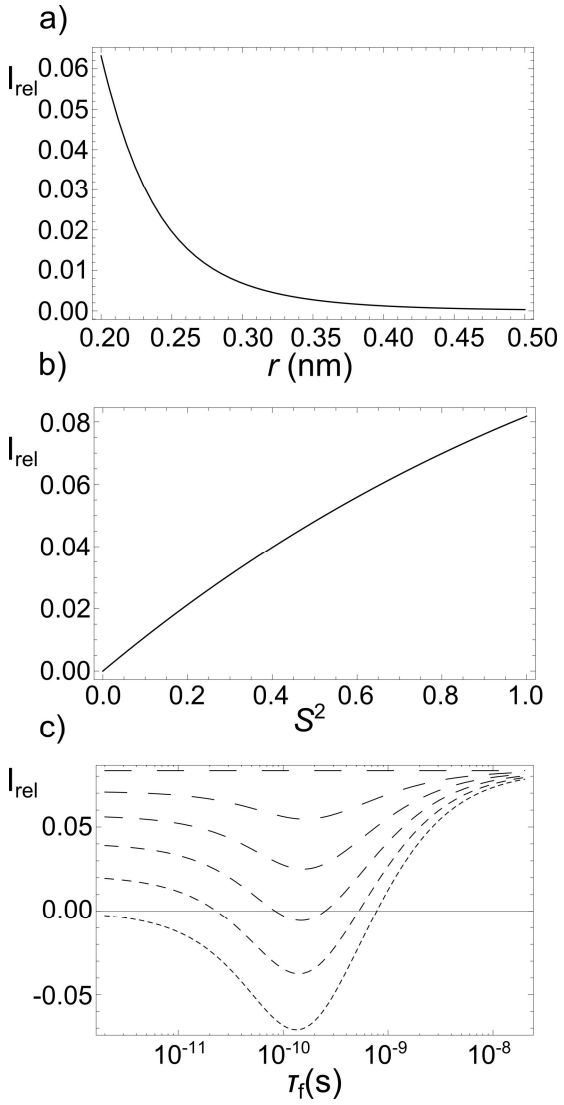

Figure 4.4. Curves illustrating the dependence of NOE crosspeak intensity for an isolated proton pair on a) interproton distance r, b) Lipari-Szabo order parameter S^2, and c) correlation time τ_f for fast internal motion. The common parameters are identical to those in Figure 4.2. Curves were plotted for a constant temperature of T = 40 °C (313 K), resulting in τ_c = 1 ns. Parameters specific to the individual panels are as follows: a) S^2 = 0.7. b) τ_f = 0 (fast intramolecular motion limit); r = 0.2 nm. c) S^2 varying from 0 to 1 in steps of 0.2, for curves from shortest to longest dash in the bundle; r = 0.2 nm.

protons, such that both auto- and crossrelaxation rates decrease with increasing distance. In the real situation, where third protons give additional contributions to relaxation, the decrease in crosspeak intensity with increasing distance may be even stronger. As described above, intramolecular motions of the polypeptide can be described by the two parameters S^2 and τ_f. Figure 4.4b shows that the crosspeak intensity also decreases with decreasing order parameter, which arises due to increased sampling of conformational space. In the limit of fast intramolecular motion, as shown in the figure, the NOE vanishes for $S^2 = 0$. In other cases, a residual positive or negative intensity would remain. Order parameters are frequently reported in the literature for amide bonds, since those can be determined from heteronuclear [^{1}H,^{15}N]-NOE measurements using ^{15}N labeled proteins.[44] Common order parameters range from ca. 0.5 to 1.0 in folded proteins,[44,153] whereas for unfolded polypeptides, values such as from 0.2 to 0.5 have been reported.[154-155] Even though the polypeptide backbone proton – proton distances measured in a homonuclear [^{1}H,^{1}H]-NOESY experiment are different from amide bonds, it may be reasonable to expect at least similar degrees of disorder.

Upon loss of secondary structure, distances characteristic for the type of secondary structure will increase – ultimately beyond the limit detectable by NOE – while at the same time the order parameter decreases. Both of these effects give rise to reduced NOE crosspeak intensity. The third parameter, τ_f, gives rise to a more complicated behavior. Figure 4.4c has been plotted with sufficient range to show the limiting cases of fast intramolecular motion, where the spectral density decreases linearly with S^2, and of slow intramolecular motion, where the spectral density reduces

to that of the rigid molecule. In-between lies a minimum, so that the crosspeak intensity in fact can increase again if τ_f decreases below a threshold of a few hundred picoseconds. This effect is opposite to those previously discussed, however under the present conditions appears relatively small in comparison.

In addition to the parameters considered above, effects such as the exchange of labile protons may play a further role in changing NOE crosspeak intensity. While the magnitude of this effect may be more difficult to predict theoretically, it results in a loss of NOE intensity upon increased exchange due to increased temperature. It thus compounds the effect of other parameters, such as increase in distance upon denaturation, discussed above. Because of the various contributions, the observed NOE intensity does not directly follow the denaturation curve for the polypeptide. Nevertheless, the combination of effects that relate to denaturation is expected to give rise to loss in the NOE intensity. Therefore, the NOE has the potential to serve as an indicator for peptide denaturation.

For the trpzip4 peptide, NOEs and amide proton exchange rates can be used to confirm the secondary structure present in the peptide at the lowest temperature (9 °C). Cross-peaks between H^N of Glu 42 and H^N of Thr 55, H^N of Thr 44 and H^N of Thr 53, H^N of Asp 46 and H^N of Thr 51, H^α of Trp 43 and H^α of Trp 54, H^α of Trp 45 and H^α of Trp 52, H^N of Glu 42 and H^α of Glu 56, H^α of Trp 43 and H^N of Thr 55, H^N of Thr 44 and H^α of Thr 53, and H^N of Asp 46 and H^α of Trp 52 are indicative of the anti-parallel β-sheet secondary structure. Additionally, the presence of hydrogen bonds is confirmed by reduced hydrogen exchange rates.[156] Table 3.1 shows that amide protons of Thr 44, Asp

46, Thr 51, and Thr 53 involved in hydrogen bonds in the core of the protein have low hydrogen exchange rate constants, while solvent exposed amide protons of Trp 43, Trp 45, Asp 47, Ala 48, Trp 52, Trp 54 and Glu 56 have high rate constants. This data obtained from NOE and hydrogen exchange measurements agrees well with the published structure, from which hydrogen bonds between H^N of Glu 42 and O of Thr 55, H^N of Thr 44 and O of Thr 53, H^N of Asp 46 and O of Thr 51, and H^N of Thr 49 and O of Asp 46 can be predicted.[53]

Table 3.1**.** Amide proton exchange rates per residue of trpzip4. Rates for E42 and T49 were not determined due to spectral overlap with tryptophan signals.

Residue	Rate constant (h^{-1})	Residue	Rate constant (h^{-1})
W43	>10	T51	0.3
T44	0.4	W52	6.2
W45	>10	T53	0.4
D46	0.2	W54	>10
D47	>10	T55	2
A48	8	E56	4
K50	0.3		

In 2D-[^{1}H,^{1}H] NOESY spectra obtained from trpzip4 at increasing temperatures, it is readily apparent that crosspeaks between different protons exhibit different temperature dependence. For example, as shown in Figure 4.5, the crosspeak between Asp 46 and Thr 51 at 29 °C retains 70% of its intensity at 9 °C, whereas the crosspeak between Glu 42 and Thr 55 retains 17% of its intensity at 9 °C. While Glu 42 and Thr 55

are located at the termini, Asp 46 and Thr 51 are located near cross-strand interaction between Trp residues.

The temperature dependence of all of the observed cross-strand NOEs that have been observed in trpzip4 is plotted in Figure 4.6. Most strikingly, it can be seen that these curves follow a sigmoidal temperature dependence, which stands in contrast to the convex function from Figure 4.3. The conclusion is that, in addition to the increased molecular motion, other changes in the polypeptide significantly contribute to the temperature dependence of NOE crosspeak intensity. This experimental observation therefore lends further support to the use of the NOE for the assay of protein denaturation. At the same time, it is apparent that Equations 1-5 contain more unknown parameters than could reasonably be included in a fit, even in the absence of the effects arising from structural changes in the polypeptide. Nevertheless, in order to extract a quantitative measure reflecting the observed differences, the data of Figure 4.5 has been fit by cubic smoothing splines. From these splines, a fully empirical cutoff temperature, which is defined as the temperature at which the NOE intensity falls below one half of that at the lowest temperature measured (here, the lowest measured temperature is 9 °C) can readily be determined for each residue. Ideally, where the sigmoidal shape is fully observable in the measured temperature range, such as for the NOE between H^N of Asp 46 and H^α of Trp 52, this cutoff temperature should be relatively insensitive with respect to the choice of the lower temperature limit.

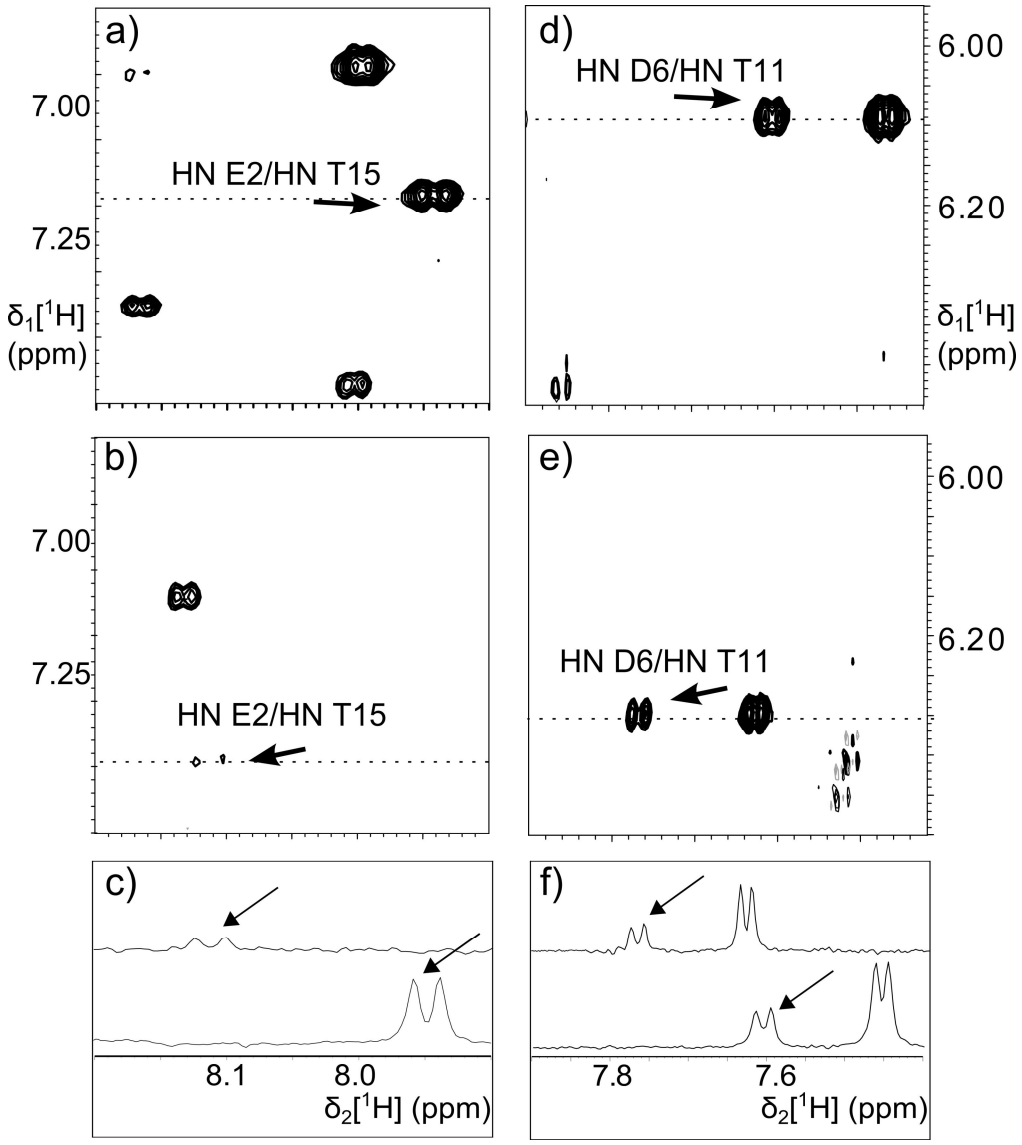

Figure 4.5. Extracts from 2D-[1H,1H] NOESY spectra of trpzip 4, showing the crosspeaks E42-T55 and D46-T51. The spectra were measured a) and d) at 9 °C and b) and e) at 29 °C. c) E42/T55 and f) D46/T51 show one-dimensional slices through the crosspeaks, taken from the positions indicated by the dotted lines in a), b), d) and e), respectively.

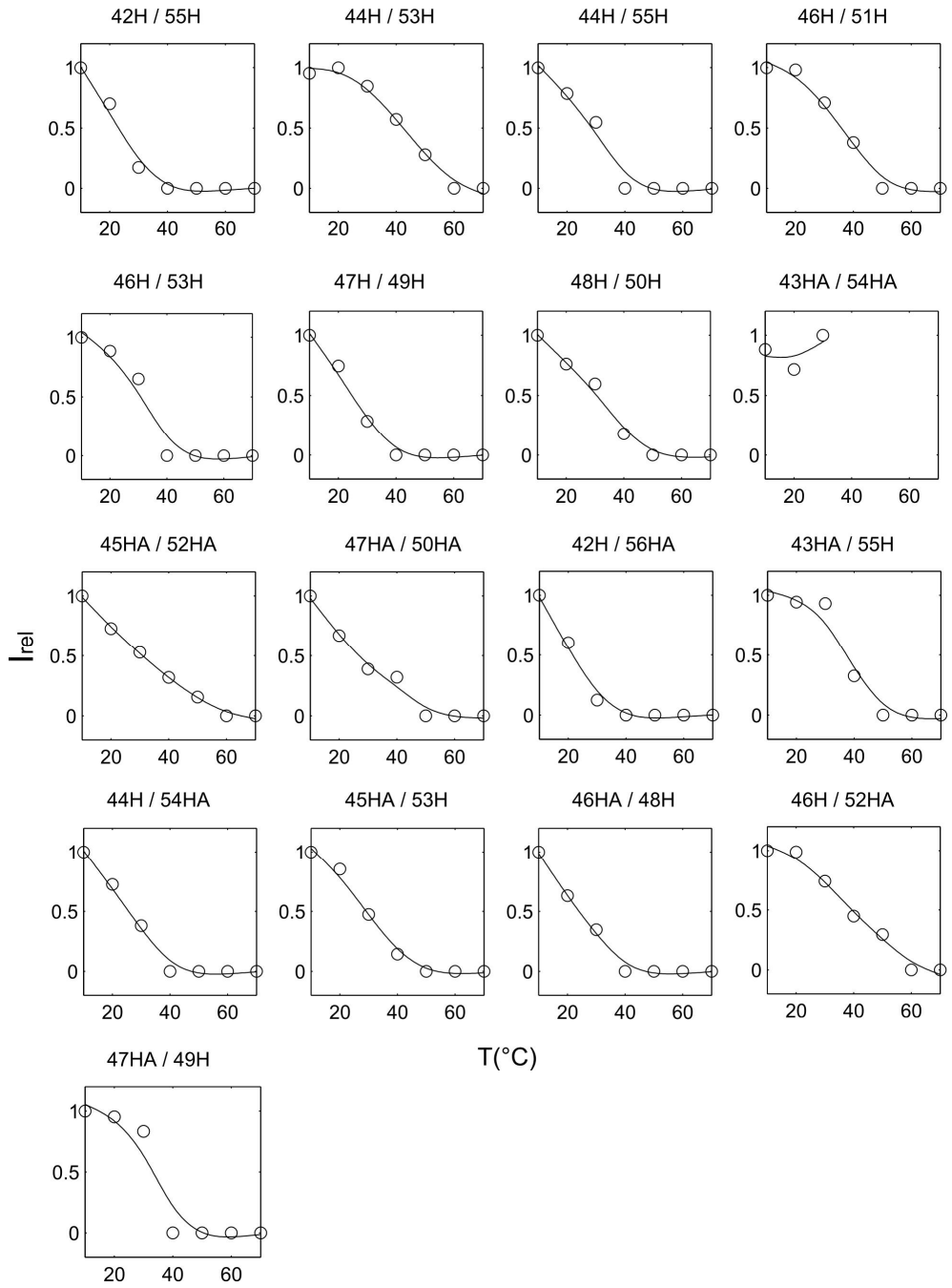

Figure 4.6. Relative intensity of backbone-backbone NOE crosspeaks in function of temperature. The line represents a cubic smoothing spline interpolation of the experimental data (see text).

In other cases, where the plateau is not yet reached at the lowest temperature (e.g. 42HN/56HA), the calculated cutoff temperature may be an overestimate. Nevertheless, the thus calculated temperature for 42HN/56HA is still lower than for example for 46HN/52HA.

The distribution of cutoff temperatures is most clearly seen in Figure 4.7, where the corresponding distances are color coded on the structure of trpzip4. The structure shown is used as obtained from the protein database (PDB ID 1LE3).[53] Interestingly, the largest cutoff temperatures are clustered in the central region of the hairpin, close to the four tryptophan residues. On the other hand, both the regions containing the termini, as well as the loop, appear to show lower thermal stability. It appears likely that indeed the tryptophan-tryptophan side-chain interactions significantly contribute to the stability of the β-hairpin structure. This result is in good agreement with a previous study that implicated the tryptophan residues in the stability of the related peptide trpzip2, by selective mutagenesis of those residues.[135] A recent molecular dynamics (MD) simulation study performed by Gao et. al. further has predicted a disfavored turn structure for trpzip4, and a hydrophobic core centric mechanism was proposed for hairpin folding, where a strong hydrophobic interaction between tryptophan residues strengthens the stability of hydrogen bonds in the middle of the strands.[141]

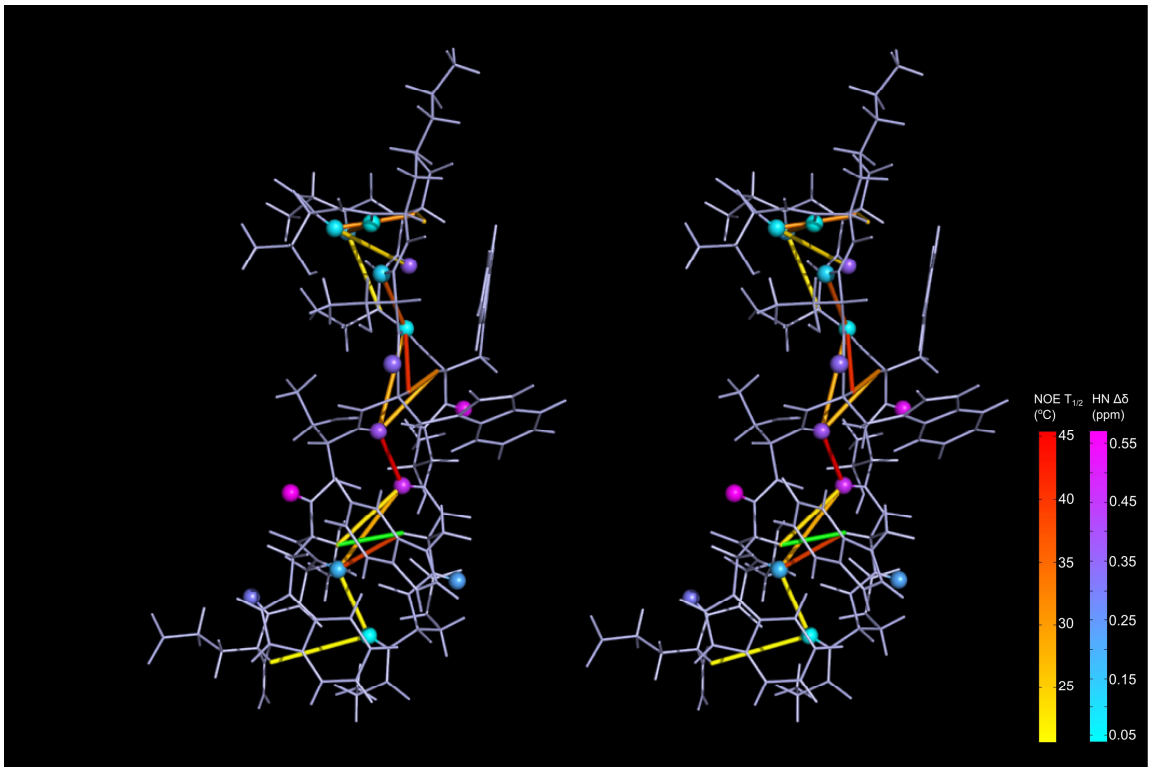

Figure 4.7. Wall-eyed stereo view of trpzip4 with backbone-backbone distances color-coded according to the temperature at which the corresponding NOE crosspeak has lost half of its volume as compared to the crosspeak at 9 °C. Yellow colored lines indicate crosspeaks that are lost at lowest temperature, and red colored lines those lost at highest temperature. The green colored line is for the distance 43HA/54HA, for which the cutoff temperature could not be determined due to overlap with the water resonance (compare to Figure 4.6). Amide- and alpha-protons are color coded according to their change in chemical shift between 9 °C and 69 °C. Cyan indicates nearly constant chemical shift, and magenta indicates the largest change.

From Figure 4.7, it is further apparent that a high NOE derived cutoff temperature in fact correlates to some extent with a large change in amide proton chemical shift upon increase of temperature. For example, the amide protons of Thr 44 and Thr 53, which are located in the core of the hairpin, at lowest temperature appear at higher chemical shift than all other amide protons. They shift in the direction towards average chemical shift with increasing temperature. Such effects are expected due to the loss of initial structure or hydrogen bonds in the core of the peptide.[145]

For the structural study of peptides of intermediate size, rotating frame Overhauser spectra (ROESY) are often preferred over NOESY spectra, since ROESY crosspeaks can be observed at all temperatures. Therefore, we have further evaluated the utility of this type of spectroscopy towards the study of the thermal denaturation process in trpzip4. From a simulation of expected ROE intensities (Figure 4.8a), it is apparent that depending on parameters, foremost the distance between atoms, the ROE is in some cases expected to initially increase with increasing temperature. This behavior was observed experimentally for the contacts between H^{α} of Trp 43 and H^{α} of Trp 54, and between H^{α} of Trp 45 and H^{α} of Trp 52. In this case, a simple empirical cutoff temperature as was used above for the analysis of NOESY spectra cannot easily be defined, and it would be necessary to employ a model that includes additional assumptions and unknown parameters. The ROE effect appears therefore less well suited for the analysis of thermal denaturation of short peptides.

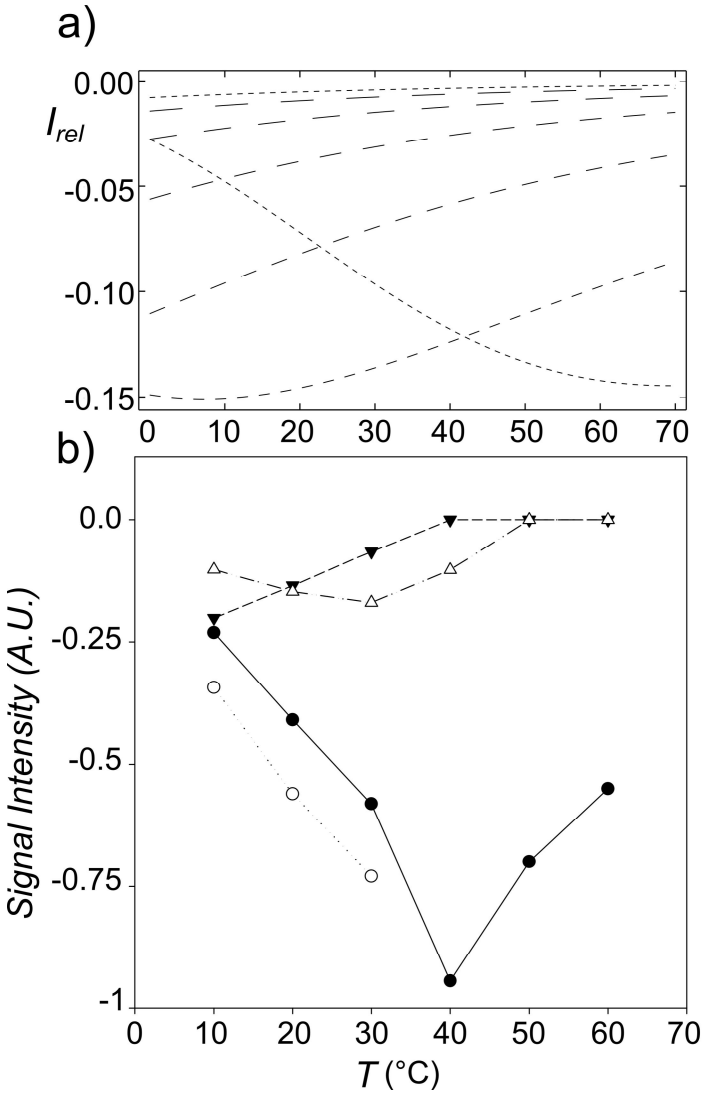

Figure 4.8. a) Temperature dependence of the ROE effect calculated for a rigid molecule. Parameters are identical to those in Figure 4.2, except for the mixing time, which was 200 ms. b) Observed ROE crosspeak intensities for trpzip4 (—●—: 45HA/52HA, · · ○ · · : 43HA/54HA, − − ▼ − − : 42HN/55HN, – -△– · : 46HN/51HA).

4.4 Conclusions

In summary, we have studied the thermal denaturation of the β-hairpin peptide trpzip4 by a NOE based method. The results indicate that the region of highest thermal stability lies in the core region, in the vicinity of the tryptophan residues. It appears likely, therefore, that side chain – side chain interactions of these amino acids play a significant role in stabilizing the structure of trpzip4, while still preserving the native hydrogen bonds typical for an antiparallel β-sheet secondary structure. Methodologically, an NOE based study appears particularly favorable compared to the more traditional chemical shift based measurements in cases such as here, where a change in aromatic side-chain conformation has a strong potential to influence chemical shift, or where the change in chemical shift is reduced due to incomplete denaturation in the accessible temperature range. The primary limitation of the NOE based method lies in the accessible temperature, since at high temperature the NOE intensity is reduced due to increased molecular tumbling. However, at lower temperature, corresponding to the onset of the denaturation process of peptides, it may well be more sensitive than other experimentally observable parameters.

CHAPTER V

SUMMARY AND CONCLUSIONS

Despite an increasing availability of information on the native structure of proteins, our understanding of the determinants for protein structure formation is relatively limited. The difficulty arises due to the presence of a balance between a large number of noncovalent interactions in a polypeptide chain that ultimately determine the protein structure. In order to investigate those noncovalent interactions, short peptides are often used since they provide a more controlled approach to analyzing specific structure information than do full-length proteins. By determining the structure and non-covalent interactions of model peptides using NMR, we investigated the driving forces for secondary and tertiary structure formation.

Two different peptides were used to study the effects of solvent-solute interactions on peptide secondary structures. First, determined structures of individual transmembrane helix peptides taken from the disulfide bond forming protein B showed stable helices. This result can be taken as an indication that DsbB follows the two-stage model for protein folding. However, comparison of individual peptide structures with the X-ray structure of full-length protein demonstrated different side-chain conformations in particular for the polar amino acids in the helices, suggesting that polar side-chains may re-orient during helix assembly for a global folding of DsbB. Mixtures of two peptides corresponding to adjacent helices in the full-length protein were employed to determine helix-helix interactions. Only relatively small changes in chemical shift were observed, indicating no strong interaction between helices in the absence of a linker peptide. In

addition to membrane protein fragments, a soluble peptide BBA5 was employed to investigate the effect of an organic co-solvent, methanol, on the structure formation. Combined methods, NMR and MD simulation, clearly show that methanol molecules strengthen the interactions between the polar backbone of the peptide due to the exclusion of surface water, enhancing the α-helix secondary structure formation. At the same time, methanol molecules were found to have favored interactions with the hydrophobic residues, which interrupt the hydrophobic cluster in the peptide and result in a higher degree of solvent exposure of these residues.

Additional information about protein folding can be gained by finding methods to observe transitions between folded and unfolded forms of a peptide. Moving toward this goal, a method using NOE information to monitor thermal denaturation of peptides was developed. The NOE based information is complementary to the commonly used observation of H^{α} or H^{N} chemical shift change. For the NOE-based approach, various factors that give rise to a change in NOE intensity upon changing the temperature are considered. The method was applied to a tryptophan zipper peptide, trpzip4.These measurements allowed to confirm that the trpzip4 structure is mainly stabilized by a hydrophobic cluster formed by tryptophan residues located in the central region of the ß-hairpin.

In summary, a combination of methodological developments and applications of NMR to peptide structural studies were presented. The results from the NMR based determination of the conformation and dynamics of three different types of peptides illustrate the important roles played by non-covalent interactions such as hydrogen

bonding, side chain - side chain hydrophobic interactions and solvent-polypeptide interactions in stabilizing the structure.. They will hopefully contribute towards a better understanding of the driving forces behind the formation of secondary or tertiary structures in proteins.

REFERENCES

(1) Creighton, T. E. *Proteins: Structures and molecular properties.* New York, 1993.

(2) Stefani, M.; Dobson, C. M. *J. Mol. Med.* **2003**, *81*, 678.

(3) Dobson, C. M. *Philos. Trans. R. Soc. Lond. B. Biol. Sci.* **2001**, *356*, 133.

(4) Bruch, M. D.; Dhingra, M. M.; Gierasch, L. M. *Proteins* **1991**, *10*, 130.

(5) Ramirez-Alvarado, M.; Kortemme, T.; Blanco, F. J.; Serrano, L. *Bioorg. Med. Chem.* **1999**, *7*, 93.

(6) Bierzynski, A.; Kim, P. S.; Baldwin, R. L. *Proc. Natl. Acad. Sci. USA* **1982**, *79*, 2470.

(7) Tanford, C. *J. Am. Chem. Soc.* **1962**, *84*, 4240.

(8) Pace, C. N.; Fu, H.; Fryar, K. L.; Landua, J.; Trevino, S. R.; Shirley, B. A.; Hendricks, M. M.; Iimura, S.; Gajiwala, K.; Scholtz, J. M.; Grimsley, G. R. *J. Mol. Biol.* **2011**, *408*, 514.

(9) Shao, Q. A.; Wei, H. Y.; Gao, Y. Q. *J. Mol. Biol.* **2010**, *402*, 595.

(10) Yang, L.; Shao, Q.; Gao, Y. Q. *J. Phys. Chem. B* **2009**, *113*, 803.

(11) Myers, J. K.; Pace, C. N. *Biophys. J.* **1996**, *71*, 2033.

(12) Güntert, P.; Mumenthaler, C.; Wüthrich, K. *J. Mol. Biol.* **1997**, *273*, 283.

(13) Honig, B.; Yang, A. S. *Adv. Protein Chem.* **1995**, *46*, 27.

(14) Lazaridis, T.; Archontis, G.; Karplus, M. *Adv. Protein Chem.* **1995**, *47*, 231.

(15) Huyghues-Despointes, B. M.; Klingler, T. M.; Baldwin, R. L. *Biochemistry* **1995**, *34*, 13267.

(16) Inaba, K.; Murakami, S.; Suzuki, M.; Nakagawa, A.; Yamashita, E.; Okada, K.; Ito, K. *Cell* **2006**, *127*, 789.

(17) Sonnichsen, F. D.; Van Eyk, J. E.; Hodges, R. S.; Sykes, B. D. *Biochemistry* **1992**, *31*, 8790.

(18) Searle, M. S.; Zerella, R.; Williams, D. H.; Packman, L. C. *Protein Eng.* **1996**, *9*, 559.

(19) Fioroni, M.; Diaz, M. D.; Burger, K.; Berger, S. *J. Am. Chem. Soc.* **2002**, *124*, 7737.

(20) O'Brien, E. P.; Dima, R. I.; Brooks, B.; Thirumalai, D. *J. Am. Chem. Soc.* **2007**, *129*, 7346.

(21) Makarov, V.; Pettitt, B. M.; Feig, M. *Acc. Chem. Res.* **2002**, *35*, 376.

(22) Hubert, P.; Sawma, P.; Duneau, J. P.; Khao, J.; Henin, J.; Bagnard, D.; Sturgis, J. *Cell. Adh. Migr.* **2010**, *4*, 313.

(23) Arora, A.; Abildgaard, F.; Bushweller, J. H.; Tamm, L. K. *Nat. Struct. Biol.* **2001**, *8*, 334.

(24) Hiller, S.; Garces, R. G.; Malia, T. J.; Orekhov, V. Y.; Colombini, M.; Wagner, G. *Science* **2008**, *321*, 1206.

(25) Doyle, D. A.; Morais Cabral, J.; Pfuetzner, R. A.; Kuo, A.; Gulbis, J. M.; Cohen, S. L.; Chait, B. T.; MacKinnon, R. *Science* **1998**, *280*, 69.

(26) Zhou, Y.; Cierpicki, T.; Jimenez, R. H.; Lukasik, S. M.; Ellena, J. F.; Cafiso, D. S.; Kadokura, H.; Beckwith, J.; Bushweller, J. H. *Mol. Cell* **2008**, *31*, 896.

(27) Lemmon, M. A.; Flanagan, J. M.; Treutlein, H. R.; Zhang, J.; Engelman, D. M. *Biochemistry* **1992**, *31*, 12719.

(28) Gurezka, R.; Laage, R.; Brosig, B.; Langosch, D. *J. Biol. Chem.* **1999**, *274*, 9265.

(29) Therien, A. G.; Grant, F. E.; Deber, C. M. *Nat. Struct. Biol.* **2001**, *8*, 597.

(30) Popot, J. L.; Engelman, D. M. *Biochemistry* **1990**, *29*, 4031.

(31) Popot, J. L.; Trewhella, J.; Engelman, D. M. *EMBO J.* **1986**, *5*, 3039.

(32) MacKenzie, K. R.; Engelman, D. M. *Proc. Natl. Acad. Sci. USA* **1998**, *95*, 3583.

(33) Engelman, D. M.; Chen, Y.; Chin, C. N.; Curran, A. R.; Dixon, A. M.; Dupuy, A. D.; Lee, A. S.; Lehnert, U.; Matthews, E. E.; Reshetnyak, Y. K.; Senes, A.; Popot, J. L. *FEBS Lett.* **2003**, *555*, 122.

(34) Wimley, W. C.; Creamer, T. P.; White, S. H. *Biochemistry* **1996**, *35*, 5109.

(35) Wimley, W. C.; White, S. H. *Nat. Struct. Biol.* **1996**, *3*, 842.

(36) Radford, S. E.; Dobson, C. M.; Evans, P. A. *Nature* **1992**, *358*, 302.

(37) Elove, G. A.; Chaffotte, A. F.; Roder, H.; Goldberg, M. E. *Biochemistry* **1992**, *31*, 6876.

(38) Neri, D.; Billeter, M.; Wider, G.; Wuthrich, K. *Science* **1992**, *257*, 1559.

(39) Kleckner, I. R.; Foster, M. P. *Biochim. Biophys. Acta.* **2011**, *1814*, 942.

(40) Schanda, P.; Forge, V.; Brutscher, B. *Proc. Natl. Acad. Sci. USA* **2007**, *104*, 11257.

(41) Wishart, D. S.; Sykes, B. D.; Richards, F. M. *Biochemistry* **1992**, *31*, 1647.

(42) Cierpicki, T.; Otlewski, J. *J. Biomol. NMR* **2001**, *21*, 249.

(43) Solomon, I. *Phys. Rev.* **1955**, *99*, 559.

(44) Kay, L. E.; Torchia, D. A.; Bax, A. *Biochemistry* **1989**, *28*, 8972.

(45) Volkman, B. F.; Lipson, D.; Wemmer, D. E.; Kern, D. *Science* **2001**, *291*, 2429.

(46) Muhandiram, D. R.; Yamazaki, T.; Sykes, B. D.; Kay, L. E. *J. Am. Chem. Soc.* **1995**, *117*, 11536.

(47) Yang, D. W.; Mittermaier, A.; Mok, Y. K.; Kay, L. E. *J. Mol. Biol.* **1998**, *276*, 939.

(48) Englander, S. W.; Mayne, L. *Annu. Rev. Biophys. Biomol. Struct.* **1992**, *21*, 243.

(49) Sharma, S.; Zheng, H.; Huang, Y. J.; Ertekin, A.; Hamuro, Y.; Rossi, P.; Tejero, R.; Acton, T. B.; Xiao, R.; Jiang, M.; Zhao, L.; Ma, L. C.; Swapna, G. V.; Aramini, J. M.; Montelione, G. T. *Proteins* **2009**, *76*, 882.

(50) Olofsson, A.; Lindhagen-Persson, M.; Sauer-Eriksson, A. E.; Ohman, A. *Biochem. J.* **2007**, *404*, 63.

(51) Abel, E. W.; Coston, T. P. J.; Orrell, K. G.; Sik, V.; Stephenson, D. *J Magn Reson* **1986**, *70*, 34.

(52) Pace, C. N. *Methods Enzymol.* **1995**, *259*, 538.

(53) Cochran, A. G.; Skelton, N. J.; Starovasnik, M. A. *Proc. Natl. Acad. Sci. USA* **2001**, *98*, 5578.

(54) Trevino, S. R.; Schaefer, S.; Scholtz, J. M.; Pace, C. N. *J. Mol. Biol.* **2007**, *373*, 211.

(55) Pace, C. N.; Grimsley, G. R.; Scholtz, J. M. *J. Biol. Chem.* **2009**, *284*, 13285.

(56) Tokuriki, N.; Tawfik, D. S. *Curr. Opin. Struct. Biol.* **2009**, *19*, 596.

(57) Tokuriki, N.; Stricher, F.; Schymkowitz, J.; Serrano, L.; Tawfik, D. S. *J. Mol. Biol.* **2007**, *369*, 1318.

(58) Bellapadrona, G.; Chiaraluce, R.; Consalvi, V.; Ilari, A.; Stefanini, S.; Chiancone, E. *Proteins* **2007**, *66*, 975.

(59) De Prat Gay, G.; Ruiz-Sanz, J.; Neira, J. L.; Itzhaki, L. S.; Fersht, A. R. *Proc. Natl. Acad. Sci. USA* **1995**, *92*, 3683.

(60) Wu, L. C.; Laub, P. B.; Elove, G. A.; Carey, J.; Roder, H. *Biochemistry* **1993**, *32*, 10271.

(61) Wahlgren, N. M.; Dejmek, P.; Drakenberg, T. *J. Dairy Res.* **1994**, *61*, 495.

(62) Reddy, A. P.; Tallon, M. A.; Becker, J. M.; Naider, F. *Biopolymers* **1994**, *34*, 679.

(63) Klibanov, A. M. *Nature* **2001**, *409*, 241.

(64) Jander, G.; Martin, N. L.; Beckwith, J. *EMBO J.* **1994**, *13*, 5121.

(65) Inaba, K.; Murakami, S.; Nakagawa, A.; Iida, H.; Kinjo, M.; Ito, K.; Suzuki, M. *EMBO J.* **2009**, *28*, 779.

(66) Struthers, M.; Ottesen, J. J.; Imperiali, B. *Fold Des* **1998**, *3*, 95.

(67) Popot, J. L.; Engelman, D. M. *Annu. Rev. Biochem.* **2000**, *69*, 881.

(68) Engelman, D. M.; Steitz, T. A. *Cell* **1981**, *23*, 411.

(69) Tafer, H.; Hiller, S.; Hilty, C.; Fernandez, C.; Wuthrich, K. *Biochemistry* **2004**, *43*, 860.

(70) Xue, R.; Wang, S.; Qi, H.; Song, Y.; Wang, C.; Li, F. *Biochim. Biophys. Acta.* **2008**, *1778*, 1444.

(71) Duarte, A. M.; Wolfs, C. J.; Koehorst, R. B.; Popot, J. L.; Hemminga, M. A. *J. Pept. Sci.* **2008**, *14*, 389.

(72) Arshava, B.; Taran, I.; Xie, H.; Becker, J. M.; Naider, F. *Biopolymers* **2002**, *64*, 161.

(73) Dmitriev, O.; Jones, P. C.; Jiang, W.; Fillingame, R. H. *J. Biol. Chem.* **1999**, *274*, 15598.

(74) Pervushin, K. V.; Arseniev, A. S. *FEBS Lett.* **1992**, *308*, 190.

(75) Pervushin, K. V.; Orekhov, V.; Popov, A. I.; Musina, L.; Arseniev, A. S. *Eur. J. Biochem.* **1994**, *219*, 571.

(76) Duarte, A. M.; de Jong, E. R.; Wechselberger, R.; van Mierlo, C. P.; Hemminga, M. A. *Biochim. Biophys. Acta.* **2007**, *1768*, 2263.

(77) Katragadda, M.; Alderfer, J. L.; Yeagle, P. L. *Biophys. J.* **2001**, *81*, 1029.

(78) Duarte, A. M.; Wolfs, C. J.; van Nuland, N. A.; Harrison, M. A.; Findlay, J. B.; van Mierlo, C. P.; Hemminga, M. A. *Biochim. Biophys. Acta.* **2007**, *1768*, 218.

(79) Chopra, A.; Yeagle, P. L.; Alderfer, J. A.; Albert, A. D. *Biochim. Biophys. Acta.* **2000**, *1463*, 1.

(80) Neumoin, A.; Arshava, B.; Becker, J.; Zerbe, O.; Naider, F. *Biophys. J.* **2007**, *93*, 467.

(81) Lomize, A. L.; Pervushin, K. V.; Arseniev, A. S. *J. Biomol. NMR* **1992**, *2*, 361.

(82) MaslennikovIv; Arsen'ev, A. S.; Chikin, L. D.; Kozhich, A. T.; Ivanov, V. T. *Bioorg. Khim.* **1993**, *19*, 5.

(83) Abdulaeva GV, S., A. G., Arseniev, A. S., Tsetlin, V. I., and Bystrov, V. F. *Biol Membrany (USSR)* **1991**, *8*, 30.

(84) Grabchuk, I. A.; Orekhov, V.; Arseniev, A. S. *Pharm. Acta. Helv.* **1996**, *71*, 97.

(85) Pervushin, K. V.; Arseniev, A. S.; Kozhich, A. T.; Ivanov, V. T. *J. Biomol. NMR* **1991**, *1*, 313.

(86) Valiyaveetil, F. I.; Zhou, Y.; MacKinnon, R. *Biochemistry* **2002**, *41*, 10771.

(87) Opella, S. J.; Marassi, F. M.; Gesell, J. J.; Valente, A. P.; Kim, Y.; Oblatt-Montal,

M.; Montal, M. *Nat. Struct. Biol.* **1999**, *6*, 374.

(88) Scott, A. I.; Roessner, C. A.; Stolowich, N. J.; Karuso, P.; Williams, H. J.; Grant, S. K.; Gonzalez, M. D.; Hoshino, T. *Biochemistry* **1988**, *27*, 7984.

(89) Inaba, K.; Murakami, S.; Nakagawa, A.; Iida, H.; Kinjo, M.; Ito, K.; Suzuki, M. *EMBO J.* **2009**, *28*, 779.

(90) Mareci TH, F. R. *J. Magn. Reson.* **1983**, *51*, 531.

(91) Braunschweiler L, E. R. *J. Magn. Reson.* **1983**, *53*, 521.

(92) Jeener J, M. B., Bachmann P, Ernst RR. *J. Chem. Phys.* **1979**, *71*, 4546.

(93) Bax A, D. D. *J. Magn. Reson.* **1985**, *65*, 355.

(94) Delaglio, F.; Grzesiek, S.; Vuister, G. W.; Zhu, G.; Pfeifer, J.; Bax, A. *J. Biomol. NMR* **1995**, *6*, 277.

(95) Keller, R., Diss. ETH Nr. 15947, 2004.

(96) Wüthrich, K. *NMR of Proteins and Nucleic Acids*; Wiley, New York, 1986.

(97) Koradi, R.; Billeter, M.; Wüthrich, K. *J. Mol. Graph.* **1996**, *14*, 51.

(98) Braun, W.; Vasak, M.; Robbins, A. H.; Stout, C. D.; Wagner, G.; Kagi, J. H.; Wüthrich, K. *Proc. Natl. Acad. Sci. USA* **1992**, *89*, 10124.

(99) White SH, v. H. G. *Curr. Opin. Struct. Biol.* **2005**, *15*, 378.

(100) Starzyk, A.; Barber-Armstrong, W.; Sridharan, M.; Decatur, S. M. *Biochemistry* **2005**, *44*, 369.

(101) Liu, L. P.; Li, S. C.; Goto, N. K.; Deber, C. M. *Biopolymers* **1996**, *39*, 465.

(102) Liu, L. P.; Deber, C. M. *Biochemistry* **1997**, *36*, 5476.

(103) Liu, L. P.; Deber, C. M. *J. Biol. Chem.* **1998**, *273*, 23645.

(104) Brown, L. R.; Bosch, C.; Wüthrich, K. *Biochim. Biophys. Acta.* **1981**, *642*, 296.

(105) Hilty, C.; Wider, G.; Fernandez, C.; Wüthrich, K. *Chembiochem* **2004**, *5*, 467.

(106) Reiersen H, R. A. *Protein Eng.* **2000**, *13*, 739.

(107) Roccatano, D.; Colombo, G.; Fioroni, M.; Mark, A. E. *Proc. Natl. Acad. Sci. USA* **2002**, *99*, 12179.

(108) Sundaralingam, M.; Drendel, W.; Greaser, M. *Proc. Natl. Acad. Sci. USA* **1985**, *82*, 7944.

(109) H. Desvaux, P. B., N. Birlirakis, and M. Goldman *J. Mag. Reson. Series A* **1994**, *108*, 219.

(110) Schleich, K. K. a. T. *J. Mag. Reson. Series A* **1995**, *114*, 219.

(111) Idiyatullin, D.; Krushelnitsky, A.; Nesmelova, I.; Blanco, F.; Daragan, V. A.; Serrano, L.; Mayo, K. H. *Protein Sci.* **2000**, *9*, 2118.

(112) Renner, C.; Cramer, J.; Behrendt, R.; Moroder, L. *Biopolymers* **2000**, *54*, 501.

(113) Uversky, V. N.; Narizhneva, N. V.; Kirschstein, S. O.; Winter, S.; Lober, G. *Fold Des* **1997**, *2*, 163.

(114) Buck, M. *Q Rev Biophys* **1998**, *31*, 297.

(115) Harding, M. M.; Williams, D. H.; Woolfson, D. N. *Biochemistry* **1991**, *30*, 3120.

(116) Cox, J. P. L.; Evans, P. A.; Packman, L. C.; Williams, D. H.; Woolfson, D. N. *J. Mol. Biol.* **1993**, *234*, 483.

(117) Albert, J. S.; Hamilton, A. D. *Biochemistry* **1995**, *34*, 984.

(118) Babu, K. R.; Douglas, D. J. *Biochemistry* **2000**, *39*, 14702.

(119) Gast, K.; Siemer, A.; Zirwer, D.; Damaschun, G. *Eur. Biophys. J.* **2001**, *30*, 273.

(120) Kinoshita, M.; Okamoto, Y.; Hirata, F. *J. Am. Chem. Soc.* **2000**, *122*, 2773.

(121) Zhao, J. H.; Liu, H. L. *Chem Phys Lett* **2006**, *420*, 235.

(122) Perham, M.; Liao, J.; Wittung-Stafshede, P. *Biochemistry* **2006**, *45*, 7740.

(123) Kony, D. B.; Hunenberger, P. H.; van Gunsteren, W. F. *Protein Science* **2007**, *16*, 1101.

(124) Hamada, D.; Kuroda, Y.; Tanaka, T.; Goto, Y. *J. Mol. Biol.* **1995**, *254*, 737.

(125) Yamazaki, K.; Iwura, T.; Ishikawa, R.; Ozaki, Y. *Journal of Biochemistry* **2006**,

140, 49.

(126) Hirota, N.; Mizuno, K.; Goto, Y. *J. Mol. Biol.* **1998**, *275*, 365.

(127) Timasheff, S. N. *Annu Rev Bioph Biom* **1993**, *22*, 67.

(128) Wang, D. Q.; Jaun, B.; van Gunsteren, W. F. *Chembiochem* **2009**, *10*, 2032.

(129) Rogers, J. M. G.; Lippert, L. G.; Gai, F. *Analytical Biochemistry* **2010**, *399*, 182.

(130) Rohl, C. A.; Chakrabartty, A.; Baldwin, R. L. *Protein Science* **1996**, *5*, 2623.

(131) Rothemund, S.; Weißhoff, H.; Beyermann, M.; Krause, E.; Bienert, M.; Mügge, C.; Sykes, B. D.; Sönnichsen, F. D. *J. Biomol. NMR* **1996**, *8*, 93.

(132) Huang, R.; Wu, L.; McElheny, D.; Bour, P.; Roy, A.; Keiderling, T. A. *J. Phys. Chem. B* **2009**, *113*, 5661.

(133) Du, D. G.; Zhu, Y. J.; Huang, C. Y.; Gai, F. *Proc. Natl. Acad. Sci. USA* **2004**, *101*, 15915.

(134) Yang, W. Y.; Pitera, J. W.; Swope, W. C.; Gruebele, M. *J. Mol. Biol.* **2004**, *336*, 241.

(135) Wu, L.; McElheny, D.; Huang, R.; Keiderling, T. A. *Biochemistry* **2009**, *48*, 10362.

(136) Takekiyo, T.; Wu, L.; Yoshimura, Y.; Shimizu, A.; Keiderling, T. A. *Biochemistry* **2009**, *48*, 1543.

(137) Hughes, R. M.; Waters, M. L. *Curr. Opin. Struct. Biol.* **2006**, *16*, 514.

(138) Kiehna, S. E.; Waters, M. L. *Protein Sci.* **2003**, *12*, 2657.

(139) Tatko, C. D.; Waters, M. L. *J. Am. Chem. Soc.* **2002**, *124*, 9372.

(140) Zhang, J.; Qin, M.; Wang, W. *Proteins* **2006**, *62*, 672.

(141) Shao, Q.; Gao, Y. Q. *J. Chem. Theory Comput.* **2010**, *6*, 3750.

(142) Glickson, J. D.; Urry, D. W.; Havran, R. T.; Walter, R. *Proc. Natl. Acad. Sci. USA* **1972**, *69*, 2136.

(143) Llinas, M.; Klein, M. P.; Neilands, J. B. *J. Mol. Biol.* **1970**, *52*, 399.

(144) Llinas, M.; Neilands, J. B. *Biophys. Struct. Mech.* **1976**, *2*, 105.

(145) Baxter, N. J.; Williamson, M. P. *J. Biomol. NMR* **1997**, *9*, 359.

(146) Mahalakshmi, R.; Raghothama, S.; Balaram, P. *J. Am. Chem. Soc.* **2006**, *128*, 1125.

(147) Gellman, S. H.; Dado, G. P.; Liang, G. B.; Adams, B. R. *J. Am. Chem. Soc.* **1991**, *113*, 1164.

(148) Otlewski, T. C. J. *J. Biomol. NMR* **2001**, *21*, 249.

(149) Cavanagh, J. *Protein NMR Spectroscopy: Principles and Practice*; Academic Press, San Diego, 1996.

(150) Luginbühl, P.; Wüthrich, K. *Prog. Nucl. Magn . Reson. Spectrosc.* **2002**, *40*, 199.

(151) Lipari, G.; Szabo, A. *J. Am. Chem. Soc.* **1982**, *104*, 4546.

(152) Lide, D. R. *CRC HANDBOOK OF CHEMISTRY AND PHYSICS*; 91st ed.; CRC Press, Inc.: Boca Raton, FL, 2010.

(153) Marlow, M. S.; Wand, A. J. *Biochemistry* **2006**, *45*, 8732.

(154) Chugha, P.; Oas, T. G. *Biochemistry* **2007**, *46*, 1141.

(155) Shojania, S.; O'Neil, J. D. *J. Biol. Chem.* **2006**, *281*, 8347.

(156) Krishna, M. M.; Hoang, L.; Lin, Y.; Englander, S. W. *Methods* **2004**, *34*, 51.

VITA

Name: Soyoun Hwang

Address: Department of Chemistry, Texas A&M University, MS 3255
College Station, TX 77843

Email Address: shwang@mail.chem.tamu.edu

Education: B.S., Chemistry, Chungnam National University, South Korea, 2003
M.S., Chemistry, Pohang University of Science and Technology, South Korea, 2005
Ph.D., Chemistry, Texas A&M University, 2012